SOUTHERN PLAINS
TRANSPORTATION CENTER

DEVELOPMENT OF A SFE DATABASE FOR SCREENING OF MIXES FOR MOISTURE DAMAGE IN OKLAHOMA

Syed Ashik Ali
Rouzbeh Ghabchi, Ph.D.
Musharraf Zaman, Ph.D., P.E.
Rifat Bulut, Ph.D.

SPTC15.2-19-F

Southern Plains Transportation Center
201 Stephenson Parkway, Suite 4200
The University of Oklahoma
Norman, Oklahoma 73019

TECHNICAL REPORT DOCUMENTATION PAGE

1. REPORT NO.	2. GOVERNMENT ACCESSION NO.	3. RECIPIENTS CATALOG NO.
SPTC15.2-19-F		

4. TITLE AND SUBTITLE	5. REPORT DATE
Development of a SFE Database for Screening of Mixes for Moisture Damage in Oklahoma	December 31, 2019
	6. PERFORMING ORGANIZATION CODE
7. AUTHOR(S)	8. PERFORMING ORGANIZATION REPORT
Syed Ashik Ali, Rouzbeh Ghabchi, Musharraf Zaman and Rifat Bulut	
9. PERFORMING ORGANIZATION NAME AND ADDRESS	10. WORK UNIT NO.
School of Civil Engineering and Environmental Science The University of Oklahoma 202 W. Boyd, Street, CEC 334 Norman, Oklahoma 73019	11. CONTRACT OR GRANT NO. DTRT13-G-UTC36
12. SPONSORING AGENCY NAME AND ADDRESS	13. TYPE OF REPORT AND PERIOD COVERED
Southern Plains Transportation Center 201 Stephenson Pkwy, Suite 4200 The University of Oklahoma Norman, OK 73019	Final March 2016 – December 2019
	14. SPONSORING AGENCY CODE

15. SUPPLEMENTARY NOTES

University Transportation Center

16. ABSTRACT

Moisture-induced damage is one of the major distresses responsible for deterioration of asphalt pavement at early age. There is a need to identify mechanistic methods for evaluating moisture-induced damage as the conventional test methods, such as Hamburg wheel tracking test (HWT) and indirect tensile strength test (IDT) do not address the mechanism leading to failure of asphalt pavements. In this study, surface free energy (SFE) technique were used to mechanistically quantify bonding characteristics of aggregate-asphalt binder systems and consequently moisture-induced damage potential of asphalt mixes. For this purpose, unmodified and polymer-modified asphalt binders from four different sources were collected and mixed with different additives, such as warm mix asphalt (WMA) additive, anti-stripping agent (ASA), polyphosphoric acid (PPA) and reclaimed asphalt pavement (RAP). The SFE components of the binder blends were determined using two different methods, namely, dynamic Wilhelmy plate (DWP) and sessile drop (SD) test. Also, the SFE components of aggregates from five different sources were determined using universal sorption device (USD) and sessile drop (SD) test. Fourier transform infrared, X-ray fluorescence and total acid number tests were conducted on the blended binders to understand the effects of chemical compositions on the SFE components. Asphalt mixes consisting of different additives were produced in the laboratory for moisture-induced damage evaluation using HWT, IDT and Louisiana semi-circular bend (LA-SCB) tests. Correlations between the moisture-induced damage performance parameters from laboratory performance tests and the SFE technique were investigated. The SFE technique was found to be able to differentiate asphalt mixes with different additives based on their moisture-induced damage potentials. It was also found that the LA-SCB test with MIST conditioning can be used as an alternative method to conventional moisture-induced damage test. As a part of this project, a SFE database of asphalt binders and aggregates was developed. The database is expected to be helpful to screen materials during mix design.

17. KEY WORDS	18. DISTRIBUTION STATEMENT
Moisture-induced Damage, Surface Free Energy Database, USD, Wilhelmy Plate, Sessile Drop, Chemical Analysis, Semi-circular Bend test	No restrictions. This publication is available at www.sptc.org and from the NTIS.

19. SECURITY CLASSIF. (OF THIS REPORT)	20. SECURITY CLASSIF. (OF THIS PAGE)	21. NO. OF PAGES	22. PRICE
Unclassified	Unclassified	146 + cover	

SI* (MODERN METRIC) CONVERSION FACTORS

APPROXIMATE CONVERSIONS TO SI UNITS

SYMBOL	WHEN YOU KNOW	MULTIPLY BY	TO FIND	SYMBOL
		LENGTH		
in	inches	25.4	millimeters	mm
ft	feet	0.305	meters	m
yd	yards	0.914	meters	m
mi	miles	1.61	kilometers	km
		AREA		
in^2	square inches	645.2	square millimeters	mm^2
ft^2	square feet	0.093	square meters	m^2
yd^2	square yard	0.836	square meters	m^2
ac	acres	0.405	hectares	ha
mi^2	square miles	2.59	square kilometers	km^2
		VOLUME		
fl oz	fluid ounces	29.57	milliliters	m
gal	gallons	3.785	liters	L
ft^3	cubic feet	0.028	cubic meters	L
yd^3	cubic yards	0.765	cubic meters	m^3
	NOTE: volumes greater than 1000 L shall be shown in m^3			m^3
		MASS		
oz	ounces	28.35	grams	g
lb	pounds	0.454	kilograms	kg
T	short tons (2000 lb)	0.907	megagrams (or "metric ton")	Mg (or "t")
		TEMPERATURE (exact degrees)		
^oF	Fahrenheit	5 (F-32)/9 or (F-32)/1.8	Celsius	^oC
		ILLUMINATION		
fc	foot-candles	10.76	lux	lx
fl	foot-Lamberts	3.426	$candela/m^2$	cd/m^2
		FORCE and PRESSURE or STRESS		
lbf	poundforce	4.45	newtons	N
lbf/in^2	poundforce per square inch	6.89	kilopascals	kPa

APPROXIMATE CONVERSIONS FROM SI UNITS

SYMBOL	WHEN YOU KNOW	MULTIPLY BY	TO FIND	SYMBOL
		LENGTH		
mm	millimeters	0.039	inches	in
m	meters	3.28	feet	ft
m	meters	1.09	yards	yd
km	kilometers	0.621	miles	mi
		AREA		
mm^2	square millimeters	0.0016	square inches	in^2
m^2	square meters	10.764	square feet	ft^2
m^2	square meters	1.195	square yards	yd^2
ha	hectares	2.47	acres	ac
km^2	square kilometers	0.386	square miles	mi^2
		VOLUME		
mL	milliliters	0.034	fluid ounces	fl oz
L	liters	0.264	gallons	gal
m^3	cubic meters	35.314	cubic feet	ft^3
m^3	cubic meters	1.307	cubic yards	yd^3
		MASS		
g	grams	0.035	ounces	oz
kg	kilograms	2.202	pounds	lb
Mg (or "t")	megagrams (or "metric ton")	1.103	short tons (2000 lb)	T
		TEMPERATURE (exact degrees)		
^oC	Celsius	1.8C+32	Fahrenheit	^oF
		ILLUMINATION		
lx	lux	0.0929	foot-candles	fc
cd/m^2	$candela/m^2$	0.2919	foot-Lamberts	fl
		FORCE and PRESSURE or STRESS		
N	newtons	0.225	poundforce	lbf
kPa	kilopascals	0.145	poundforce per square inch	lbf/in^2

*SI is the symbol for the International System of Units. Appropriate rounding should be made to comply with Section 4 of ASTM E380. (Revised March 2003)

ACKNOWLEDMENTS

The authors are thankful to the Southern Plains Transportation Center (SPTC) and the Oklahoma Department of Transportation (ODOT) for providing financial support for this study. The authors acknowledge and thank Richard Steger and Ingevity for their continuous support and assistance throughout the study. Material donations from Silver Star Construction Co., Dolese Bros. Co., Martin Marietta, Hanson Aggregates WRP Inc, Lion Oil Co., Asphalt Terminals & Transportation LLC, Valero Ardmore Refinery and ArrMaz are gratefully acknowledged. The authors also want to thank Ms. Shivani Rani and Mohammad Ashiqur Rahman for their help with material collection and laboratory testing. The authors are grateful to Dr. Edgar O'Rear for his valuable suggestions and comments during this study. The authors offer special thanks to Kenneth Hobson for his great help and cooperation throughout the study.

Special thanks are extended to Mr. Michael Schmitz (Mike) for his technical support in the laboratories. The authors are also grateful to Molly Smith and Margaret Vennochi for their administrative assistance in this project.

DEVELOPMENT OF A SFE DATABASE FOR SCREENING OF MIXES FOR MOISTURE DAMAGE IN OKLAHOMA

Final Report

SPTC15.2-19

December 31, 2019

Prepared by

Syed Ashik Ali, Ph.D. Candidate[1]

Rouzbeh Ghabchi, Ph.D.[1]

Musharraf Zaman, Ph.D., P.E.[1]

Rifat Bulut, Ph.D.[2]

[1]School of Civil Engineering and Environmental Science

The University of Oklahoma

202 W. Boyd, Street, CEC 334

Norman, Oklahoma 73019

[2]School of Civil and Environmental Engineering

Oklahoma State University

Stillwater, OK 74078

Submitted to

Southern Plains Transportation Center

201 Stephenson Pkwy, Suite 4200,

Norman, OK 73019

TABLE OF CONTENTS

LIST OF TABLES

LIST OF FIGURES

EXECUTIVE SUMMARY

With recent developments in testing equipment, test methods and studies focused on performance testing, asphalt mix design methods are moving increasingly from empirical to mechanistic. In spite of these developments, the moisture-induced damage potential of asphalt mixes is generally evaluated using the retained indirect tensile strength ratio (TSR) test or from the stripping inflection point (SIP) in the Hamburg wheel tracking (HWT) test. Although widely used as indicators of moisture-induced damage potential, neither of these tests directly addresses the mechanisms governing stripping of asphalt pavements. A mechanistic approach is needed for screening of asphalt mixes at the design stage to combat moisture-induced damages of pavements that cost millions of dollars annually. According to recent studies, the Surface Free Energy (SFE) characteristics of asphalt mixes can be used effectively to quantify bond strength and debonding of binder-aggregate system in presence of water. In this study, unmodified and polymer-modified asphalt binders from four different sources were collected. Different additives, such as warm mix asphalt (WMA) additive, anti-stripping agent (ASA), polyphosphoric acid (PPA) and reclaimed asphalt pavement (RAP) were mixed with the binder. The SFE components of the binder blends were determined using dynamic Wilhelmy plate (DWP) and sessile drop (SD) test methods under RTFO-aged and PAV-aged conditions. Also, aggregates from five different sources of Oklahoma were collected and the SFE components were determined using universal sorption device (USD) and sessile drop (SD) test. Furthermore, chemical analyses of the blended binders and aggregates were conducted to understand the effects of chemical compositions on the SFE components. Asphalt mixes consisting of WMA additive, ASA, PPA and RAP were produced in the laboratory for moisture-induced damage evaluation using Hamburg wheel tracking (HWT), indirect tensile strength (IDT) and Louisiana semi-circular bend (LA-SCB) tests. Correlations between the moisture-induced damage performance parameters from laboratory performance tests and the SFE technique were also investigated. From this study, SFE technique was found to be a useful tool to screen asphalt mixes for moisture-induced damage. The effect of the addition of different additives on binders' SFE components were observed to vary with binder types and sources. Also, from SFE technique, granite and rhyolite aggregates were found to exhibit high and limestone aggregates exhibited low moisture-induced damage potential when used in an asphalt mix. The LA-SCB test with MIST conditioning exhibited potential to be used as an alternative method to conventional moisture-induced damage test. The results of this study were included in an easy-to-use interactive database that can be readily used by designers and

others for selection of materials and screening of mixes for moisture-induced damage. As a part of this project, a workshop was organized to train personnel from ODOT and private sectors on this innovative and cost-effective mechanistic approach. The findings of this study and the SFE database will be extremely helpful to DOTs as well as the private sector to combat moisture-induced damage in Oklahoma.

1. INTRODUCTION

1.1. Background

Moisture-induced damage is one of the major distresses which contributes to the significant premature deterioration of asphalt pavements. The loss of strength and durability of asphalt mixes due to loss of bond between aggregate and binder in presence of moisture is generally known as moisture-induced damage (Harvey and Lu, 2005; Masad et al., 2006; Bhasin et al., 2007b). Although the effect of moisture on the performance of asphalt pavement was first recognized in the early 1930s, it was not considered a major issue until early 1960s (Caro et al., 2008a; Abuawad et al., 2015). Generally, moisture-induced damage is not a failure mode by itself (Abuawad et al., 2015). However, it can lead to serious distresses in asphalt pavements such as bleeding, particle degradation and disintegration, potholes, shoving, rutting and cracking (Wasiuddin et al., 2007b; Caro et al., 2008b). State Departments of Transportations (DOTs) spend significant amounts of resources to maintain and reconstruct pavements subjected to moisture-induced damage (Caro et al., 2008a; Abuawad et al., 2015).

The evaluation of moisture-induced damage is a complex problem (Wasiuddin et al., 2007b; Abuawad et al., 2015). This phenomenon starts with the transport of moisture into the pavement which subsequently leads to pavement deterioration due to the loss of either cohesive or adhesive bonds or both (Wasiuddin et al., 2007b; Caro et al., 2008b). Loss of adhesion, also known as stripping, is generally caused by breaking of adhesive bond between the aggregate and the binder in the presence of water. However, loss of cohesion generally refers to softening of the binder due to the effect of moisture (Wasiuddin et al., 2007b; Abuawad et al., 2015). From a mechanistic point of view, the moisture-induced damage can be assessed by evaluating the bond strength between binder and aggregate, in presence of moisture. A better resistance to moisture-induced damage can be ensured by improving the adhesion bond in the binder-aggregate system (Harvey and Lu, 2005; Masad et al., 2006).

The first effort to quantify the moisture-induced damage was reported in the late 1960s through visual inspection (Caro et al., 2008b). Over the past few decades, a number of empirical test methods were developed to evaluate this phenomenon (Caro et al., 2008a; Caro et al., 2008b). Recently, modified Lottman test, indirect tensile strength ratio (TSR), resilient modulus ratio, Marshall stability ratio, stripping inflection point (SIP) from Hamburg wheel tracking (HWT) test and fracture energy ratio have been used for evaluating the moisture-induced damage

potential of asphalt mixes (Bagampadde et al., 2006; Gorkem and Sengoz, 2009; Ghabchi et al., 2015; Mirzababaei, 2016). However, none of these test methods does not appear to address the failure mechanisms governing the moisture-induced damage of asphalt pavements and does not correlate well with field performance (Caro et al., 2008b).

A number of recent studies have used the thermodynamic theory or adhesion by applying the surface free energy (SFE) approach to mechanistically quantify the adhesion between aggregate and binder (Bhasin and Little, 2006; Bhasin et al., 2006; Hefer et al., 2006; Bhasin, 2007; Bhasin et al., 2007a; Bhasin et al., 2007b; Wasiuddin et al., 2007b; Wasiuddin et al., 2008; Buddhala et al., 2011; Ghabchi et al., 2013). Also, the SFE approach was used successfully to evaluate the changes in the moisture-induced damage potential of asphalt mixes containing different additives (Wasiuddin et al., 2007b; Moghadas Nejad et al., 2012; Arabani and Hamedi, 2014).

The physical and chemical properties of the asphalt binder and aggregate are known to affect the moisture-induced damage potential of the asphalt mix (Curtis et al., 1992). The chemical characteristics of the binder and additives are an important factor in determining the strength of the binder-aggregate bond. Several chemical analysis techniques are currently being used to characterize the chemical components of asphalt binder and aggregate (Le Guern et al., 2010; Hossain et al., 2012; Hesp and Shurvell, 2013). These techniques were found to provide important and useful information about the chemical properties of asphalt binder and aggregates in a relatively short period of time. As the use of different chemicals and rejuvenators such as warm mix asphalt (WMA) additives, poly-phosphoric acid (PPA), anti-stripping agents (ASA) and reclaimed asphalt pavement (RAP) in asphalt mixes continues to increase, the mechanistic evaluation of the moisture-induced damage potential becomes even more important.

1.2. Objectives

In this study, the moisture-induced damage potential of asphalt binders-aggregate systems and asphalt mixes was evaluated using thermodynamic approaches, chemical properties and mechanical tests. The effects of the addition of different additives on the moisture-induced damage potential of asphalt mixes were investigated. As an outcome of this study, a more mechanistic based test method is proposed to evaluate moisture-induced damage of asphalt mixes. The specific objectives of this study were as follows:

i. Evaluate the effect of WMA additive, antistripping agent, RAP binder, and polyphosphoric acid on the SFE components of commonly used unmodified and polymer-modified asphalt binders in Oklahoma;
ii. Evaluate the effect of oxidation and aging on moisture-induced damage potential by determining the SFE components of short-term and long-term aged binders;
iii. Determine the SFE components of commonly used aggregates in Oklahoma and evaluate the effect of the addition of lime on the SFE components;
iv. Using SFE technique, evaluate the compatibilities between binders' containing different types of additives with different types of aggregates;
v. Develop an easy-to-use and interactive SFE database including aggregates, asphalt binders, RAP, WMA, PPA, ASA, and lime;
vi. Conduct elemental analyses of asphalt binders and aggregates and determine correlations between chemical compositions and SFE components;
vii. Prepare asphalt mixes with different types of additives and conduct TSR, HWT and SCB tests on laboratory-compacted mixes and correlate the results with the SFE data;
viii. Evaluate the SCB test's suitability as a simple test method for screening of asphalt mixes for moisture-induced damage;
ix. Conduct a technology transfer workshop for DOT and private sector personnel and others to increase awareness of mechanistic approaches for evaluation of moisture-induced damage of asphalt mixes and availability of the interactive database.

1.3. Scope of the Work

In this project, effects of RAP, WMA, PPA, ASA, and aging (short-term and long-term) on the moisture-induced damage potential of asphalt mixes were studied by using the SFE technique. Also, elemental analyses of asphalt binders and aggregates were conducted. The data obtained from the elemental analysis are expected to provide valuable information about the surface energy characteristics of the materials. In addition, conventional tests, namely TSR (AASHTO T 283) and HWT (AASHTO T 324) were conducted on the asphalt mixes containing binders and aggregates from local sources. Furthermore, moisture-induced damage potential of asphalt mixes was evaluated by fracture energy approach using semi-circular bend (SCB) test (ASTM D 8044). Correlations between different mechanical testing and surface free energy parameters were developed to better understand the mechanisms of moisture-induced damage in asphalt pavements.

2. LITERATURE REVIEW

2.1. Theories Related to Moisture-induced Damage of Asphalt Pavements

The moisture-induced damage is defined as the deterioration of mechanical properties of asphalt mixes due to the presence or intrusion of moisture in a liquid or vapor state (Caro et al., 2008a). According to Caro et al. (2008a), moisture-induced damage is a two-step mechanism: the first step involves infiltration of the moisture into the pavement either in liquid or vapor state and reaching the binder-aggregate interface. The three primary modes of transport through which moisture can reach the binder-aggregate interface are infiltration of surface water, capillary rise of subsurface water and permeation or diffusion of water vapor (Masad et al., 2007; Caro et al., 2008a). The second step includes the response of the system i.e., adhesive and/or cohesive failures and reduction in the structural capacity of the pavement. Five different theories have been proposed by researchers to explain the adhesion bonding in binder-aggregate system: weak boundary layer theory, electrostatic theory, chemical bonding theory, mechanical bonding theory and thermodynamic theory (Hefer et al., 2005; Caro et al., 2008a). The details associated with the mechanisms and capabilities of these theories to evaluate moisture-induced damage on a quantitative basis were explained by Hefer et al. (2005). Caro et al. (2008a) presented a comprehensive literature review on the damage mechanisms using these theories. According to the weak boundary layer theory, adhesive failure is associated with the presence of an interface of low cohesive strength which can result from the presence of dust in the aggregate surface and/or dissolution of surface complexes in the presence of water. In the electrostatic theory, the adhesive strength of an asphalt mix is explained using coulombic forces. The interactions between aggregate surface and liquid media with dissolved ions were reported to be important to explain moisture-induced damage. The chemical bonding theory evaluates the binder-aggregate adhesion on a microscopic scale. According to this theory, the adhesion bond is assumed to result from the chemical reaction between binder and aggregate and formation of a new material at their interface. This mechanical bonding theory assumes that the adhesion bonding is caused by forcing asphalt binder into the cavities, pores and asperities of the surface of the aggregate and producing a physical interlock. The surface chemistry of the binder and aggregate was found to dominate the adhesive bond strength of a given binder-aggregate system. The thermodynamic theory using the surface free energy concept was reported to have the potential to quantify the adhesion of a binder-aggregate system (Bhasin et al., 2007b; Caro et al., 2008a). Also, the compatibility of various binder-aggregate combinations can be assessed using the thermodynamic theory. The details of the thermodynamic theory are

presented in the subsequent sections. However, Caro et al. (2008a) concluded that all the thermodynamic, chemical, physical and mechanical components are needed to be considered during modelling and characterizing moisture-induced damage in asphalt pavements.

2.2. Current Practices of Evaluating Moisture-induced Damage

The evaluation of moisture-induced damage as a complex phenomenon is a challenging task for transportation agencies (Abuawad et al., 2015). Several test methods have been developed and improved over the last few decades to characterize moisture-induced damage potential of asphalt mixes (Caro et al., 2008a; Caro et al., 2008b). However, many of these methods are empirical and have several drawbacks, such as inability to simulate field condition, dependency on moisture conditioning process, and poor correlation with field performance (Caro et al., 2008b; Abuawad et al., 2015). Previously, moisture-induced damage tests were classified based on the state of mix (loose or compact), mode of loading, moisture conditioning process and scale of performance measure. Caro et al. (2008b) introduced a new classification with three parts based on the generic nature of the test methods. The three parts of this classification system are subjective quantification, quantification using performance index and ratio of a parameter for dry and moisture-conditioned specimens. Among these three parts, the use of parametric ratio between dry and wet conditioned specimens from a particular test is commonly used to characterize moisture-induced damage by state DOTs. Moisture conditioning in the laboratory is an integral part of this type of testing. The purpose of laboratory moisture conditioning is to simulate the environment and moisture affecting the performance of an asphalt mix in the field.

The TSR test using a freeze thaw cycle (AASHTO T 283) and submerged HWT test are the most commonly used tests among DOTs (Abuawad et al., 2015). In a TSR test, the average tensile strength of dry specimens from an indirect tensile strength test is compared with the average tensile strengths of moisture-conditioned specimens. According to the AASHTO T 283 test method (also known as Lottman test), a saturated compacted specimen (with a saturation between 70% to 80%) is kept at -18 °C for 16 hours followed by a thawing cycle by keeping it at 60 °C for 24 hours to simulate moisture conditioning. In a HWT test, stripping inflection point (SIP) is determined from rutting curve to evaluate moisture-induced damage. The SIP is defined as the number of wheels passes on the rutting curve at which a sudden increase in rut depth occurs. Graphically, the SIP is represented as the intersection of the fitted lines that

characterize the creep phase and the stripping phase on the rutting curve (Figure 2.1). A higher value of SIP for a mix corresponds to a lower moisture-induced damage potential.

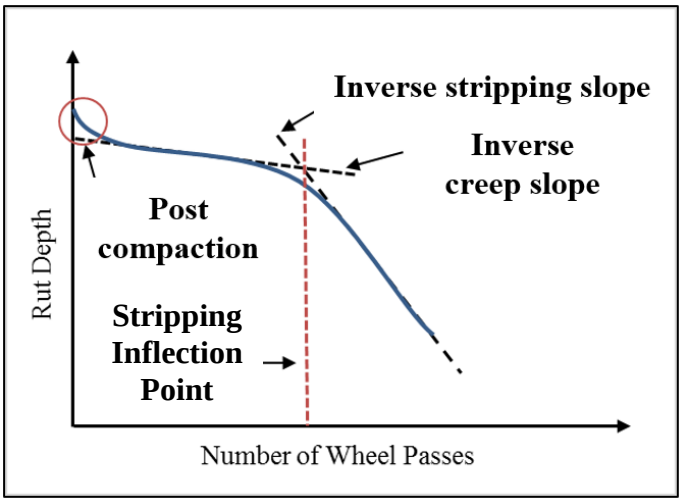

Figure 2.1 Determination of stripping inflection point from Hamburg wheel tracking test

A number of other tests and moisture conditioning procedures are also being investigated by researchers and the asphalt industry (Gorkem and Sengoz, 2009; Liu et al., 2014; Tarefder and Ahmad, 2014; LaCroix et al., 2016). For example, Gorkem and Sengoz (2009) used the Nicholson stripping test and the modified Lottman test to evaluate the effect of the addition of hydrated lime, elastomeric and plastomeric polymers on the moisture-induced damage potential of loose and compacted asphalt mixes. Analysis of microscopically captured images using a software was found to improve the estimation of degree of stripping. Liu et al. (2014) conducted a study to evaluate the moisture-induced damage of aggregates and binders using five empirical test methods, namely static immersion test, rolling bottle test (RBT), boiling water test (BWT), total water immersion test, and the ultrasonic method. Among the different test methods, the BWT and the RBT were observed to be the most sensitive while the static immersion test and the ultra-sonic test were found to be the least sensitive. The moisture-induced damage potential of asphalt mixes due to two different wet conditioning methods, namely, moisture-induced sensitivity testing (MIST) and AASHTO T 283 method was evaluated and the relationship with permeability was determined by Tarefder and Ahmad (2014). The indirect tensile strength tests conducted on samples conditioned according to the AASHTO T 283 method were found to result in reduced TSR values with an increase in permeability. However, the TSR values of samples conditioned in a MIST equipment were found to be unaffected by permeability. Mirzababaei (2016) used different conventional test methods,

namely AASHTO T 283 (modified Lottman test), resilient modulus ratio (RMR), Marshall stability ratio (MSR), fracture energy ratio (FER) and boiling water to determine the effect of zycotherm® on the moisture-induced damage potential of the tested asphalt mixes. LaCroix et al. (2016) used both AASHTO T 283 and MIST to condition their samples and tested them for moisture-induced damage. It was found that the current AASHTO T 283 method affects the adhesive strength of the binder and the aggregate whereas the MIST affects the cohesive strength. It was suggested that a combination of both conditioning methods be used to ensure evaluation of the relative contributions of adhesion and cohesion mechanisms to moisture-induced damage. Vargas-Nordcbeck et al. (2016) used the modified Lottman indirect tension test procedure with different conditioning levels and found that an increase in the number of conditioning cycles was required to accurately simulate field performance. Also, the use of simple performance tests was found to serve as an alternative method for the evaluation of moisture-induced damage in asphalt mixes.

Currently there is no general agreement on a single test and moisture conditioning method for evaluating moisture-induced damage. Also, conventional test methods evaluate the performance of mixes as a whole and do not consider the contribution of constituent materials i.e., properties of asphalt and aggregate (Bhasin, 2007). Therefore, emphasis should be given on the development of efficient tools to assess compatibility between aggregates and binders to resist moisture-induced damage (Bhasin, 2007; Caro et al., 2008b).

2.3. Thermodynamic Approach of Evaluating Moisture-induced Damage

Thermodynamic theory (also known as adsorption theory) is one of the most widely used concepts in adhesion science (Hefer et al., 2005). According to this theory, the physio-chemical adhesion between two materials is a thermodynamic phenomenon and a function of surface free energies of those materials. Generally, molecules in bulk of a material are surrounded by other molecules and have higher bond energy than the molecule on the surface. Therefore, work needs to be done to bring the molecule from the bulk to surface, i.e., to create a new surface. The surface free energy (SFE) of a material is generally defined as the work required to increase the surface of a material by a unit area under vacuum (Van Oss et al., 1988). According to the Good-Van Oss-Chaudhury theory, the SFE of a material can be divided into three independent components, namely a non-polar or Lifshitz-van der Waals component, a monopolar acidic component, and a monopolar basic component. These components can be obtained by measuring the work of adhesion of that material with other liquids or vapors (Van

Oss et al., 1988). The total SFE of an asphalt binder/aggregate can be expressed by Equations (1) and (2).

$$\Gamma_A^{Total} = \Gamma_A^{AB} + \Gamma_A^{LW} \quad (1)$$

$$\Gamma_A^{AB} = \sqrt{(\Gamma_A^+ \Gamma_A^-)} \quad (2)$$

where,

Γ^+ = Lewis acid component;

Γ^- = Lewis base component;

Γ^{LW} = Lifshitz-van der Waals component;

Γ^{Total} = total SFE component.

For convenience, subscripts *A, L, S, and W* are used to represent asphalt binder, probe liquids, aggregate (stone) and water, respectively.

The tendency of a binder and an aggregate to bind together or form an binder-aggregate system in dry condition can be represented by the work of adhesion ($W_{A/S}$). The $W_{A/S}$ of an binder-aggregate system can be calculated from Equation (3) using the SFE components of the binder and aggregate. Generally, a higher $W_{A/S}$ value indicates a stronger bond between a binder and an aggregate under dry condition.

$$W_{AS} = 2\sqrt{(\Gamma_A^{LW} \Gamma_S^{LW})} + 2\sqrt{(\Gamma_A^+ \Gamma_S^-)} + 2\sqrt{(\Gamma_A^- \Gamma_S^+)} \quad (3)$$

In presence of water, the amount of work required for debonding of the binder from the aggregate surface is defined as work of debonding (W_{ASW}^{wet}) and can be determined using Equation (4).

$$W_{ASW}^{wet} = \Gamma_{AW} + \Gamma_{SW} - \Gamma_{AS} \quad (4)$$

where,

Γ_{AW} = interfacial energy between binder and water;

Γ_{SW} = interfacial energy between aggregate and water;

Γ_{AS} = interfacial energy between binder and aggregate.

Generally, the value of W_{ASW}^{wet} is negative indicating an overall reduction in free energy of the system due to debonding of the asphalt binder from aggregate interface in presence of

water. Therefore, debonding of asphalt binder from aggregate is a thermodynamically favorable phenomenon (Bhasin et al., 2007b).

The interfacial energy between materials *i* and *j* can be determined using Equation (5).

$$\Gamma_{ij} = \Gamma_i + \Gamma_j - 2\sqrt{(\Gamma_i^{LW}\Gamma_j^{LW})} - 2\sqrt{(\Gamma_i^{+}\Gamma_j^{-})} - 2\sqrt{(\Gamma_i^{-}\Gamma_j^{+})} \quad (5)$$

The tendency of the binder to spread and coat the surface of the aggregate can be determined using the wettability or spreading coefficient ($S_{A/S}$). The spreading coefficient is generally a positive value. A higher value of spreading coefficient is required to ensure a better coating of the binder to the aggregate surface (Buddhala et al., 2011). The $S_{A/S}$ can be calculated using Equation (6).

$$S_{A/s} = \Gamma_S - \Gamma_{AS} - \Gamma_A \quad (6)$$

The details of the thermodynamic concepts and surface free energy theories can be found in Hefer et al. (2005) and Bhasin (2007).

A number of methods are currently available to determine the SFE components of binder and aggregate. For binder, the SFE components can be determined by measuring the contact angle of the binder with different probe liquids of known SFE components. Hefer et al. (2006) introduced the dynamic Wilhelmy plate (DWP) method of contact angle measurement as well as data analysis technique for calculating surface free energy. In a DWP test, contact angles are measured indirectly by immersing a plate uniformly coated with a thin layer of binder into a liquid and calculating the angle from the measured forces. This is a dynamic contact angle measurement technique as the plate is in motion and provides two different contact angles known as advancing (Figure 2.2 (a)) and receding contact angles (Figure 2.2 (b)). The contact angle between the plate and liquid is measured considering force equilibrium during the test using Equation (7).

$$Cos\theta = \frac{\Delta F + V_{im}(\rho_L - \rho_{air}g)}{P_t\gamma_L} \quad (7)$$

where,

θ = contact angle between the plate and liquid;

ΔF = difference in force;

V_{im} = volume of coated plate immersed in water;

ρ_L = density of water;

ρ_{air} = density of air;

P_t = perimeter of the coated plate;

γ_L = the total surface energy of liquid.

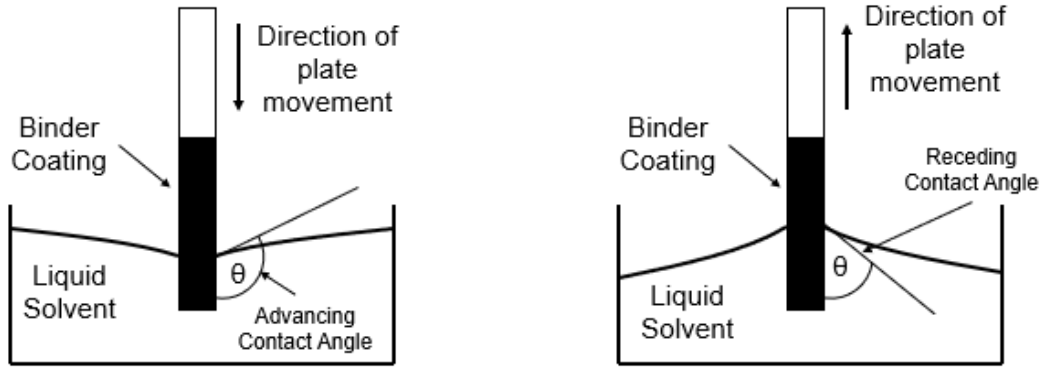

(a) (b)

Figure 2.2 Dynamic Wilhelmy plate test method for (a) advancing contact angle and (b) receding contact angle

The SFE components of binder can be calculated by solving equation (8) using contact angle values measured with three different probe liquids of known SFE components.

$$\Gamma_L^{Total}(1+cos\theta) = 2(\Gamma_A^{LW}\Gamma_L^{LW} + \Gamma_A^{+}\Gamma_L^{-} + \Gamma_A^{-}\Gamma_L^{+}) \qquad (8)$$

Hefer et al. (2006) and Bhasin (2007) found that the advancing contact angles correlated well with the theoretical requirements to determine surface free energy components. Also, the selection of appropriate probe liquids was observed to be important for conducting DWP test.

The theory and methodology for using sorption measurements to determine the surface energy components of aggregates were presented by Bhasin and Little (2007). According to Bhasin and Little (2007), the SFE components of aggregate can be calculated from spreading pressures of the probe vapors on the aggregate surface. The reduction in surface energy due to the adsorption of a probe vapor is known as the spreading pressure of that probe vapor on the aggregate surface. The spreading pressures can be determined by obtaining a full adsorption isotherm of the vapor on the aggregate. The equilibrium spreading pressure (π_e) can be

calculated based on the mass absorbed at maximum saturated vapor pressure using Equation (9).

$$\pi_e = \frac{RT}{MA}\int_0^{Po}\frac{n}{p}dp \qquad (9)$$

where,

R = universal gas constant;

T = temperature,

n = mass absorbed per unit mass of aggregate at a vapor pressure *p*;

M = molecular weight of the probe vapor;

P_0 = maximum saturation vapor pressure;

A is the specific surface area of the aggregate.

The interfacial work of adhesion and π_e can be related using Equation (10). The work of adhesion, spreading pressure and the SFE components can be related using Good-van-Oss-Chaudhury (GVOC) theory using Equation (11).

$$W_{SL} = \pi_e + 2\gamma_{LV} \qquad (10)$$

$$\pi_e + 2\gamma_{LV} = 2\sqrt{(\Gamma_S^{LW}\Gamma_L^{LW})} + 2\sqrt{(\Gamma_S^{+}\Gamma_L^{-})} + 2\sqrt{(\Gamma_S^{-}\Gamma_L^{+})} \qquad (11)$$

Three SFE components of solids are the three unknowns in Equation (11). The SFE components of aggregate can be determined by arranging a set of at least three equations using spreading pressures with three different probe vapors.

2.4. Studies Related to Thermodynamic Approach

A number of studies have used the surface free energy components of aggregates and binders to evaluate the moisture-induced damage potential of asphalt mixes. Bhasin et al. (2006) evaluated a total of 16 field mixes from Texas, Ohio, Kansas, and Nevada and classified using qualitative inspection of pavements and field cores as well as mechanical testing of asphalt mix. The results were compared with the bond energy parameters from SFE technique. The surface free energy measurements and concomitant bond energy calculations were found to be an effective tool to identify compatible binder-aggregate pairs.

The effect of different types of modifications on the surface free energy components of the binder was evaluated by Bhasin et al. (2007a). The changes in surface free energy due to the addition of polymers and anti-stripping agent and oxidative aging were determined and different energy parameters were calculated to correlate with the performance of the asphalt mixes. In another study, Bhasin and Little (2007) compared the surface free energy characteristics of five aggregates of different chemical compositions. The specific surface area of the aggregate determined using standard nitrogen sorption device was found to agree well with the areas obtained using the sorption equipment. It was found that the base component of the aggregate was much higher than the acid component and acted as a primary contributor to the differences in the compatibility ratio with any given binder.

Also, Bhasin et al. (2007b) combined the effect of work of adhesion and work of debonding and proposed a single valued parameter to evaluate moisture damage. The energy ratio parameter can be calculated using Equation (12).

$$ER_1 = \left|\frac{W_{AS}}{W_{ASW}^{wet}}\right| \qquad (12)$$

To consider the effect of the wettability, a modified version of Equation (11) was also proposed by Bhasin et al. (2007b). The parameter is known as ER_2 and can be calculated using Equation (13).

$$ER_2 = \left|\frac{W_{AS}-W_{AA}}{W_{ASW}^{wet}}\right| \qquad (13)$$

where W_{AA} is the cohesive bond energy of the asphalt binder. However, Bhasin et al. (2007b) recommended to use all the parameters, such as work of adhesion, work of debonding, wettability and energy ratio to evaluate moisture-induced damage potential of asphalt mixes.

Wasiuddin et al. (2007b) evaluated the effect of antistrip additives on asphalt binders using the SFE technique. A chemical model was proposed to explain the change in SFE components with the addition of antistrip additives. In a different study, thermal degradation of the antistripping agent as a result of aging of binder was evaluated by Wasiuddin et al. (2007a) using the same technique. Also, the influence of different warm mix asphalt additives on the moisture-induced damage potential of binders was studied and reported by Wasiuddin et al. (2008).

Arabani and Hamedi (2010) evaluated the effects of polyethylene polymer coating on aggregates on the basis of the SFE characteristics of aggregates. It was observed that the

polyethylene polymer coating treatment brought the total SFE of aggregates to the same level although they exhibited significant differences before treatment. In another study, Arabani and Hamedi (2014) used surface free energy (SFE) concept to evaluate the effect of liquid antistrip additives. A good correlation was observed between the moisture-induced damage results from dynamic modulus test and SFE technique. Alvarez et al. (2012a) evaluated the effect of filler on binder-aggregate interfaces of asphalt mixes based on surface free energy approach. In a different study, asphalt rubber-aggregate and polymer modified binders-aggregate interfaces were evaluated using the same procedure (Alvarez et al., 2012b).

The cohesion and adhesion of asphalt mastic were also studied by Tan and Guo (2013). Sessile drop and column wicking method were used to measure the SFE components of asphalt and fillers, respectively. The van der Waals force of surface free energy was found to play an important role in the cohesion and adhesion of asphalt mastic. Ghabchi et al. (2014) evaluated the effect of the addition of different amounts of RAP to the asphalt binders on their surface energies. The compatibilities of different amounts of RAP blended binders with six different types of aggregates were evaluated using wettability, work of adhesion, work of debonding and energy ratio parameters. Zhang and Luo (2017) conducted adsorption tests on selected aggregates using a gravimetric sorption analyzer. From the adsorption results, the surface pores of the aggregates were characterized as micro-pores, meso-pores and macro-pores according to their size. The measured adsorption isotherms were modeled using different isotherm models such as Toth model (Tóth, 1981), Dubinin-Astakhov (DA) model (Langmuir, 1918) and the modified Brunauer-Emmett-Teller (BET) model (Brunauer et al., 1938). The DA model was identified to be the most appropriate model and was able to address the volume filling of micropores and the adsorption in mesopores and macro-pores.

2.5. Effect of Chemical Compositions of Asphalt Binder and Aggregate on the Moisture-induced Damage

The interaction between the asphalt and aggregate in a mix depends on the chemistry and physical properties of both the materials (Curtis et al., 1992). Asphalt binder is a complex material and the complexity gets more critical with the addition of additives (Hossain et al., 2012). To understand the effect of additives on the binder's performance properties, it is important to examine the interaction between additives and the binder constituents. Hossain et al. (2012) found reasonable agreement between rheological and chemical properties using spectroscopic analysis. It was observed that an increase in stiffness due to the addition of WMA

additives were resulted from an increase in aliphatic content of the binder. Also, an increase in the nitrogen content in the surface composition of the binder was reported as a result of the addition of an antistripping agent. According to Wei et al. (2014), understanding the relationship between chemical composition and the surface free energy of asphalt binder is important for assessment of adhesive bond between asphalt and aggregate. It was found that the saturates, aromatics, wax or asphaltenes had negative influence whereas, resins exhibited positive influence on the surface free energy. Different elemental contents such as C%, N%, and S% exhibited a good correlation with the surface free energy of the binder. Tarefder and Zaman (2009) evaluated the effect of the chemical functional group on the moisture-induced damage potential of the asphalt binders using atomic force microscopy (AFM). The adhesion forces between asphalt and silicon-nitride (resembles aggregate) and cohesion forces between asphalt molecules and carboxyl (-COOH), methyl (-CH3), and hydroxyl (-OH) functional groups were determined by probing the asphalt surface with chemically functionalized tips. It was observed that the addition of 3% polymer to the binder exhibited the highest adhesion/cohesion forces in wet asphalts and hence reduced moisture-induced damage. Also, the interaction with PPA is very complex and needs different approaches to explain pertinent physical and chemical phenomena (Fee et al., 2010). Baumgardner et al. (2005) analyzed the chemical compositions of PPA-modified binders using different chemical analysis tools and concluded that the mechanism of PPA action depends on the constituents of the base binder. However, a general mechanism reported by Fee et al. (2010) is based on the notion that the PPA reacts with various functional groups in the binder and breaks the asphaltene agglomerates into smaller fractions and disperse them in the maltene phase. Those smaller asphaltene units form long-range networks and affect the rheology and physical characteristics of the binder.

Recently, researchers are using various chemical analysis tools such as X-Ray fluorescence (XRF), Fourier transform infrared (FTIR) spectroscopy, differential scanning calorimetry, nuclear magnetic resonance (NMR), AFM and X-ray photo electron spectroscopy (XPS) to analyze the chemical constituents of asphalt binder (Le Guern et al., 2010; Hossain et al., 2012; Hesp and Shurvell, 2013). For example, Reinke and Glidden (2010) used the XRF technique to detect the amount of phosphorus in the binder and to quantify PPA content. Also, the XRF has been used to ensure the quality of asphalt binder by conducting elemental analysis (Soleimani et al., 2009; Hesp and Shurvell, 2010; Hesp and Shurvell, 2013). Mouillet et al. (2008) used infrared microscopy to investigate the chemical mechanisms of aging of polymer-modified binders by continuous oxidation. Also, FTIR spectroscopy has been used to investigate

the evolution of the binder structural and functional grouping during aging (Lamontagne et al., 2001).

In the present study, XRF and FTIR techniques were used to determine the effect of additives on surface free energy characteristics of binders. The acidity of a binder is known to have important influence on its bond strength with the aggregates (Wasiuddin et al., 2007b; Ghabchi et al., 2013). The acidity of binder from total acid number (TAN) test was used to correlate with the SFE components of the binders.

2.6. Effect of Different Additives on the Moisture-induced Damage

2.6.1. WMA Additives

Recently, the use of WMA for construction of pavements has been increasing to reduce energy consumption, preserve the environment and ensure sustainable development. The WMA technologies are reported to reduce the asphalt production temperature by 2 to 38 °C than that of hot mix asphalt (HMA), which results in a significant savings of fuel costs (D'Angelo et al., 2008; West et al., 2014). Three categories of WMA technologies, namely, asphalt foaming, organic additives and chemical additives are currently available to the asphalt industry (West et al., 2014). At present, a number of chemical additives are available to help coat the aggregate with binder at a lower mixing temperature. Moisture-induced damage susceptibility of WMA is a major concern for pavement engineers as low mixing and compaction temperatures can cause insufficient drying of aggregates, which may result in moisture-induced damage in the asphalt mix (Xiao et al., 2010; Khodaii et al., 2012). A number of studies have reported an increase in moisture-induced damage potential for WMA mixes from laboratory tests (Prowell et al., 2007; Ghabchi et al., 2013). For example, Wasiuddin et al. (2008) evaluated the effect of the addition of Sasobit® and Aspha-min® additives using the SFE approach. Sasobit® was found to reduce the adhesion between asphalt binders and aggregates whereas Aspha-Min® did not exhibit any specific trend. Ghabchi et al. (2013) reported an increase in the wettability of the asphalt binder over the aggregates with the addition of Sasobit®, Advera®, and Evotherm® additives. Also, WMA-modified binders exhibited a higher magnitude of work of adhesion and a lower magnitude of work of debonding of the binder-aggregate system than that of the neat binder.

2.6.2. Liquid Antistripping Agent

Liquid antistripping agents are typically surface-active agents (surfactants) and are widely used by the pavement industries (Taylor and Khosla, 1983). Antistripping agents are

amines or chemical compounds containing amine which are strongly basic in nature (Tunnicliff and Root, 1983). The amines have a long chain hydrocarbon portion and an amine group. The amine group of the antistripping agent reacts with aggregate and forms ammonium salts whereas the hydrocarbon portion is directed into the binder. As a result, the hydrocarbon chain acts as a bridge between the binder and aggregate surface and improves bonding (Wasiuddin et al., 2007a). Aksoy et al. (2005) evaluated the effect of two liquid heat stable anti-stripping agents using Marshall stability ratio and TSR tests. The additives were found to reduce the level of moisture-induced damages in asphalt mixes. Wasiuddin et al. (2007b) added two amine-based liquid antistrip additives to binders and evaluated moisture-induced damage potential using SFE technique. The basic antistrip additives were found to reduce the acid components and increase the basic components of SFE of the asphalt binder. Arabani and Hamedi (2014) used dynamic modulus test and found out that the wet to dry ratio of dynamic modulus increased with the addition of antistripping agent. Recently, Abuawad et al. (2015) conducted several laboratory tests including modified Lottman test, wheel track test and fracture test using semi-circular bend specimens and observed that the use of antistripping agent were effective in reducing moisture damage potential. However, there is a need to study the effect of antistripping agent on the polymer-modification and aging of the binder.

2.6.3. Polyphosphoric Acid (PPA)

Asphalt binder modification has become an integral part of asphalt production to improve performance of asphalt pavements over the past few decades. The use of different types of modifiers such as polymers, crumb rubber, and polyphosphoric acid (PPA) have increased significantly with the advent of Superpave specification (Baumgardner, 2010). The use of PPA in binder modification to change the high temperature rheological properties was first reported on early 1970s (Baumgardner, 2010). A number of studies has reported increase in the high-temperature performance grade (PG) of the neat binder with negligible effect on the low-temperature properties with the addition of PPA (Baumgardner, 2010; D'Angelo, 2010; Fee et al., 2010). Also, PPA can be added to polymer-modified binder as a cross-linking agent or as a partial replacement for polymer modification (Arnold et al., 2009). One of the major concern for the PPA-modified binder is its performance in presence of moisture. Arnold et al. (2009) reported that, at a higher level of PPA modification, the sensitivity of the binder to moisture absorption increased significantly. Several studies have reported increased moisture-induced damage potential of asphalt mixes with PPA-modified binder (Orange et al., 2004; Fee et al.,

2010; Al-Qadi et al., 2014). Also, there is a need to study the effect of the addition of PPA on the moisture-induced damage potential of polymer-modified binders.

2.6.4. Reclaimed Asphalt Pavement (RAP)

Incorporating RAP in asphalt mixes is a major initiative towards the implementation of green paving technologies. According to a report by the National Asphalt Pavement Association (NAPA), more than 99% of the asphalt is being reused and recycled (NAPA 2011). The incorporation of RAP in the asphalt mix was found to reduce the fatigue life (Shu et al., 2008; Mohammad et al., 2016). Ghabchi et al. (2014) evaluated the effect of the addition of different amounts of RAP to the asphalt binder on the moisture-induced damage potential of asphalt mixes using the SFE approach. It was found that the addition of extracted RAP binder increased the acid SFE components of the binder while the base SFE components remained almost unchanged. Also, it was also observed that the moisture-induced damage potential of the binders reduced with an increase in the RAP content to the binders. In a different study, Ghabchi et al. (2016) evaluated moisture-induced damage potential using TSR test and obtained satisfactory result up to 25% RAP incorporation in asphalt mixes.

2.7. Studies Related to Semi-circular Bend (SCB) Test Method

Fracture in asphalt pavement has been historically evaluated using laboratory tests, numerical simulations, and field evaluations. Currently, a number of test method such as single edge notch beam, disc-shaped compact tension; and semi-circular bend (SCB) tests are being used to characterize fracture of asphalt mix (Wagoner et al., 2005; Li et al., 2008; Kim et al., 2012). The application of SCB test was first reported in rock mechanics to determine fracture resistance of rock material (Chong and Kuruppu, 1984). A similar concept of SCB test was applied to understand the fracture characteristics of asphalt materials using monotonic loading (Saha and Biligiri, 2016). The SCB test method has been used to characterize fatigue and low temperature fracture resistance of asphalt mixes by many researchers (Mull et al., 2002; Wu et al., 2005; Li and Marasteanu, 2010; Kim et al., 2012; Mohammad et al., 2016; Ozer et al., 2016; Saeidi and Aghayan, 2016). It was found that the SCB test is a reliable and relatively simple test method for assessment of cracking performance of asphalt mixes. Figure 2.3 (a) presents a schematic of SCB test on asphalt mix specimen. The results of the SCB test can be analyzed using linear elastic fracture mechanics principle and the fracture properties of asphalt mixes can be characterized by critical energy release rate or J-integral. The J-integral is calculated by plotting the area under the load-deformation curve until peak load against notch depths (Figure

2.3 (b)). The slope of the strain energy vs notch depth curve is considered in the calculation of J-integral using Equation (14). The mechanics behind the determination of J-integral from SCB test using specimens of different notch depths can be found in the literature (Wu et al., 2005).

$$J_c = -(\frac{1}{b})\frac{dU}{da} \quad (14)$$

where,

J_c = critical Strain energy release rate;

b = specimen width;

U = strain energy to failure;

a = notch depth.

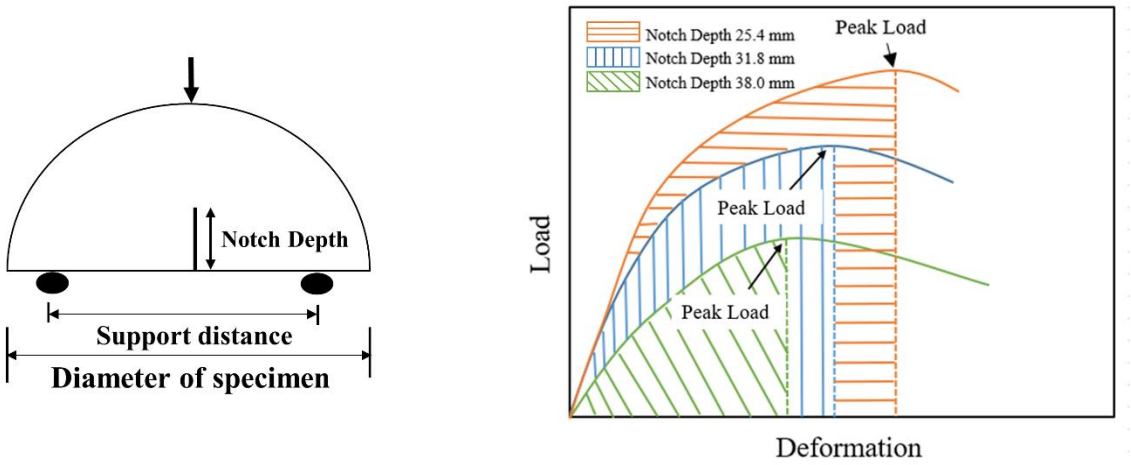

(a) (b)

Figure 2.3 (a) Schematic of a SCB test and (b) typical load vs deformation curves for specimens with different notch depths from SCB test

Wu et al. (2005) investigated the applicability of J-integral for evaluating fracture resistance of asphalt mixes. It was found that the mixes with higher tensile strengths exhibited more brittleness and less fracture resistant than those with lower tensile strengths. Also, the J-integral was found sensitive to all mix variables selected, including binder type, nominal maximum aggregate size (NMAS), and compaction effort. Kim et al. (2012) observed a good correlation between the SCB-measured J-integral and the IDT-measured toughness index (TI) values, especially for laboratory-produced mixes. A good agreement was also observed between the J-integral values and field cracking performance data. Mohammad et al. (2016) also compared the laboratory and field performances of asphalt mixes and found that the J-integral correlates well with the field data. Furthermore, specification has been developed for

SCB test for the Louisiana Department of Transportation and Development. Cooper Jr et al. (2016) developed a predictive SCB model to estimate the J-integral to use during the mix design process. As the infiltration of moisture leads to the damage of the pavement, the incorporation of fracture mechanics through SCB test are expected to better explain the mechanisms behind the moisture-induced damage phenomenon.

In this study, thermodynamic approach i.e., SFE technique was used to evaluate the effects of the addition of different additives such as WMA, PPA, ASA, and RAP on the moisture-induced damage potential of asphalt mixes. Also, the compatibility of the binder-aggregate system was evaluated based on their energy ratios obtained from SFE technique. As mentioned in previous literatures, the XRF and FTIR tests were conducted to determine the chemical compositions of the binder blends. Also, the compositions of aggregates were determined using XRF test. The results obtained from these analyses were used to explain the surface energy characteristics of the materials. In addition to asphalt binder and aggregate tests, moisture-induced damage potential of the asphalt mixes was evaluated using conventional tests, namely IDT and HWT and unconventional test, namely semi-circular bend (SCB) test. In this study, the fracture energy approach using SCB test was used to determine the moisture-induced damage potential of asphalt mixes.

3. MATERIAL AND METHODOLOGY

3.1. Material Selection, Collection and Preparation

3.1.1. Asphalt Binder

For the purpose of this study, two neat PG 64-22 binders and two polymer-modified PG 76-28 binders from different Oklahoma refineries were collected. Also, a chemical WMA additive, one type of PPA and an antistripping agent were collected from local material suppliers. Simulated RAP binder was prepared following the procedure describe by Ghabchi et al. (2014) using a pressure aging vessel (PAV). Asphalt binders were blended with the additives using a high shear mixer at 1,000 rpm for 45 minutes. To ensure consistency, the additives were blended with PG 64-22 and PG 76-28 binders at 155 °C and 170 °C, respectively. The oxidative aging of binders similar to that of mixing in the asphalt plant and compacting in the field were simulated using a rolling thin film oven (RTFO) following the AASHTO T 240 test method. Binders were then long-term aged using a pressure aging vessel (PAV) following the AASHTO R 28 method. Tests were conducted on both long term-aged and short term-aged samples. Table 3.1 presents the test matrix used in this study for asphalt binders.

3.1.2. Aggregate

Aggregates were collected from different Oklahoma quarries for determining the surface free energy and chemical components. The SFE of aggregates was measured using a universal sorption device (USD) and a sessile drop (SD) device. Elemental analysis of the aggregates was performed using XRF test. For aggregate sample preparation for USD test, the size fraction with particles larger than 2.36 mm (retaining on a No. 8 sieve) and smaller than 4.75 mm (passing a No. 4 sieve) was selected. The selected fraction of aggregates was washed several times with distilled water to obtain dust-free clean surfaces. Then the aggregates were oven-dried at 120°C for 24 hours and allowed to cool to room temperature in a desiccator sealed with silica gel, before testing. As a part of the study, the effect of lime treatment on the surface free energy of aggregate was evaluated. For lime treatment, approximately 3% water (by weight of aggregate) was added to the dried aggregate. Dry hydrated lime was then added and mixed with the aggregate for 3 minutes. After mixing, the lime-treated aggregates were marinated for 15 minutes to allow reaction. The lime-treated aggregates were then heated to 163°C for 2 hours. The aggregate samples were cooled to room temperature for 12 hours before testing.

Table 3.1 Test Matrix for Asphalt Binders

Binder type	Source	Additives	Amount (%)	Aging condition	DWP Test	SD Test	XRF Test	FTIR Test	TAN Test
PG 64-22	S1 and S2		0	RTFO	x	x	x	x	x
PG 64-22	S1 and S2	RAP	20	RTFO	x	x	x	x	x
PG 64-22	S1 and S2		0	PAV	x	--	--	--	--
PG 64-22	S1 and S2	RAP	20	PAV	x	--	--	--	--
PG 64-22	S1 and S2		0	RTFO	x	x	x	x	x
PG 64-22	S1 and S2	WMA	0.5	RTFO	x	x	x	x	x
PG 64-22	S1 and S2		0	PAV	x	--	--	--	--
PG 64-22	S1 and S2	WMA	0.5	PAV	x	--	--	--	--
PG 64-22	S1 and S2		0	RTFO	x	x	x	x	x
PG 64-22	S1 and S2	ASA	0.5	RTFO	x	x	x	x	x
PG 64-22	S1 and S2		0	PAV	x	--	--	--	--
PG 64-22	S1 and S2	ASA	0.5	PAV	x	--	--	--	--
PG 76-28	S3 and S4		0	RTFO	x	x	x	x	x
PG 76-28	S3 and S4	RAP	20	RTFO	x	x	x	x	x
PG 76-28	S3 and S4		0	PAV	x	--	--	--	--
PG 76-28	S3 and S4	RAP	20	PAV	x	--	--	--	--
PG 76-28	S3 and S4		0	RTFO	x	x	x	x	x
PG 76-28	S3 and S4	WMA	0.5	RTFO	x	x	x	x	x
PG 76-28	S3 and S4		0	PAV	x	--	--	--	--
PG 76-28	S3 and S4	WMA	0.5	PAV	x	--	--	--	--
PG 76-28	S3 and S4		0	RTFO	x	x	x	x	x
PG 76-28	S3 and S4	ASA	0.5	RTFO	x	x	x	x	x
PG 76-28	S3 and S4		0	PAV	x	--	--	--	--
PG 76-28	S3 and S4	ASA	0.5	PAV	x	--	--	--	--
PG 76-28	S3 and S4		0	RTFO	x	x	x	x	x
PG 76-28	S3 and S4	PPA	1.5	RTFO	x	x	x	x	x
PG 76-28	S3 and S4		0	PAV	x	--	--	--	--
PG 76-28	S3 and S4	PPA	1.5	PAV	x	--	--	--	--

For SD test, large aggregate specimens (cobble) ranging in size from about 10 cm to about 25 cm in average diameter were obtained from the quarry. In order to measure contact angles of the aggregate surfaces using the SD device, the aggregate surfaces must be flat, smooth, and clean. The cobble size rock specimens were cut with thicknesses varying from about 1 cm to about 2 cm using a mechanical diamond saw. Although the diamond saw creates nice, flat surfaces, there were still traces caused by the blade. To remove those traces and to reduce the amount of the roughness on the sample surface, a polishing test was undertaken using different grades of specific silicon carbide grit powders with grit numbers 220 (66 μm), 400 (22.1 μm), 600 (14.5 μm), and 1000 (9.2 μm), as well as using the 5 micron aluminum oxide powder. During the cutting and polishing processes, the aggregates were usually contaminated with oil and grit powder material. Since oil and powder can change the cohesive and adhesive properties of solids (i.e., aggregates), any changes in the surface properties of the materials were expected to change the surface tension and contact angles directly. In order to remove the soil and grit powder material from the surface of the aggregates, the samples were washed thoroughly with soap and warm distilled water. The flat rock specimens were then cleaned using hexane. After the cleaning process, the rock specimens were put inside an oven at 105±5 °C for 12 hours for drying. The samples were then allowed to cool down to room temperature in a desiccator with anhydrous calcium sulfate crystals. Table 3.2 shows test types and the aggregates to be tested in this study.

Table 3.2 Test Matrix for Aggregate

Aggregate Type	Source	XRF Test	SD Test	USD Test Without Lime Treatment	USD Test With Lime Treatment
Granite	Oklahoma	x	x	x	x
Rhyolite	Oklahoma	x	--	x	x
Limestone 1	Oklahoma	x	x	x	x
Limestone 2	Oklahoma	x	x	x	x
Limestone 3	Oklahoma	x	x	x	x

3.1.3. Asphalt Mix

A mix design with a nominal maximum aggregate size (NMAS) of 12.5 mm as well as aggregates and asphalt binders were collected from a local asphalt plant. A total of five different mixes were prepared in the laboratory following the mix design. The Mix-1 through Mix-4 were

prepared using a PG 64-22 and an asphalt binder content of 5.2% with an aggregate gradation shown in Figure 3.1. The Mix-1 was prepared without any additives. Mix-2, Mix-3 and Mix-4, however, contained 0.5% WMA additive, 0.5% ASA and 1.5% PPA by the weight of total binder, respectively. Mix-5 was prepared with 20% RAP. The amounts of different aggregates were adjusted to incorporate 20% RAP and maintain the same gradation presented in Figure 3.1. Mix-5 was found to require a higher (5.5%) total binder content (neat binder- 4.5%, binder from RAP- 1.0%) to meet the mix design requirements by the Oklahoma DOT. Additives were added to the binder at their mixing temperatures. The mixing compaction temperatures were 163° and 149°C, respectively, for all mixes, except Mix-2, lower mixing (135°C) and compaction (128°C) temperatures were used for Mix-2 as it contained a WMA additive. All the mixes were short-term conditioned for four hours using AASHTO R30 method (AASHTO, 2015) before compaction. The cylindrical samples of different dimensions needed to conduct HWT, TSR and SCB tests were compacted using a Superpave gyratory compactor (SGC) and will be sawed to dimensions, notch depths and geometries as required by AASHTO T 324, AASHTO T 283, and Louisiana Transportation Research Center (LTRC) test protocol, respectively. Tests were conducted on samples that satisfies the air voids requirements of 7%±0.5%. Table 3.3 presents the test matrix for asphalt mixes for this study.

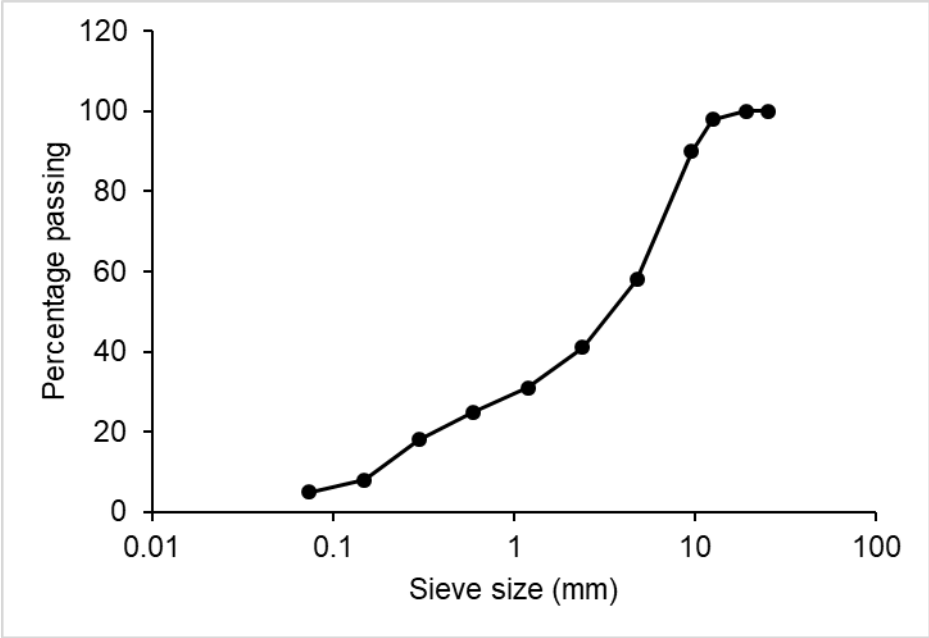

Figure 3.1 Gradation of the Asphalt Mixes

Table 3.3 Test Matrix for Asphalt Mixes

Mix ID	NMAS (mm)	Additive	HWT Test (Submerged)	TSR Test (Wet)	TSR Test (Dry)	SCB test (MIST)	SCB Test (Dry)
Mix# 1	12.5	--	x	x	x	x	x
Mix# 2	12.5	WMA	x	x	x	x	x
Mix# 3	12.5	Antistripping agent	x	x	x	x	x
Mix# 4	12.5	PPA	x	x	x	x	x
Mix# 5	12.5	RAP	x	x	x	x	x

3.2. Moisture Conditioning of Asphalt Mixes

3.2.1. AASHTO T 283 Method

The AASHTO T 283 (AASHTO, 2014) method was used for simulating the moisture-induced damage in the laboratory on the compacted specimens before conducting IDT test. According to this procedure, samples were conditioned by saturating with water (70-80% saturation) followed by a freezing cycle (-18°C for 16 hours) and a thawing cycle (60°C water bath for 24 hours).

3.2.2. Moisture Induced Sensitivity Test (MIST) Conditioning (ASTM D7870, 2013)

As a part of the development of new test method using LA-SCB test, compacted asphalt samples were subjected to moisture conditioning in a Moisture Induced Sensitivity Test (MIST) equipment before testing. Samples were conditioned at 60°C for 20 hours in water to simulate chemical and adhesion effects. After the adhesion phase, samples were subjected to 3,500 pressure cycles at 280 kPa to generate the effect of pore pressure buildup inside the sample. The MIST conditioning simulated the distress experienced by a wet pavement from a passing vehicle tire.

3.3. Laboratory Testing on Asphalt Binders

3.3.1. Dynamic Wilhelmy Plate (DWP) Test

The dynamic Wilhelmy plate (DWP) test was used to determine the SFE components of the asphalt binder blends using three different probe liquids, namely water, glycerin and

formamide. For this purpose, the contact angles of the binder blends with the three probe liquids were determined using a dynamic contact angle (DCA) analyzer. The asphalt binder samples for DWP testing were prepared using a 24 mm x 50 mm glass plate coated with the asphalt binder blends. The details of the testing procedure are described by Ghabchi et al. (2013). In this study, the advancing contact angles of binder blends was measured and used for further analysis as they were found to be more consistent than the receding contact angles (Hefer et al., 2006). Five replicates were tested for each solvent to ensure consistency and repeatability of the test results.

3.3.2. Sessile Drop Test

In this study, the contact angles of the RTFO-aged asphalt binders were also measured using the Sessile Drop (SD) device. The experimental set up was in close resemblance to the procedures reported in Koc (2013) and Thoroppady Kittu (2013). Three probe liquids, namely water, ethylene glycol (EG) and diiodomethane (DIM) were utilized for determining the contact angles on the asphalt binder specimens. The SD Device system is equipped with a software application (i.e., FTA) to analyze the images in order to determine the contact angle. The probe liquid was filled in the syringe and dispensed on the specimen using the FTA software on the SD device. The drop volume was about 12 µL as recommended by Koc (2013) and Thoroppady Kittu (2013). The time over which the drop is dispensed was kept as 24 seconds in this study. The pump was switched off while the pendant drop was still hanging from the needle. The specimen platform was raised up until the specimen touches the drop, at which point the drop detaches and falls on the specimen. To ensure accuracy, considerable attention was paid so as not to touch the needle to the surface of asphalt binder. The camera mounted on the device was used to capture a series of images of the binder-probe liquid interface for a period of time. The 'trigger' function of the camera was activated manually to start the process of image capture. In this study, 30 images per second were used for a total period of 15 seconds. The software processed a total of 450 images and the average contact angle was determined from these images. Contact angle measurements were conducted six times on one slide by dispensing six drops of the liquid on one face of the slide at different locations. Only one face of a slide was used for the measurements. The same procedure was repeated on the other two slides for obtaining 18 measurements with one probe liquid and on one asphalt binder sample.

3.3.3. X-Ray Fluorescence (XRF) Test

The elemental analysis of binder blends was conducted using the XRF technique. In XRF, the emission of characteristic "secondary" (or fluorescent) X-rays from the test sample excited by high-energy X-rays is used to identify the chemical compositions of materials being studied. The working principles and mechanism of the XRF technique can be found elsewhere (Hesp and Shurvell, 2010; Hesp and Shurvell, 2013). All the tests were conducted in the chemical laboratory of Ingevity using a Rigaku NexCG X-Ray Fluorescence Device. The device is capable of providing rapid, non-destructive, multi-element analyses from very low to high concentrations of elements ranging from sodium (Na) to uranium (U). Peak heights in the spectrum were used to detect and quantify the presence of the elements. Three samples were tested from each binder blends to ensure consistency.

3.3.4. Fourier Transform Infrared Spectroscopy (FTIR) Test

The FTIR spectroscopy was used to examine the effect of the addition of different additives to asphalt binders. This method detected and quantified the CH_3, CH_2, aromatic carbon, carboxyl and sulfoxide groups in binder samples. The results of the FTIR tests on asphalt binders were compared with the SFE test results in order to evaluate and explore their correlation with SFE components and moisture damage.

3.3.5. Total Acid Number (TAN) Test

The TAN test was used to determine the acidity of asphalt binders with respect to the amount of potassium hydroxide in milligrams needed to neutralize the acids in one gram of sample (Jingyan et al., 2012). The acidity of the binder blends was determined and its correlation with the SFE components of binders and moisture damage was investigated.

3.4. Laboratory Testing on Aggregates

3.4.1. Universal Sorption Device (USD) Test

The SFE components of the collected aggregates were measured using a USD in accordance with the methodology discussed by Bhasin and Little (2007). This technique is based on the development of a vapor sorption isotherm, i.e., the amount of vapor adsorbed, or desorbed, on the solid surface at a fixed temperature and relative pressure (RP). The adsorption isotherms were determined by conducting the adsorption tests at 25°C and different RP ranging from 0.05 to 1.00. At each RP step, the system monitored sample weight until

reaching to an equilibrium condition. About 20 grams of the prepared aggregate sample were introduced in the sample chamber of the USD device to obtain adsorption isotherms for water, MPK, and n-hexane. The collected data was then used for determining the spreading pressure of each aggregate tested with each probe vapor.

3.4.2. Sessile Drop (SD) Test

The contact angles of the aggregate specimens with three different probe liquids (water, diiodomethane, and ethylene glycol) were determined using the sessile drop device. The test was conducted on multiple sets of each sample with each probe liquid until the desired repeatability and standard deviation were achieved. To avoid the contamination of the syringe in the SD device with the different probe liquids, each probe liquid was dedicated with one syringe. The SD device was calibrated before each testing set. The syringe that contains the probe liquid was refilled before the test. Once the device was calibrated and the specimens were at the testing temperature (at room temperature), the specimen was taken out of the desiccator and placed under the needle on the sample stage in the SD device. The SD device is equipped with an automated pump system to dispense a small amount of liquid on the specimen using the syringe. About 10-15 μL of probe liquid was dispensed from the needle using the FTA software in the SD device computer system. While the liquid was still in the form of a pendant drop and at its full volume, the platform that holds the specimen was elevated slowly until the specimen touches the drop. The drop detached from the needle and forms the sessile drop on the flat surface of the specimen. The high-resolution camera in the SD device constantly captures the images of the liquid-solid interface and sends it to the FTA software for processing. In this study, 30 images per second are used. The time period for a single test, for the collection of the digital images, was 10 seconds. The software processes all the images and an average contact angle was determined. Contact angle measurements were conducted eight times on one side of the specimen by dispensing eight drops of the liquid on the surface of the specimen at different locations. Only one face of the specimen was used for the measurements.

3.4.3. X-Ray Fluorescence (XRF) Test

In this study, the elemental analysis of aggregates was carried out, using the XRF technique through a Rigaku NexCG X-Ray Fluorescence Device. The working principle for this test was similar to that of the binder test. The results from the elemental analysis by XRF were used to develop correlations between the amount and types of different elements in aggregates and their SFE components to the extent feasible.

3.5. Laboratory Testing on Asphalt Mixes

3.5.1. Hamburg Wheel Tracking (HWT) Test

The HWT test was conducted on asphalt mix specimens produced for this study in accordance with the AASHTO T 324 test method (AASHTO, 2014) to determine their rutting and moisture-induced damage potentials. The diameter and height of the compacted samples were 150 mm and 60 mm, respectively. The HWT test was conducted on two sets of samples to ensure repeatability. In this method, two cylindrical specimens were cut to a desired shape and were placed in the mounting tray. The mounting tray was then fixed in the HWT machine for testing. The HWT tests were conducted at 50°C with a wheel pass frequency of 52 passes/minute. The tests were terminated after reaching a maximum rut depth of 20 mm or 20,000 wheel passes, whichever reached first. The rutting potentials of the mixes were evaluated based on conventional method by determining post compaction deformation and creep slope. The stripping potential was determined through stripping slope and stripping inflection point from the HWT test results (Figure 3.2 (a)). Yildirim and Kennedy (2002) used the rut depth at 1,000 wheel passes as the post-compaction point. The linear region of the rut progression curve after post compaction point is called creep region which represents rutting due to plastic flow. The creep slope is defined as the rut depth per wheel pass in the creep region. The stripping inflection point is used to characterize the moisture-induced damage of the asphalt mix. The stripping slope was obtained by drawing lines between the stripping inflection point and the final wheel pass.

In addition to conventional method, a new method known as TAMU method (Figure 3.2 (b)), proposed by Yin et al. (2014) was applied and compared with the current practice used for analyzing the HWT test results. Yin et al. (2014) proposed a procedure to separate visco-plastic strain and stripping strain from the rut depth obtained from the HWT test. A parameter called stripping number (LC_{SN}) was introduced to represent the maximum number of load cycles that an asphalt mix can resist in the HWT test before the adhesive fracture occurs. Also, the rut depth accumulation resulting from stripping was quantified using a parameter called stripping life (LC_{ST}). The LC_{ST} was represented as the number of wheel passes required to produce a stripping strain of 12.5 mm. The visco-plastic strain increment ($\Delta\varepsilon_{10,000}^{vp}$) which was the slope of the visco-plastic strain at 10,000 wheel passes was proposed to quantify the resistance to rutting. The details of the procedure can be found in Yin et al. (2014).

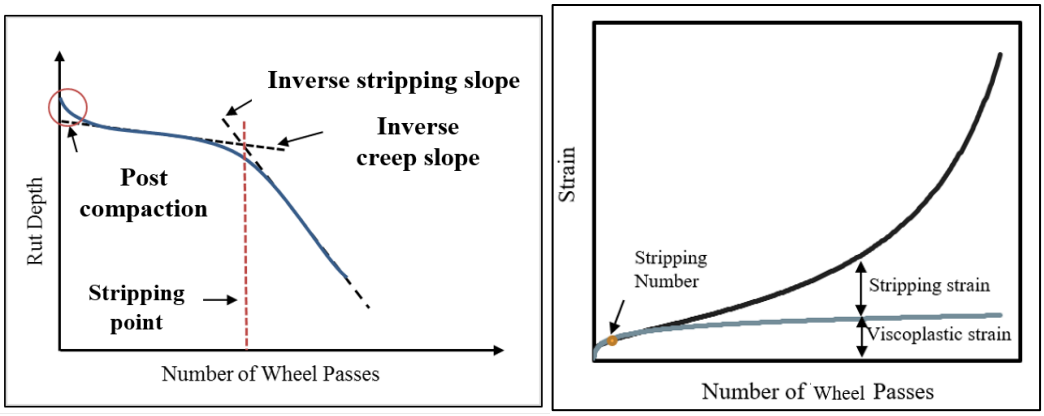

(a) (b)

Figure 3.2 Analysis of HWT test results using (a) conventional method and (b) TAMU method

3.5.2. Retained Indirect Tensile Strength Ratio (TSR) Test

The IDT test was conducted in accordance with the AASHTO T 283 test method (AASHTO, 2014). The reduction in tensile strength due to the accelerated moisture and temperature conditioning was measured and used as an indicator of the moisture-induced damage. For this purpose, asphalt mix specimens of 150 mm diameter and 95 mm height were prepared in the laboratory. The AASHTO T 283 method (AASHTO, 2014) was used for simulating the moisture-induced damage in the laboratory on the compacted specimens. Then the IDT test was conducted on dry and moisture-conditioned specimens. The TSR value was determined by dividing the average tensile strength of moisture-conditioned to that of dry-conditioned specimens using Equation (15). Another parameter, known as the toughness index (TI) ratio of a moisture-conditioned sample to that of a dry sample was calculated as a new mechanistic approach based on fracture mechanics to determine the moisture-induced damage potential (Kim et al., 2012). The TI was calculated from the IDT test results using Equation (16) to characterize the post-peak failure behavior of the mixes. Figure 3.3 shows the area under the strength vs strain curve considered in TI calculation from IDT test. The TI value of an ideal brittle material with no post-peak load-carrying capacity is zero, whereas the TI value should be 1 for an elastic perfectly plastic material with no loss in load-carrying capacity after peak load (Shu et al., 2008; Huang et al., 2010). Kim et al. (2012) used a tensile strain of 3% as a terminal strain for dry specimens. In this study, the TI values were calculated up to a tensile strain of 4% as the moisture-conditioned specimens were found not to reach peak strength at 3% strain.

$$TSR = \frac{ITS\ of\ wet{-}conditioned\ Specimens\ (ITS_{wet})}{ITS\ of\ Dry{-}conditioned\ Specimens\ (ITS_{dry})} \qquad (15)$$

$$TI = \frac{A_\varepsilon - A_p}{\varepsilon - \varepsilon_p} \qquad (16)$$

where,

ε = strain corresponding to 4% tensile strain;

ε_p = strain corresponding to peak strength;

A_ε = area under normalized stress-strain curve up to 4% tensile strain (ε);

A_p = area under normalized stress-strain curve up to peak strength (ε_p).

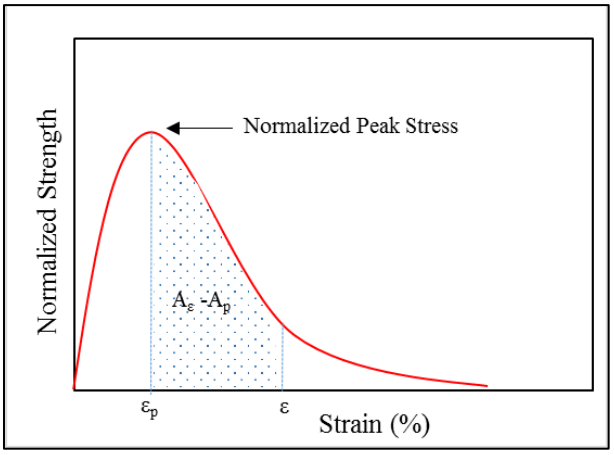

Figure 3.3 Schematic diagram to calculate toughness index (TI) from IDT test

3.5.3. Louisiana Semi-Circular Bend (LA-SCB) Test

The semi-circular specimens having a diameter of 150 mm, a height of 75 mm, and a thickness of 50 mm were prepared for conducting LA-SCB test. For this purpose, cylindrical SGC samples of 150 mm diameter and 120 mm height were compacted in the laboratory. The samples were divided into two subsets. One subset was kept at 25°C while the other subset was moisture-conditioned using a MIST equipment. After conditioning, specimens for LA-SCB test were prepared by cutting the samples into desired shapes and cutting notches of 25.4, 31.8 and 38 mm depth. The test was conducted at room temperature (25°C) by applying a monotonically increasing load at a rate of 0.5 mm/min until failure. The results of the SCB test were analyzed by calculating the critical energy release rate or J-integral (J_c) using Equation (14). The mechanics behind the determination of J-integral from SCB test using specimens of different notch depths can be found in the literature (Wu et al., 2005). Figure 2.3 exhibited the schematic of a LA-SCB test and analysis procedure to determine J-integral for asphalt mix. The J-integral ratio was calculated by dividing the J integral value of a MIST-conditioned to a dry specimen using Equation (17).

$$J_c\ ratio = \frac{J_c\ of\ MIST-conditioned\ Specimens\ (J_{c-Mist})}{J_c\ of\ Dry-conditioned\ Specimens\ (J_{c-dry})} \qquad (17)$$

4. RESULTS AND DISCUSSIONS

4.1. Asphalt Binder Test Results

In this study, the surface free energy (SFE) and chemical characteristics of four different binders (i.e. S1 PG 64-22, S2 PG 64-22, S3 PG 76-28 and S4 PG 76-28) with different additives were evaluated using dynamic Wilhelmy plate (DWP), sessile drop (SD), X-ray fluorescence (XRF), total acid number, and Fourier transform infrared (FTIR) tests. The results of the tests conducted on all the binder blends are presented in Appendices A to E. The contact angles and SFE components of binder blends from DWP tests are presented in Appendix A. Appendices B, C and D contains XRF, TAN and FTIR test results of binder blends. The SFE components of bonder blends from SD test are presented in Appendix E. Also, the test results of an unmodified PG 64-22 from source S1(S1 PG 64-22) and a polymer-modified PG 76-28 from source S3 (S3 PG 76-28) binders are presented in the following sections.

4.1.1. Dynamic Wilhelmy Plate Test

4.1.1.1. Contact Angles of Asphalt Binders with Probe Liquids

As noted earlier, the DWP test was conducted on the asphalt binders to determine their contact angles with three probe liquids, namely water, glycerin, and formamide using a dynamic contact angle analyzer (DCA). The contact angles of the asphalt binder blends with three different probe liquids were used to calculate the SFE components of the tested binders. The contact angles of RTFO-aged S1 PG 64-22, S1 PG 64-22+0.5% W1, S1 PG 64-22+0.5% A1 and S1 PG 64-22+20% R1 are presented in Figure 4.1(a). Generally, a contact angle of less than 90º indicates that the probe liquid can wet the surface of that material and vice versa (Buddhala et al., 2011). From Figure 4.1(a), it can be observed that the contact angles of S1 PG 64-22 binder with water, glycerin, and formamide reduced slightly due to the addition of 0.5% W1 additive. For example, the contact angle of RTFO-aged S1 PG 64-22 binder was found to be 107.9°, 94.3° and 90.5° when it comes in contact with water, glycerin, and formamide, respectively. The corresponding contact angles for the same binder blend containing 0.5% W1 additive were 107.8°, 94.1° and 89.8°, respectively. A similar decreasing trend in contact angles was also observed with the addition of 0.5% A1 and 20% R1 to the binder. From Figure 4.1(a), it was also observed that the contact angles of PG 64-22 binder containing 0.5% A1 additive with water, glycerin and formamide were 107.0°, 94.0° and 87.9°, respectively. The reactions between the binder and the fatty amine derivatives of the W1 additive and polyamines of A1

antistripping agent are hypothesized to be responsible for the changes in contact angles. A similar trend of reduction in contact angle with an increase in the WMA and anti-stripping additive was reported in other studies (Wasiuddin et al., 2007b; Buddhala et al., 2011; Ghabchi et al., 2013). However, the effects of additives were found to be different for polymer-modified S3 PG 76-28 binder (Figure 4.1(b)). The additions of W1 additive, A1 antistripping agent, and R1 were found to increase the contact angles of S3 PG 76-28 binder with water and formamide. The reaction of the polymer and the chemical constituents of the additives are expected to be responsible for these changes. Figure 4.1(b) also presents the contact angles of S3 PG 76-28 with 1.5% PPA. From Figure 4.1(b), the contact angles of S3 PG 76-28 with water, glycerin and formamide were found to be 114.4º, 101.2º and 97.5º, respectively. The addition of 1.5% PPA to the S3 PG 76-28 binder was found to increase the contact angles with all probe liquids. The contact angles of RTFO-aged PG 76-28+1.5% P1 binder were 117.70°, 108.83° and 106.10° for water, glycerin and formamide, respectively. The increase in contact angles of the binder with the addition of PPA are expected to reduce the wettability of the probe liquids on the surface of the binder. Reactions between the binder's chemical components with the PPA are expected to be responsible for the increase in contact angles. Also, the oxidation during short-term aging process may affect the contact angles of the binder. Furthermore, from Appendix A, the effect of the addition of different additives on binders' contact angle with different probe liquids are observed to be dependent on binder type and source (Appendix A). The differences on the base binder's compositions and their reactions with different additives are responsible for these variations.

4.1.1.2. Surface Free Energy Components of Asphalt Binders

Typically, a change in the SFE components of a binder is reported to result in a change in the moisture-induced damage potential of the corresponding binder-aggregate system. Bhasin et al. (2006) reported that the acid component of the asphalt acts as a scale factor in calculation of dry adhesive bond strength. The SFE components of all the four binders with different additives are presented in Appendix A. It was observed that the SFE components of the binders vary with binder type and binder source.

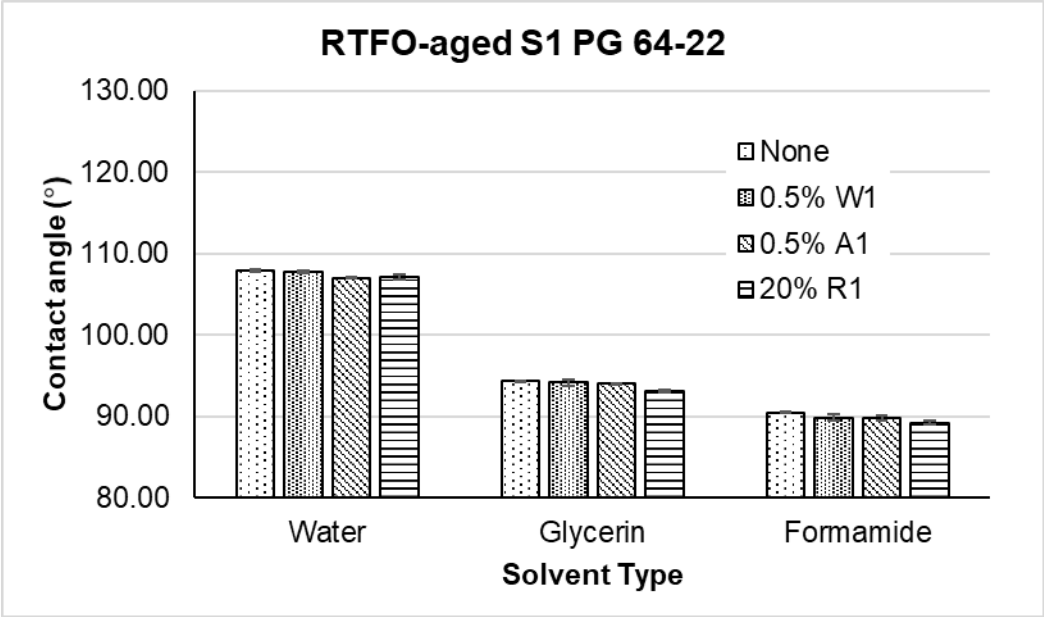

(a)

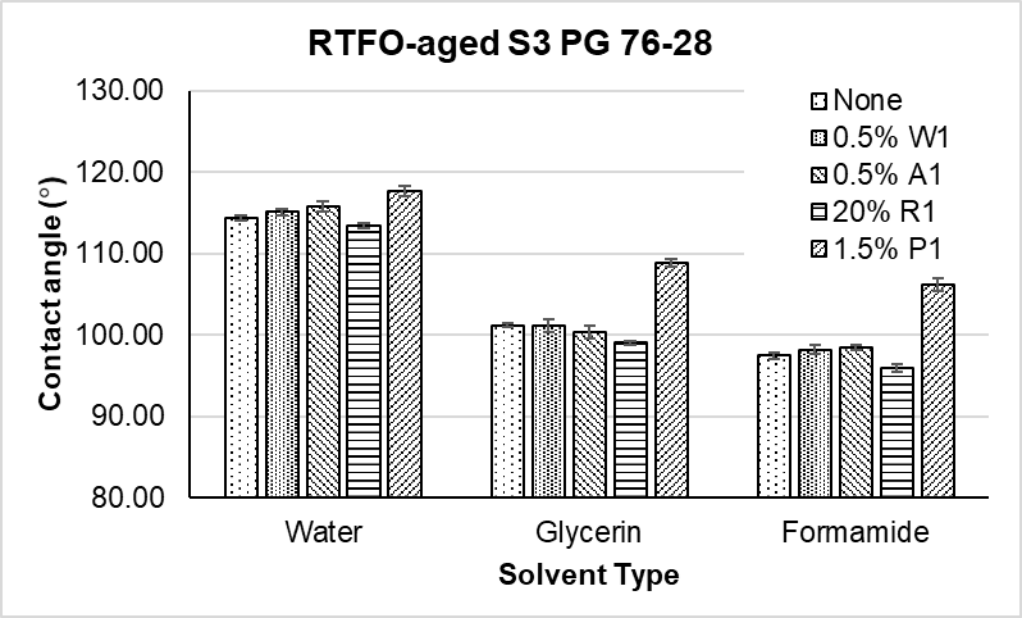

(b)

Figure 4.1 Contact angles with different solvents for (a) RTFO-aged S1 PG 64-22; and (b) RTFO-aged S3 PG 76-28 binders

Figure 4.2 (a) presents the SFE components of S1 PG 64-22, S1 PG 64-22+0.5% W1, S1 PG 64-22+0.5% A1 and S1 PG 64-22+20% R1 under RTFO-aged condition. From Figure 4.2(a) it was observed that the non-polar Lifshitz-van der Waals (Γ^{LW}) and the total SFE (Γ^{Total})

component of S1 PG 64-22 binder increased with the addition of the W1 additive to the binder blend. For example, the Γ^{LW} for S1 PG 64-22 binder was found to increase from 9.31 mJ/m^2 to 10.40 mJ/m^2 upon the addition of 0.5% W1 additive. However, the acid (Γ^+) and base (Γ^-) components of S1 PG 64-22 binder were found to reduce with the addition of W1 additive. The Γ^+ reduced from 1.81 mJ/m^2 to 1.51 mJ/m^2 and the Γ^- reduced from 0.68 mJ/m^2 to 0.64 mJ/m^2 for S1 PG 64-22+0.5%W1 binder. Also, the Γ^+/Γ^- ratio of the PG 64-22 binder was found to reduce from 2.65 to 2.36 with the addition of 0.5% W1 additive. This indicates that the asphalt binder may become more basic with the addition of W1 additive which may result in weak bonding with basic aggregates. Bhasin et al. (2006) tested several aggregates, namely granite, gravel, limestone, quartz and sandstone from different sources and found out that the Γ^- components of all the aggregates are relatively higher than the acid components. Therefore, the addition of W1 additive to S1 PG 64-22 binder are expected to result in a weak adhesive bond with basic aggregates than the neat binder.

From Figure 4.2(a), it was also observed that the Γ^{LW}, Γ^{Total} and the Γ^- components of PG 64-22 binder increased as a result of addition of anti-striping additive. The Γ^{LW} and Γ^- were found to increase by approximately 11% and 22% with the addition of 0.5% A1 antistripping additive, respectively. The Γ^+ component of PG 64-22 binder was found to reduce by approximately 18% with the addition of A1 antistripping agent. Also, the Γ^+/Γ^- component was found to reduce from 2.66 to 1.80 indicating more basic behavior with the addition of 0.5% A1 antistripping additive. The reaction of the amine-based antistripping agent, which is basic in nature, with binder constituents are expected to be responsible for the changes in the binder surface energy properties. Similar increase in the basic behavior with the addition antistripping agent was reported by Wasiuddin et al. (2007b). Also, it was observed that all the SFE components of S1 PG 64-22 binder increased due to the addition of simulated RAP. The Γ^+/Γ^- component was found to increase from 2.65 to 2.70 indicating more acidic behavior with the addition of 20% simulated RAP. Ghabchi et al. (2014) observed a similar increase in acidic nature of the binder with an increase in the amount of RAP content. The aged binder from RAP is expected to be responsible for the changes in SFE components of neat S1 PG 64-22 binder.

The SFE components of RTFO-aged S3 PG 76-28 with different additives are presented in Figure 4.2(b). The acidic nature of the S3 PG 76-28 binder was found to increase with the addition of 0.5% W1 and 0.5% A1 additives. It is hypothesized that the reaction of the polymer presents in the S3 PG 76-28 binder and the constituents of the W1 additive and A1 antistripping agent resulted in an increase in the acidic component. Also, the addition of RAP binder was

found to increase the acidic nature of the S3 PG 76-28 binder which is consistent with the findings of Ghabchi et al. (2014). The effect of the addition of PPA on S3 PG 76-28 binder can be evaluated from Figure 4.2(b). The acid (Γ^+) and the non-polar Lifshitz-van der Waals (Γ^{LW}) components of the PG 76-28 binder was found to decrease with the addition of 1.5% PPA. For example, the Γ^+ component was observed to reduce from 1.28 mJ/m^2 to 0.88 mJ/m^2 after addition of 1.5% PPA to binder blend. However, the base component (Γ^-) of the PG 76-28 binder increased with the addition of the 1.5% PPA. The Γ^- component was found to increase from 0.29 mJ/m^2 to 0.79 mJ/m^2 with the addition of 1.5% PPA. The total SFE (Γ^{Total}) components of the PG 76-28 binder also decreased from 8.90 mJ/m^2 to 6.49 mJ/m^2 with addition of 1.5% PPA. As a result of the addition of PPA, the Γ^+/Γ^- value for the PG 76-28 binder was found to reduce from 4.41 to 1.11 indicating a substantial increase in basic behavior with the addition of PPA to binder blend. Al-Qadi et al. (2014) also reported an increase in the basic SFE component of the binder with an increase in PPA amount. Therefore, the addition of PPA may result in a weak bonding with aggregates that generally have a higher basic component than acid component. Similar to contact angles, the reactions of the neat binder constituents with PPA are likely to be responsible for such changes in the binder's surface energy properties.

The SFE components of all the binders with different additives under PAV-aged conditioned are presented in Appendix A. Figures 4.3 (a) and 4.3 (b) present the SFE components of PAV-aged S1 PG 64-22 and S3 PG 76-28 binders with different additives, respectively. From Figure 4.2(a) and 4.3(a), it was observed that the non-polar Lifshitz-van der Waals (Γ^{LW}), base (Γ^-) and the total SFE (Γ^{Total}) component of S1 PG 64-22 binder increased with PAV-aging. For example, the Γ^{LW} for S1 PG 64-22 binder was found to increase from 9.31 mJ/m^2 to 9.68 mJ/m^2 upon PAV-aging. However, the acid (Γ^+) component of the S1 PG 64-22 binder was found to reduce with long-term aging. The Γ^+ was found to reduce from 1.81 mJ/m^2 to 1.39 mJ/m^2 for PAV-aged S1 PG 64-22 binder. Also, the Γ^+/Γ^- ratio of S1 PG 64-22 binder was found to reduce significantly (from 2.66 to 2.36) as a result of PAV-aging. A similar trend in reduction of Γ^+/Γ^- ratio was observed for S1 PG 64-22+0.5% W1 and S1 PG 64-22+20% RAP binders. This indicates that the asphalt binder became more basic in nature with long-term aging which may result in weak bonding with basic aggregates. However, the Γ^+/Γ^- ratio was found to increase from 1.80 to 1.88 for S1 PG 64-22+0.5% A1 binders. Wasiuddin et al. (2007a) reported that the beneficial effect of the antistripping agent severely degraded with aging. Therefore, the reduction in basic properties of amine antistripping agent with long-term aging is expected to be responsible for this observation. The effect of the long-term aging on the S3 PG

76-28 binder can be evaluated from Figure 4.2(b) and 4.3(b). The acidic components were found to increase significantly for all the S3 PG 76-28 binder blends with long-term aging.

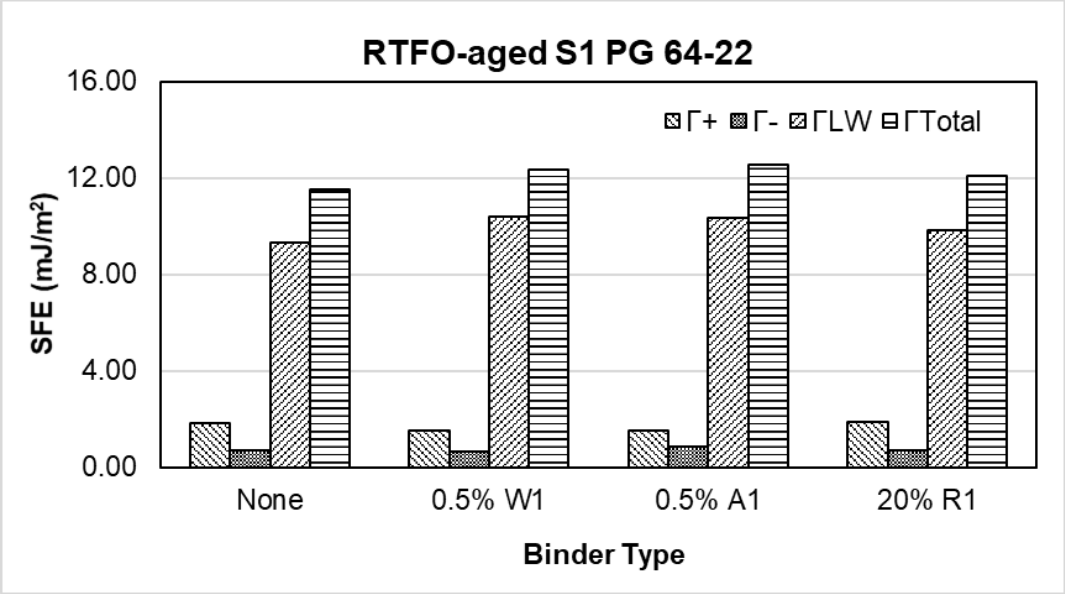

(a)

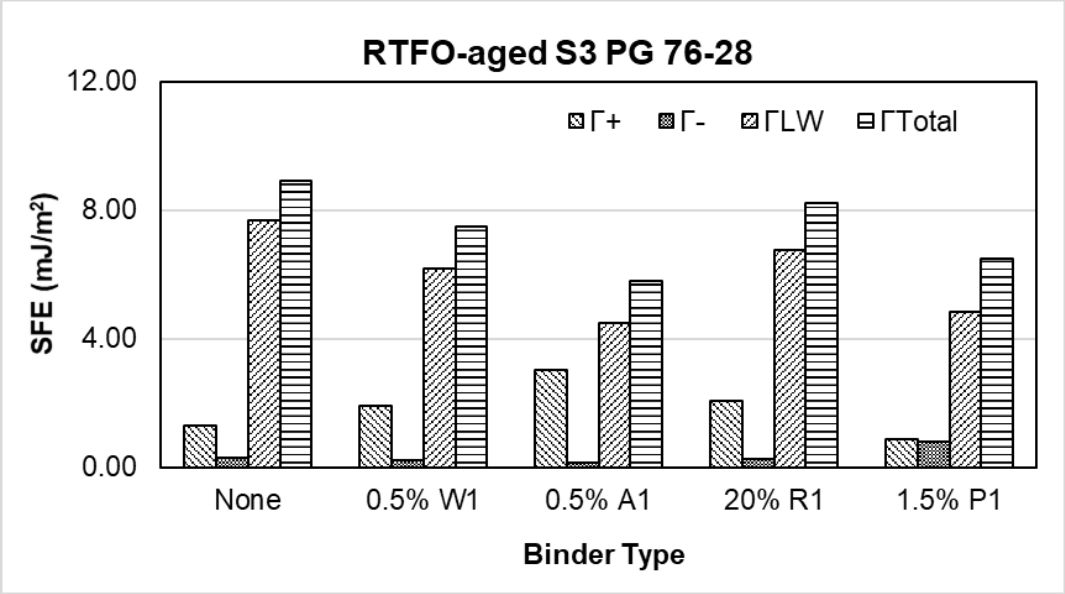

(b)

Figure 4.2 Surface free energy components of (a) RTFO-aged S1 PG 64-22 binders and (b) RTFO-aged S3 PG 76-28 binders containing different additives

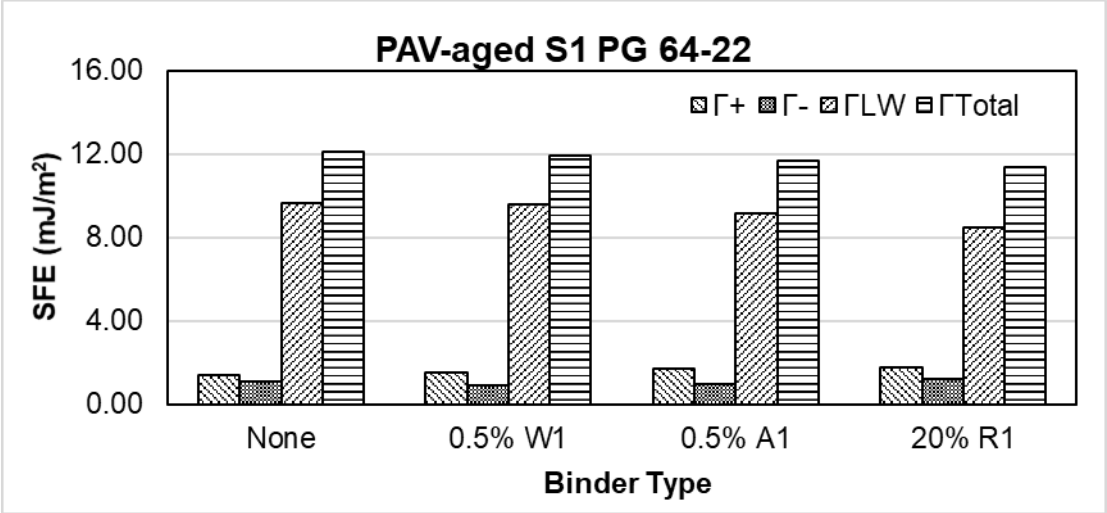

(a)

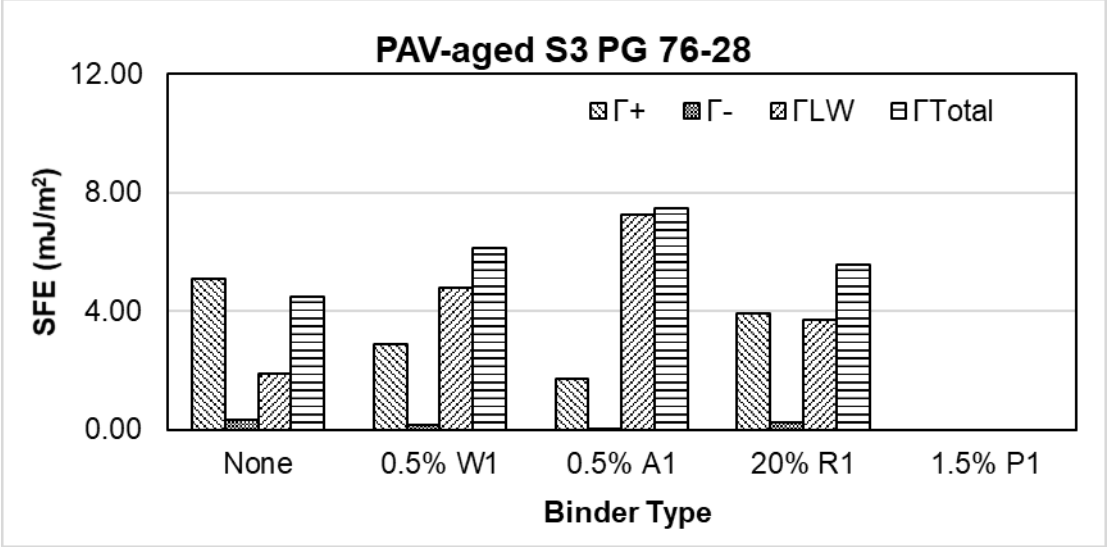

(b)

Figure 4.3 Surface free energy components of (a) PAV-aged PG 64-22 and (b) PAV-aged PG 76-28 binders containing different additives

4.1.2. X-Ray Fluorescence (XRF) Test

The results of the XRF tests for all the binder blends are presented in Appendix B. Figure 4.4 (a) and 4.4 (b) present the chemical compositions of S1 PG 64-22 and S3 PG 76-28 binders from XRF tests, respectively. During XRF tests, all elements were scanned initially. Then those elements which were not detected, or spectrum could not be seen, were deleted. Each analysis was re-calculated with only the detected elements. Figure 4.4 (a) and 4.4 (b) present the values (PPM) of those elements which were detected for S1 PG 64-22 and S3 PG

76-28 binders. The results of the XRF tests indicated that oil constitutes more that 95% of the of the binder composition. Also, it was observed from the XRF spectrum that both the binders exhibited presence of Aluminium (Al, 1.49 keV), Silicon (Si, 1.74 keV), Sulfur (S, 2.31 keV), Chlorine (Cl, 2.62 keV), Calcium (Ca, 3.69 keV), Vanadium (V, 4.95 keV), Iron (Fe, 6.40 keV), Nickel (Ni, 7.48 keV), Copper (Cu, 8.05 keV), Zinc (Zn, 8.64 keV) and Tin (Sn, 25.27 keV). Hesp and Shurvell (2010) and Hesp and Shurvell (2013) also reported the presence of the abovementioned elements in their tested asphalt binders. Among all the elements detected in S1 PG 64-22 binder, Sulfur(S) was found to exhibit the highest proportion (46,507 ppm). Other elements can be listed as Al, V, Ni, Si, Cl, Fe, Sn, Zn and Cu according to their composition from the highest to the lowest. It was found that the Al, Si, S, Cl, V, and Cu exhibited an increase in the amount with an addition of 0.5% W1 additive. For example, the S was found to increase from 46,507 ppm to 47,192 ppm upon the addition of 0.5% W1 additive. However, Ca, Fe, Zn and Sn were found to decrease with addition of W1 additive. These changes may be resulted from the reaction of the chemical components of binder and the fatty amine derivatives of the W1 additive.

The Al, Si, S, Cl, Fe, Cu, Zn and Sn exhibited an increase in the composition with the addition of A1 antistripping additive. The S was found to increase from 46,507 ppm to 46,722 ppm upon the addition of 0.5% A1 additive. However, Ca, V and Ni were found to decrease with the addition of A1 additive. The A1 additive is a polyamine-based antistripping agent. As in case of WMA additive, the changes in the chemical compositions of the binder are expected to result from the its reaction with the polyamines. With the addition of 20% RAP binder, the Al, Cu and Sn exhibited an increase in the composition, whereas, Si, S, Cl, Ca, V and Zn showed a reduction in the composition.

From Figure 4.4 (b), it can be observed that the amount of S (28,666 ppm) was the highest among all the elements detected for the PG 76-28 binder from the XRF spectrum. According to their composition from the highest to the lowest, other detected elements can be listed as Al (241 ppm), Fe (183 ppm), Si (116 ppm), P (80.1 ppm), Cl (46.3 ppm), V (45.2 ppm), Ca (26.1 ppm), Ni (25.2 ppm), Sn (14.5 ppm), Zn (8.36 ppm), Cu (3.29 ppm), Pb (2.46 ppm), and Sr (1.16 ppm). Similar to S1 PG 64-22 binder, the addition of W1 additive and A1 antistripping agent was observed to increase the Al, Si, S, Cu and Ca composition of S3 PG 76-28 binder.

Analysing the XRF spectrum of the PG 76-28+1.5% P1 binder from Figure 4.4(b), revealed that the addition of PPA can be easily detected from the increase in phosphorus

content of the binder. The amount of phosphorus increased from 80.1 ppm to 3,385 ppm with the addition of PPA to the PG 76-28 binder. Reinke and Glidden (2010) also reported presence of phosphorus element in the binder sample after PPA modification from XRF test. Furthermore, nuclear magnetic resonance (NMR) test used by Baumgardner et al. (2005) detected phosphorous compounds in the precipitated asphaltenes from the PPA-modified asphalt binders. The amount of Al, Si, and Sn exhibited an increase with addition of 1.5% PPA. For example, the Al was found to increase from 241 ppm to 264 ppm upon the addition of 1.5% PPA. On the other hand, S, Cl, Fe and Ni were found to decrease with addition of PPA.

Hefer et al. (2005) reported that the polar molecules of the binders exhibit active sites. These active sites help to interact with other active sites within the binder (cohesive bonding) and with aggregate surfaces (adhesive bonding). Among the elements detected from XRF test, Al, Ca, Fe, Cu, Zn and Sn can exist in their positive ionic configuration and are expected to be responsible for positively active sites. Therefore, the relations between the Lewis acid component and the amount of Al, Ca, Fe, Cu, Zn and Sn in the binder blends were evaluated. The Lewis acid component was found to have very a poor correlation with Ca, Fe, Zn, Cu and Sn. The highest coefficient of correlation (R^2) was observed between Al and Lewis acid component with a R^2 value of 0.49. It indicates that the presence of Al might have higher influence on Lewis acid component than the other elements. Figure 4.5 presents the variation of acid component with Al. Similarly, the Lewis base component was evaluated with the elements detected from XRF tests and the Vanadium (V) was found to exhibit the highest correlation with a R^2 values of 0.30. Figure 4.6 presents the variation of the base component with respect to V. Among all the elements detected from the XRF study, the non-polar Lifshitz-van der Waals component (Γ^{LW}) was found to increase with a decrease in Fe and increase in Ni components. The R^2 values for Lifshitz-van der Waals component (Γ^{LW}) with Fe and Ni were found to be 0.37 and 0.40, respectively. Figure 4.7 presents the changes in the non-polar Lifshitz-van der Waals component (Γ^{LW}) with the Ni for the tested binders.

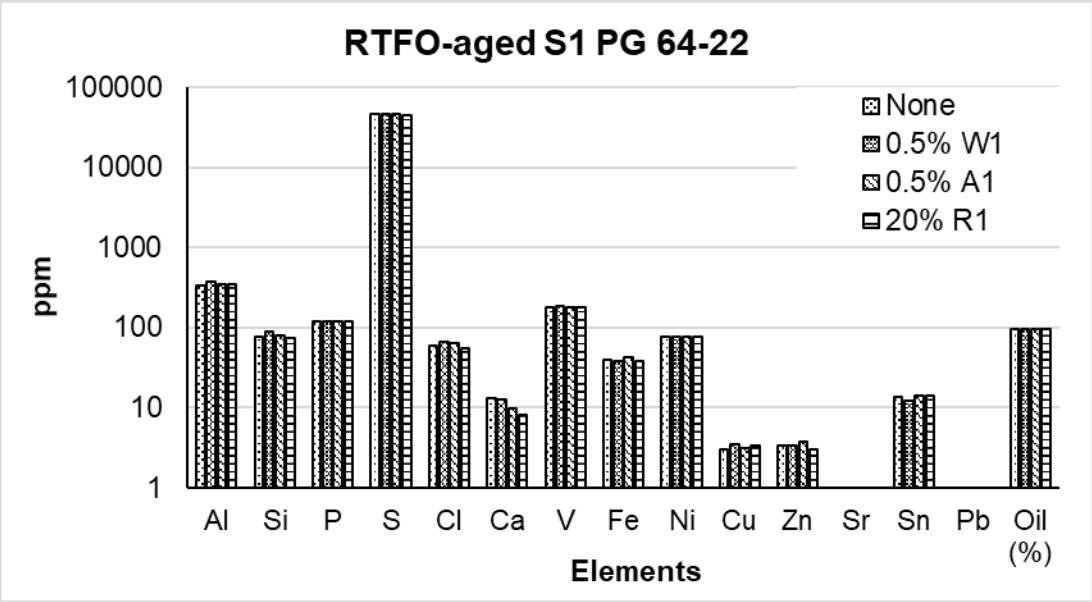

(a)

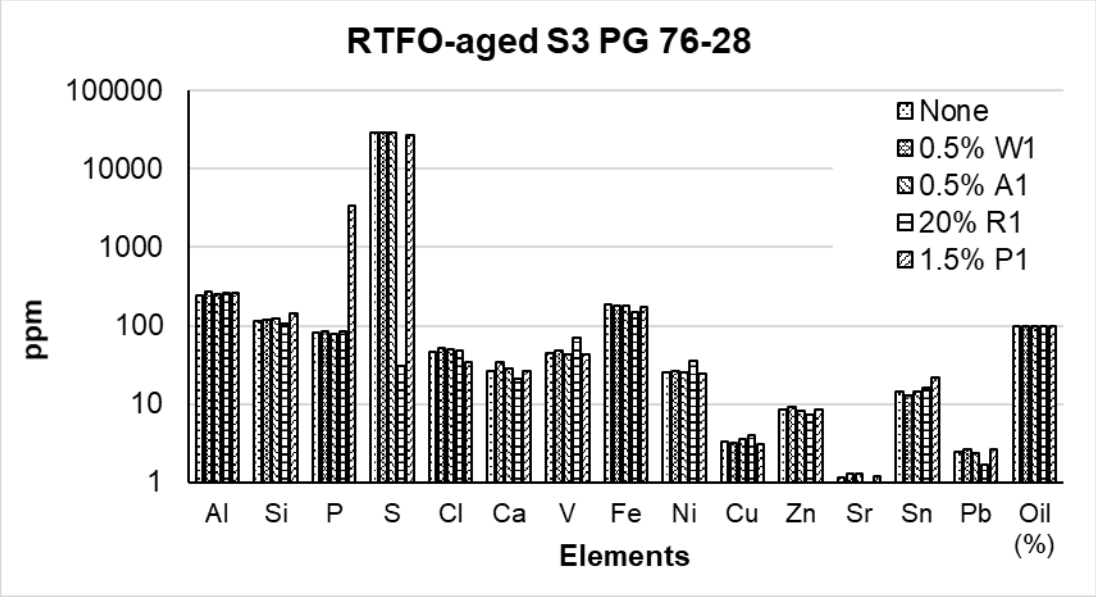

(b)

Figure 4.4 Elements detected from XRF tests of (a) RTFO-aged S1 PG 64-22 and (b) RTFO-aged S3 PG 76-28 binders with different additives

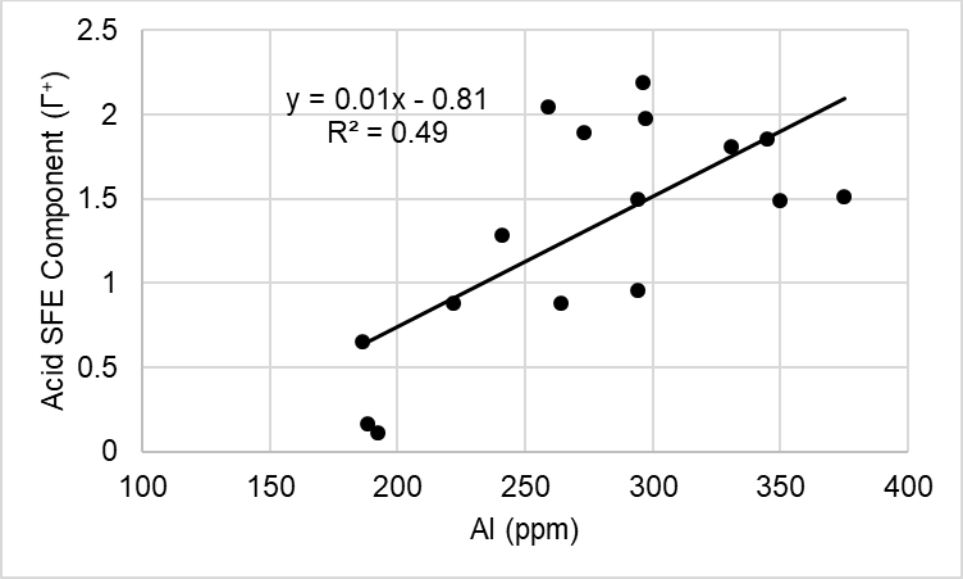

Figure 4.5 Correlation between Acid SFE Component (Γ^+) and Aluminum (Al)

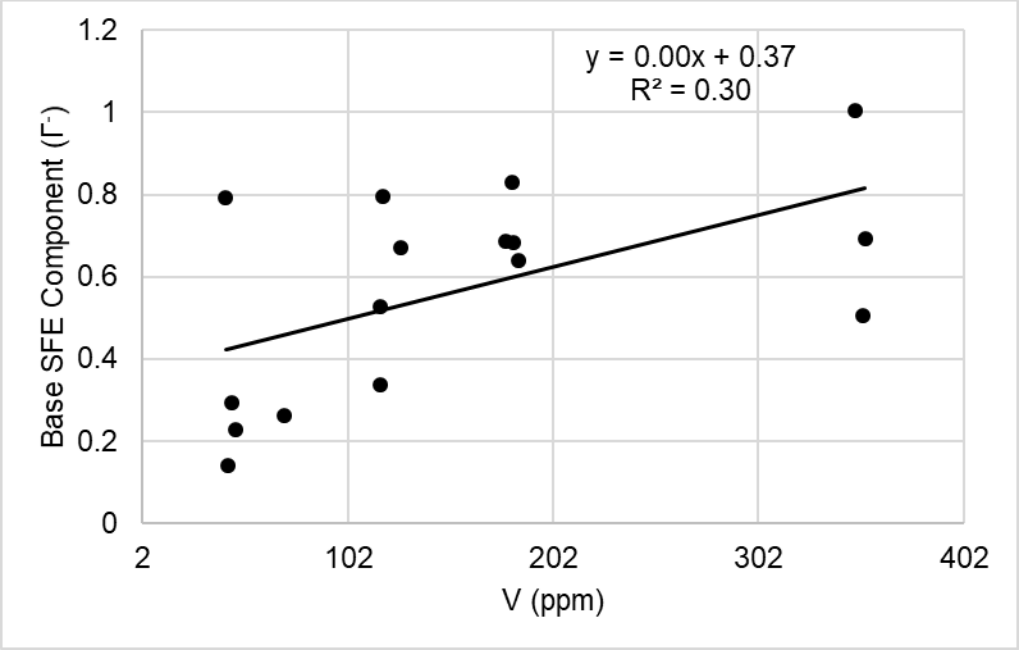

Figure 4.6 Correlation between Base SFE Component (Γ^+) and Vanadium (V)

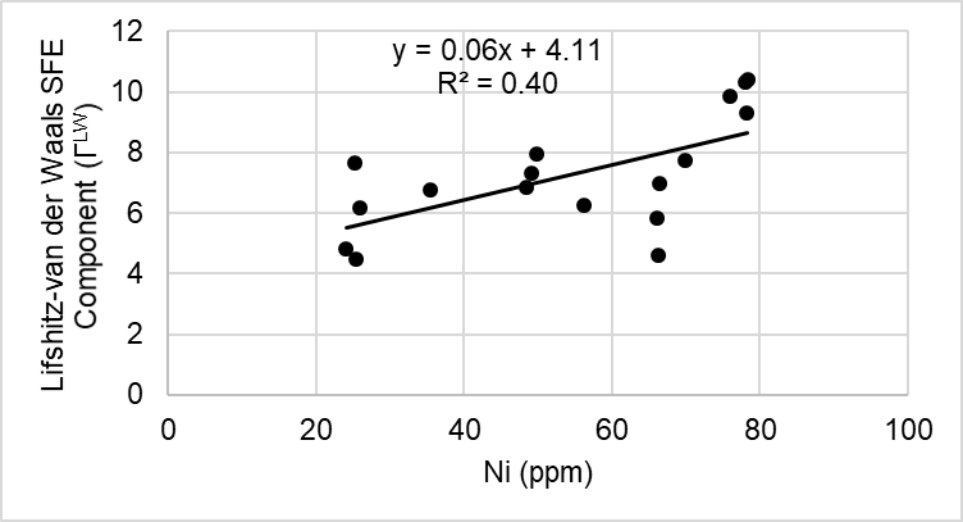

Figure 4.7 Correlation between Lifshitz-van der Waals SFE Component (Γ^{LW}) and Nickel (Ni)

4.1.3. Total Acid Number Test

Figure 4.8(a) and 4.8(b) present the results of the total acid number test conducted on S1 PG 64-22 and S3 PG 76-28 binders. From Figure 4.8(a), it was observed that the acid values of the S1 PG 64-22 reduced with the addition of W1 additive and A1 antistripping agent. Both the W1 additive and A1 antistripping agent are amine-based additives, basic in nature. Therefore, the addition of W1 and A1 additives reduced the acidic properties as well as acid value of the S1 PG 64-22 binder. The result was found to be consistent with the acid/base ratio (Γ^+/Γ^-) of S1 PG 64-22 binder. The Γ^+/Γ^- value was found to reduce from 2.66 to 2.36 and 1.80 with addition of 0.5% W1 and 0.5% A1 additives, respectively, indicating increase in basic nature of the binder.

However, for S3 PG 76-28 binder (Figure 4.8(b)), no significant changes in the acid values were observed with the addition of W1 additive. Also, the acid values increased from 0.40 to 0.46 with the addition of 0.5% A1 antistripping agent. From DWP test, the Γ^+/Γ^- component was found to increase with the addition of W1 and A1 additive, indicating increase in acidic behavior of the binder. The reaction of the polymer presents in the binder and the chemical constituents of W1 and A1 additives may be responsible for such changes in the acid values and Γ^+/Γ^- component of the S3 PG 76-28 binder. Also, the addition of 1.5% PPA was found to increase the acid number significantly. An increase in the acid number was expected as it will require more KOH to compensate for the unbonded PPA present in the binder. However, from the DWP test, PPA modification did not exhibited an increase in acid SFE

component. As the base binder's constituents, functional groups and type and amount of polymer are unknown, it is difficult to comment on the mechanism behind this phenomenon. Further studies involving different amount of PPA and aging processes are needed to properly understand this characteristic.

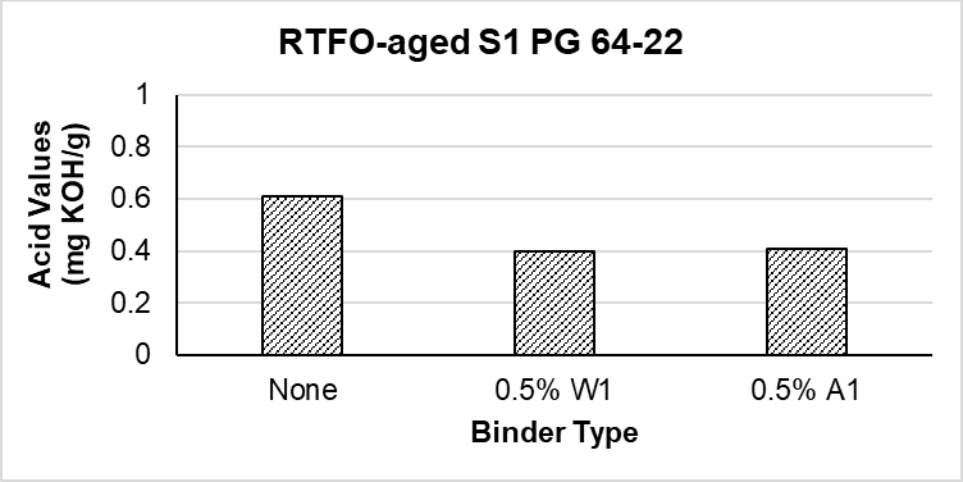

(a)

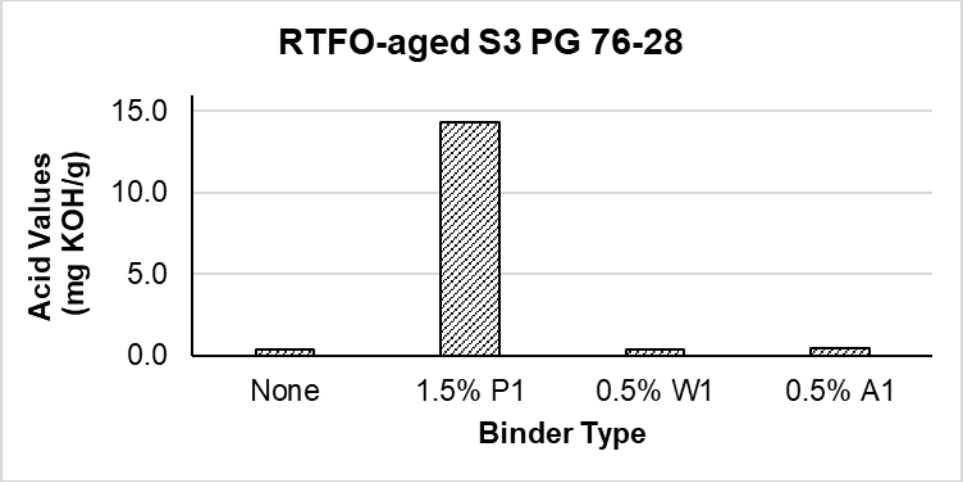

(b)

Figure 4.8 Acid values of (a) RTFO-aged S1 PG 64-22 and (b) RTFO-aged PG 76-28 binders

4.1.4. Fourier Transform Infrared Spectroscopy (FTIR) Test

The FTIR test was conducted on all the binder blends after RTFO-aged conditioning. The FTIR spectra for all the binders are presented in Appendix C. Figure 4.9 (a) and 4.9 (b) present the FTIR spectra for S1 PG 64-22 and S3 PG 76-28 binders, respectively. The FTIR

spectra of molecular compounds feature absorption bands that can be associated with specific functional groups. According to Yoon and Tarrer (1988), the functional groups of an asphalt that are adsorbed on an aggregate surface come mainly from the acid fraction of the asphalt. Bagampadde et al. (2006) used the peaks corresponding to carbonyl (C=O) stretch (1710–1690 cm^{-1}) of infrared absorbance to characterize the moisture-induced damage potential of binder. Different functional groups like carboxylic acids, 2-quinolones, ketones and anhydrides can be characterized using the peaks on that region. Yoon and Tarrer (1988) reported that the presence of ketones and phenolics is expected to improve moisture-induced damage resistance. However, on the other hand, carboxylic acids, anhydrides, and 2-quinolenes form bonds on the aggregate surface which is highly soluble to water. Therefore, the presence of these functional groups is expected to increase moisture-induced damage potential.

From Figure 4.9(a), the FTIR spectrum of S1 PG 64-22 binder was found to exhibit a prominent peak at 1,705 cm^{-1} indicating the presence of different acidic functional groups. With the addition of 0.5% W1 and 0.5% A1 additive, broader band peaks were observed around this frequency. This indicates a reduction in the acid functional groups with the addition of W1 and A1 additive. However, the addition of 20% RAP was found to exhibit a prominent peak at 1,705 cm^{-1}. The appearance of acidic functional groups at 1705 cm^{-1} peak was found to be consistent with acid values as well as the acid/base SFE ratio (Γ^+/Γ^-) of the PG 64-22 binder. Bagampadde et al. (2006) also reported a good correlation between the acid numbers and the integrated peak areas of the spectra.

From Figure 4.9(b), the presence of Styrene-Butadiene-Styrene (SBS) polymer modifier in the S3 PG 76-28 binder was detected through the appearance of butadiene peak at 965 cm^{-1}. The FTIR spectra of S3 PG 76-28 binder also exhibited a prominent peak at carbonyl region. However, with the addition of 0.5% W1, 0.5% A1 and 20% R1, the peak at carbonyl region became more prominent indicating an increase in acidic behavior. The acid values and the acid/base SFE ratio (Γ^+/Γ^-) were also found to follow a similar trend. The addition of PPA to S3 PG 76-28 binder did not add new functionality to the binder. However, the peak at 1,705 cm^{-1} was found to disappear with addition of PPA. The reduction of acid/base SFE ratio (Γ^+/Γ^-) was found to be consistent with the disappearance of the peak.

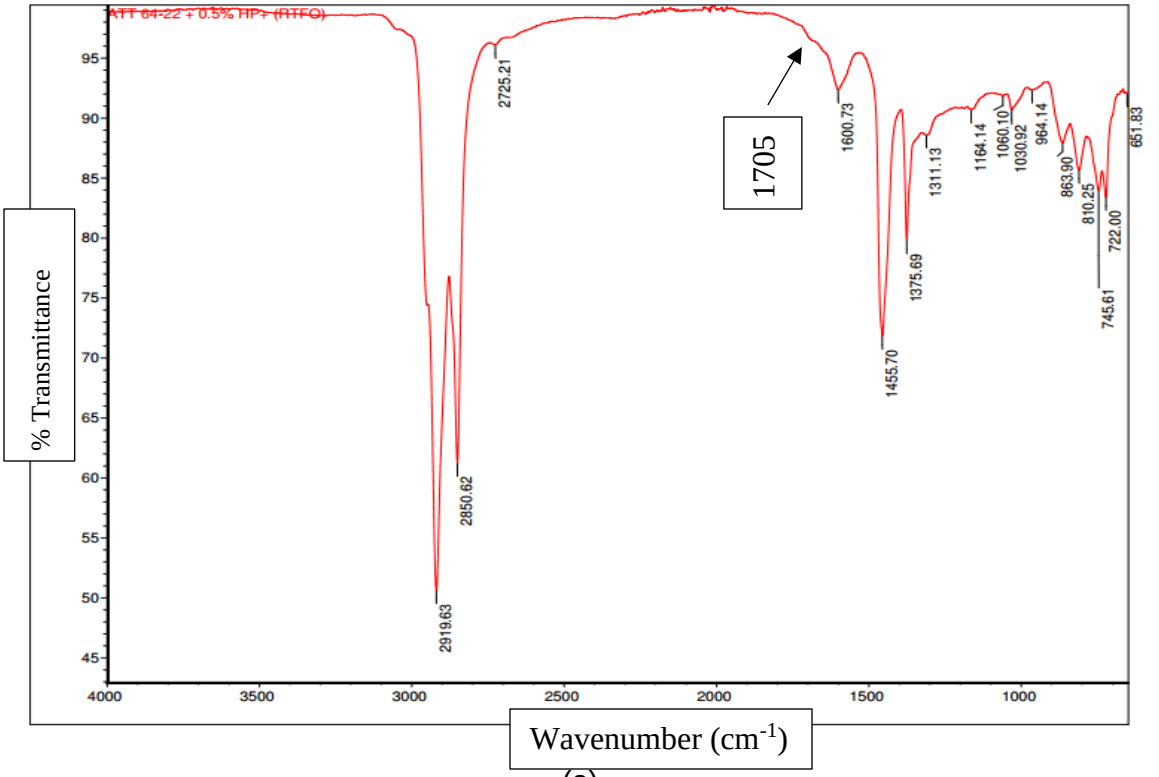

(a)

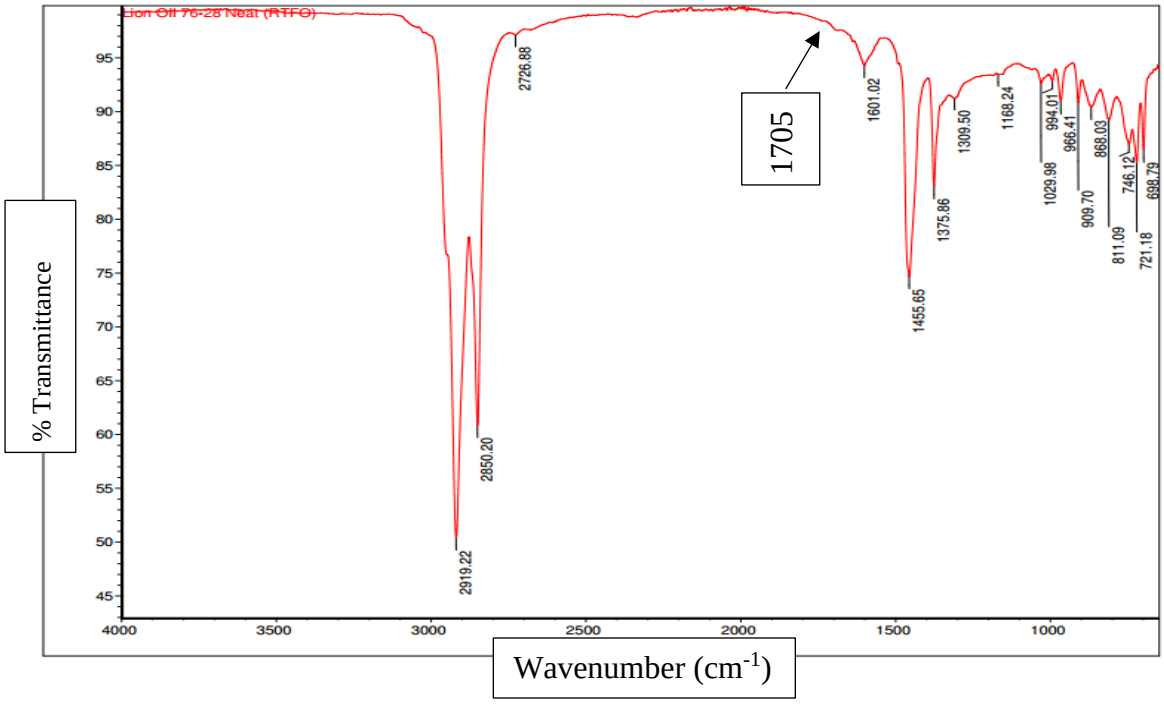

(b)

Figure 4.9 FTIR Spectra of (a) RTFO-aged S1 PG 64-22 and (b) RTFO-aged S3 PG 76-28 binders

4.1.5. Sessile Drop Test

4.1.5.1. Contact Angles of Asphalt Binders

In addition to dynamic Wilhemy plate (DWP) tests, sessile drop tests were conducted to on all the binders under RTFO-aged conditioned and are presented in Appendix E. The contact angles of the asphalt binder blends with three different probe liquids, namely water, ethylene glycol (EG) and diiodomethane (DIM) were used to calculate the SFE components of the corresponding binders. The contact angles of RTFO-aged S1 PG 64-22 and S3 PG 76-28 binders with different additives are presented in Figure 4.10 (a) and 4.10 (b). The contact angle of binder with water by SD method was found to be different than the DWP method. However, in most of the cases the changes in the contact angles with the addition of different additives were found to be similar to that of the DWP method. For example, the contact angle of the S1 PG 64-22 binder was found to reduce with the addition of W1 and A1 additives. A reduction in the contact angle with W1 and A1 additive was also observed from the DWP method.

4.1.5.2. Surface Free Energy Components of Asphalt Binder

The surface free energy components of all the binder blends were determined using SD method and are presented in Appendix E. Figures 4.11 (a) and (b) present the SFE components of S1 PG 64-22 and S3 PG 64-22 binders. It was observed that the magnitude of the energy components varies with test methods. For example, the total SFE (Γ^{Total}) component of S1 PG 64-22 binder obtained from the DWP method was 11.53 mJ/m^2 whereas the same component by the SD method was 39.03 mJ/m2. In most cases the SFE components from the SD method exhibited a similar trend as by the DWP method. However, some discrepancies were observed between the two methods. For example, the addition of PPA was found to reduce the acid SFE component in the DWP method, however, the results exhibited an increase in the acid SFE component in the SD method. The inconsistency is believed to be due to the differences in the mechanisms used by these two methods.

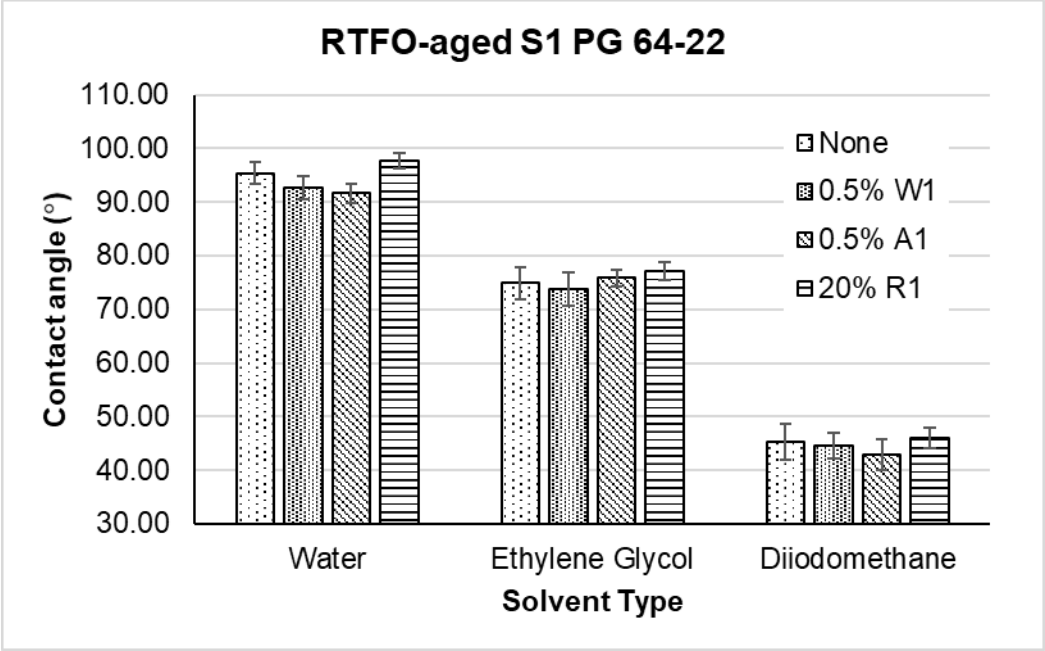

(a)

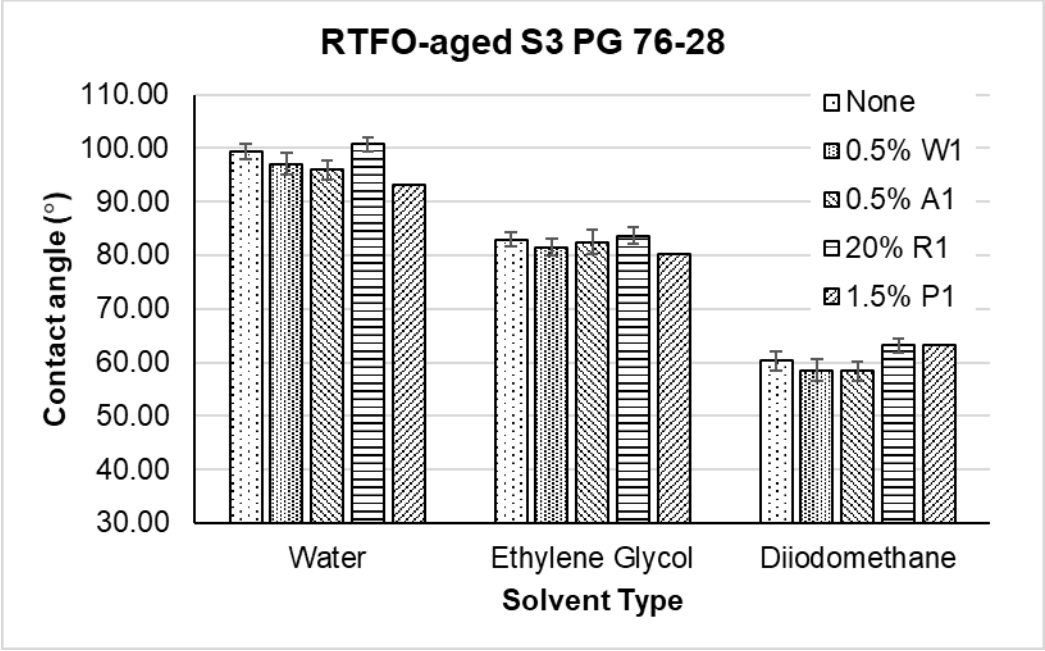

(b)

Figure 4.10 Contact Angles of (a) RTFO-aged S1 PG 64-22 and (b) RTFO-aged PG 76-28 binders with different solvents from SD method

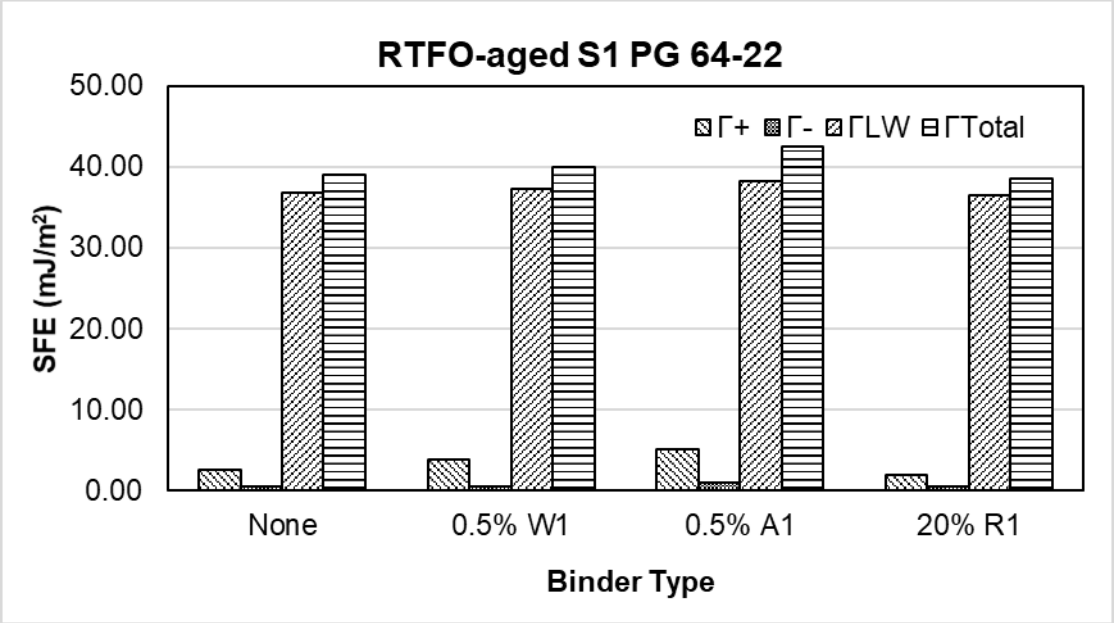

(a)

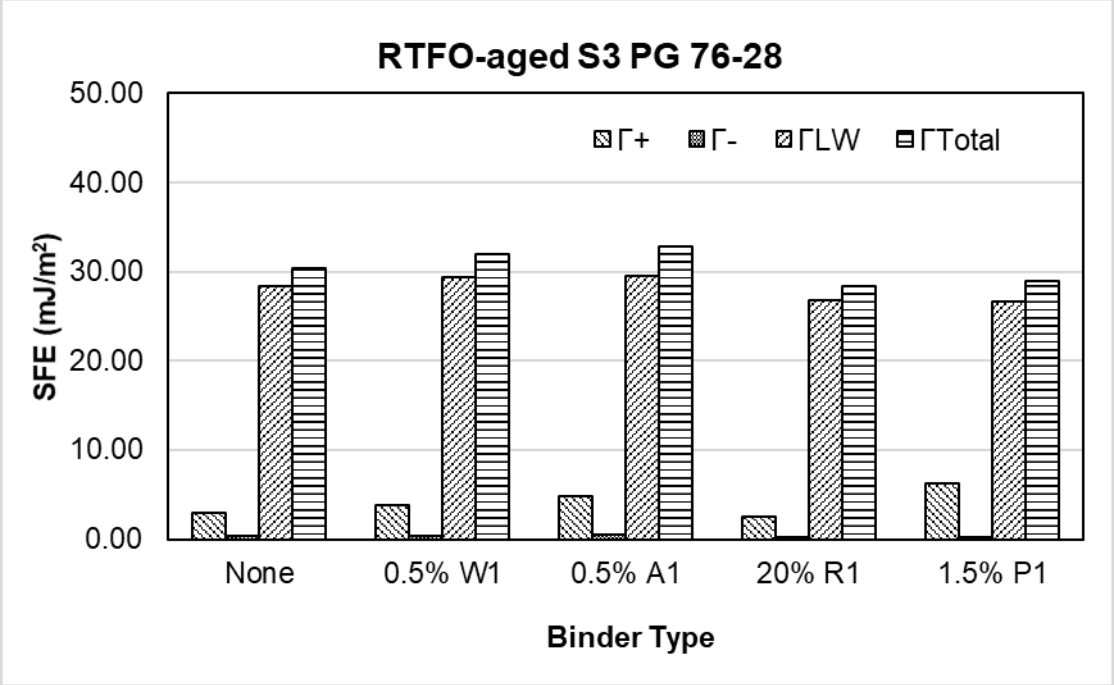

(b)

Figure 4.11 Surface free energy components of (a) RTFO-aged S1 PG 64-22 and (b) RTFO-aged PG 76-28 binders with different solvents from SD method

4.2. Aggregates Test Results

4.2.1. Universal Sorption Device (USD) Test

Surface free energy components of three different types of aggregates, namely limestone, granite and rhyolite from five different Oklahoma quarries were determined in this study. Each aggregate was tested with each of the three probe vapors, namely water, MPK and n-Hexane in a Universal Sorption Device. A proprietary software associated with this device was used to determine the adsorption isotherms for the tested aggregates. Equation (9) was used to calculate the spreading pressure for the aggregate with probe vapors. The specific surface areas of the aggregates were calculated from the adsorption isotherm of n-Hexane with a projected area of n-Hexane molecule as 56 $Å^2$. The surface free energy components of the aggregate were calculated by combining the spreading pressures from different probe vapors using equations (10) and (11). Table 4.1 presents the specific surface area and spreading pressure measured using the USD test for all the tested Oklahoma aggregates.

The specific surface area of the aggregates was found to vary from 0.30 m^2/g to 1.83 m^2/g, depending on the aggregate source. The Limestone 1 and rhyolite aggregates were found to exhibit the smallest and the largest specific surface areas, respectively. Also, the spreading pressure of the aggregates was found to vary significantly with the aggregate types and did not exhibit any particular trend with all probe vapors. The SFE components of the tested aggregates are presented in Figure 4.12. The basic components of all the aggregates were found to be higher than their acidic and Lifshitz-van der Waals (Γ^{LW}) components. The highest and the lowest basic components were observed for granite and Limestone 1 aggregates, respectively. According to Bhasin (2007), the adhesion between the binder and aggregate is significantly influenced by the large magnitude of base component of the aggregates. The magnitude of acid component is very small and was found to vary from 1.46 mJ/m^2 to 50.62 mJ/m^2. The non-polar or Lifshitz-van der Waals (Γ^{LW}) components of the surface free energy varied from 52.93 to 59.67 mJ/m^2 for different aggregates which is similar to that reported by Bhasin (2007). Although the difference in non-polar component (Γ^{LW}) between aggregates is not significant, it is expected to exhibit significant effect on adhesion bonding between binder and aggregates (Bhasin, 2007).

Table 4.1 Specific surface area and spreading pressure of aggregate

Aggregate Type	Specific Surface Area (m^2/g)	Spreading Pressure with Water (mJ/m^2)	Spreading Pressure with MPK (mJ/m^2)	Spreading Pressure with n-Hexane (mJ/m^2)
Limestone 1	0.30	189.6	78.2	27.8
Limestone 2	0.87	295.3	88.5	29.5
Limestone 3	1.50	364.3	76.8	28.0
Granite	0.74	440.7	38.5	28.8
Rhyolite	1.83	491.4	87.4	25.6

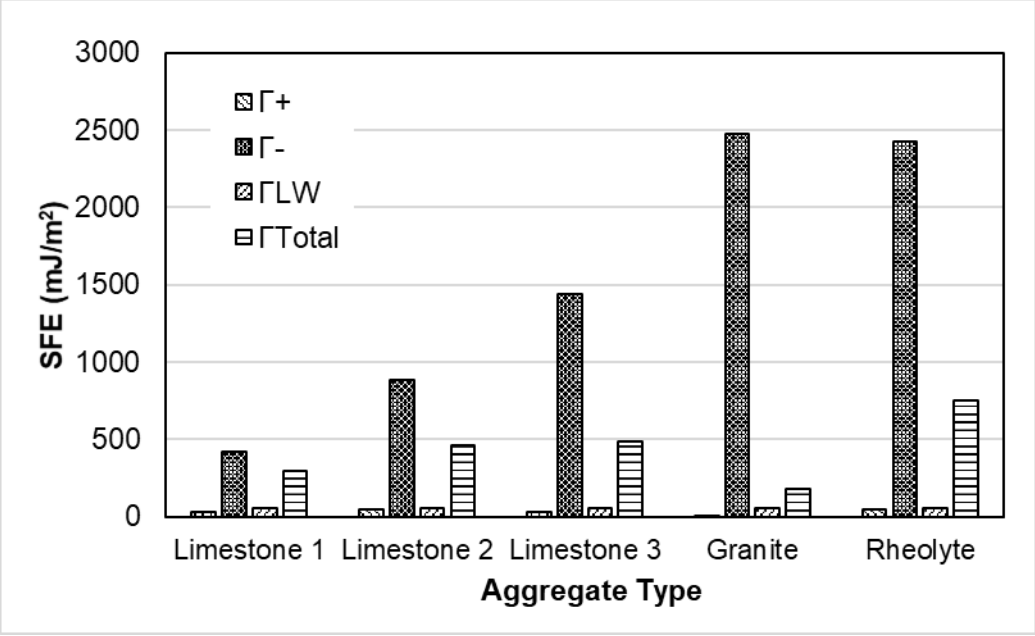

Figure 4.12 Surface free energy components of aggregates from USD test

4.2.2. X-Ray Fluorescence (XRF) Test

Tarrer and Wagh (1991) reported that the mineralogical and chemical composition of an aggregate significantly affect the moisture-induced damage potential of an asphalt mix. According to Tarrer and Wagh (1991), the surface energy and chemical reactivity of the aggregate are influenced by the mineralogical and chemical composition of the aggregate. Based on their affinity for water, aggregates are classified as hydrophilic (water loving) or hydrophobic (water hating) in nature. Typically, hydrophilic aggregates exhibit a high silica content. On the other hand, hydrophobic aggregates exhibit a low silica content.

The XRF test was conducted on all five aggregates used in this study and their mineralogical compositions are presented in Table 4.2. It was observed that all the limestone aggregates mostly composed of $CaCO_3$, carbonaceous in character. The amount of CaO was found to vary from 85.4% to 90.2 % in limestones from different sources. On the other hand, granite and rhyolite exhibited high amount of silica (SiO_2) in their composition. It was observed that the granite and rhyolite contained 74.8% and 64.9% of silica whereas the amount of silica for limestone aggregate varied between 6.5% to 9.7%. Therefore, the granite and rhyolite are expected to exhibit higher hydrophilicity than the limestone aggregates. This indicates that the use of granite and rhyolite aggregate in a mix may increase the potential to moisture-induced damage. Other studies also reported an increase in moisture-induced damage potential with granite aggregate and a reduction of the same with limestone aggregate. Among the three limestone sources, Limestone 3 contained the highest silica and may exhibit higher potential for moisture-induced damage.

Table 4.2 Mineral composition of aggregates from XRF tests

Aggregate Type	Na_2O (%)	MgO (%)	Al_2O_3 (%)	SiO_2 (%)	P_2O_5 (%)	K_2O (%)	CaO (%)	TiO_2 (%)	MnO_2 (%)	Fe_2O_3 (%)	Others (%)
Limestone 1	0.0	2.9	1.2	6.6	0.0	0.5	85.4	0.1	0.0	2.0	1.3
Limestone 2	0.0	1.4	1.0	6.5	0.0	0.2	90.2	0.0	0.0	0.3	0.3
Limestone 3	0.0	2.0	1.5	9.7	0.0	0.2	85.8	0.0	0.0	0.4	0.3
Granite	3.9	0.1	11.4	74.8	0.0	5.9	0.8	0.2	0.1	2.4	0.4
Rhyolite	3.1	1.4	12.2	68.9	0.3	4.0	1.5	1.3	0.2	6.8	0.5

4.2.3. Effect of Lime Treatment on SFE Components of Aggregate

The USD tests were conducted on all the five aggregate after treating them with 2% hydraulic lime. It was found that the specific surface area of the limestone aggregates increased with the addition of lime, whereas, the specific surface area reduces for granite and rhyolite aggregates (Appendix F). Comparing Figures 4.12 and 4.13 after lime treatment revealed that the basic components were still higher than the acidic and Lifshitz-van der Waals (Γ^{LW}) components for all the aggregates. Also, the basic SFE components of all the aggregates (except Limestone 3) were found to increase with the lime treatment. The rhyolite aggregate exhibited the highest change (2.49 times) in basic SFE component compared to that of other aggregate. Generally, the Ca^{2+} from lime migrate to the surface and replace H^+, Na^+, K^+ and other cations from the aggregate surface. The Ca^{2+} is relatively hydrophobic in nature and

responsible for increase in base components (Wasiuddin et al., 2010). The acid components were found to increase for Limestone 3, rhyolite and granite aggregates whereas, reduced for Limestone 1 and Limestone 2 aggregates. The granite aggregate exhibited the highest changes in acid components among all the aggregates after the lime treatment. It was observed that the changes in the Lifshitz-van der Waals (Γ^{LW}) components of different aggregates were insignificant after lime treatment.

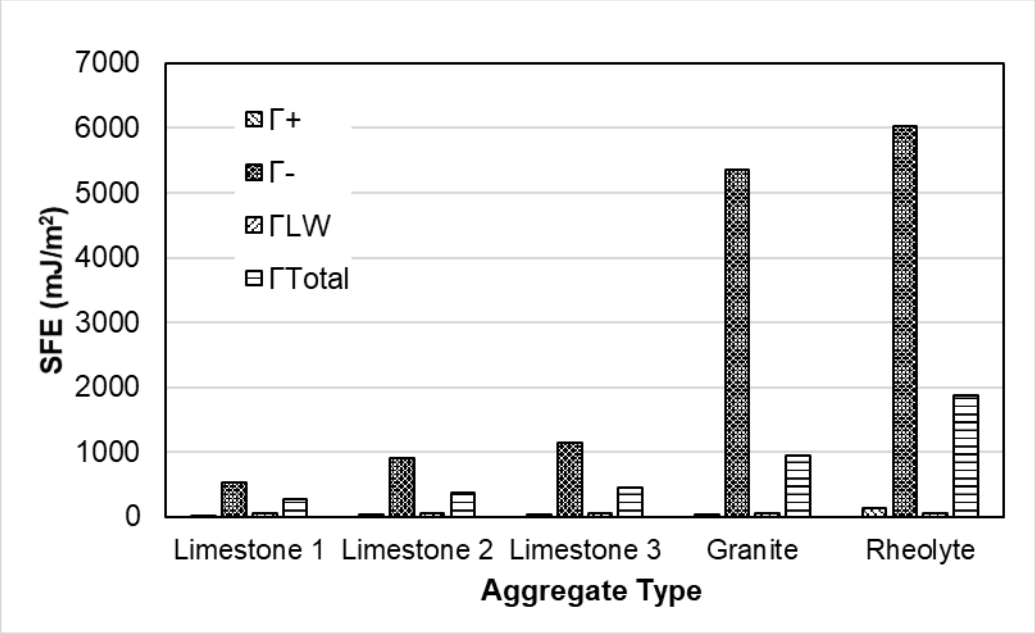

Figure 4.13 Surface free energy components of lime treated aggregates from USD test

4.2.4. Sessile Drop Test

4.2.4.1. Contact Angles and Surface Free Energy Components of the Aggregates

The contact angles of the aggregates with water, ethylene glycol and diiodomethane are presented in Figure 4.14. The contact angles were found to vary significantly with different aggregates. The contact angles were used to calculate the SFE components of the aggregates and are presented in Figure 4.15. Similar to USD test, the basic component of the aggregates was found to be higher than the other SFE components. However, the SFE components from USD method is by an order of magnitude higher than those from SD method (Koc and Bulut, 2013). The USD method is based on the absorption of probe vapor on the surface of the aggregate, whereas, the SD method uses static contact angle of a solvent on the aggregate surface to calculate SFE component. Among all the aggregates, the granite aggregate exhibited

highest basic SFE component which was also observed from USD test. Also, from Figure 4.14, differences in the SFE components of the limestone aggregates were observed for different sources.

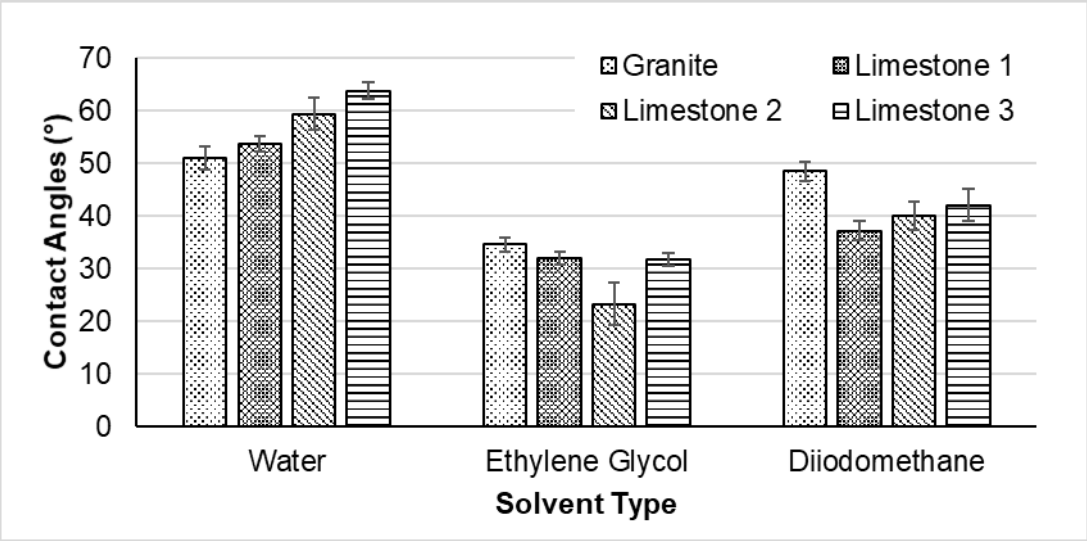

Figure 4.14 Contact angles of aggregates with different solvent from SD test

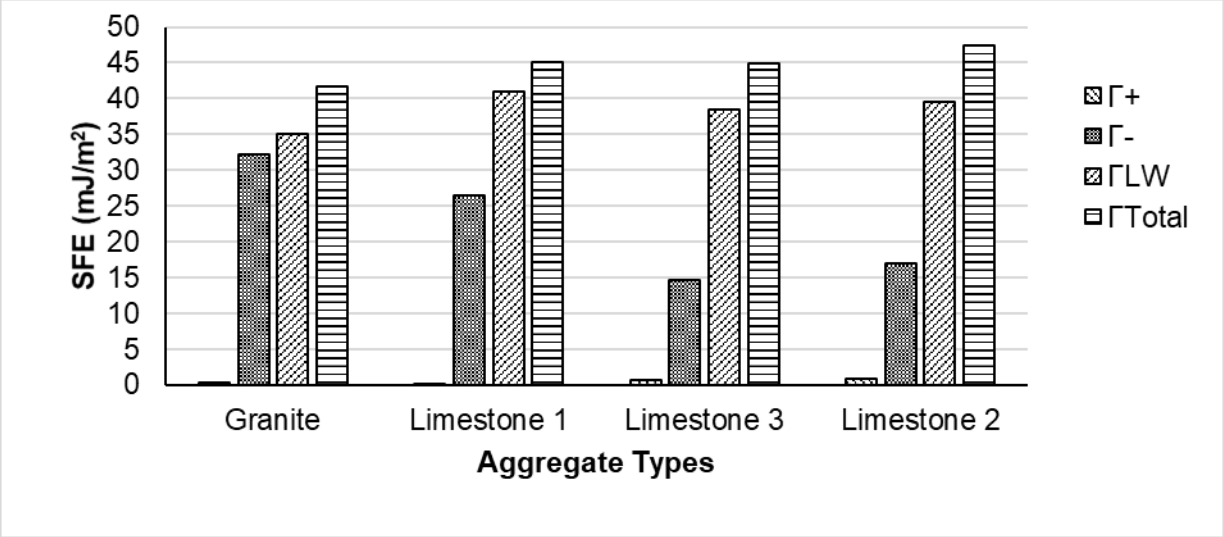

Figure 4.15 Surface free energy components of aggregates from SD test

4.3. Evaluation of Moisture-induced damage potential of binder-aggregate system using SFE Technique

In this study, the moisture-induced damage potential of different binder-aggregate combinations were evaluated using the SFE technique is the results are presented in Appendix I and J. For convenience, the moisture-induced damage potentials of S1 PG 64-22 and S3 PG

76-28 binders and Limestone 1 aggregate are presented in the following sections. Also, the SFE components obtained from the DWP method for binders and USD method for aggregates were used in the discussion. The moisture-induced damage potential of the binder-aggregate systems obtained from the SD method can be found in Appendix J.

4.3.1. Effect of WMA Additive

Figures 4.16 (a) and 4.16 (b) present the spreading coefficient ($S_{A/S}$), work of adhesion ($W_{A/S}$) and work of debonding (W_{ASW}^{wet}) of the RTFO-aged S1 PG 64-22 and RTFO-aged S3 PG 76-28 binder with Limestone 1 aggregate, respectively. The spreading coefficient is generally a positive value. A higher magnitude of spreading coefficient of an aggregate–asphalt binder system means a greater tendency of the liquid asphalt binder to wet and coat the surface of that aggregate (Buddhala et al., 2011). This indicates possibility of better bonding between asphalt binder and aggregate systems which may reduce the moisture-induced damage potential of the asphalt mixes. From Figure 4.16(a), the $S_{A/S}$ of S1 PG 64-22 binder was found to reduce with the addition of 0.5% W1 additive. For example, the S1 PG 64-22 binder containing 0.5% chemical WMA additive exhibited 5% reduction in the $S_{A/S}$ when it was compared with the neat S1 PG 64-22 binder. However, an increase in the spreading coefficient was observed when 0.5% WMA additive was used with S3 PG 76-28 binder. This observation indicated that the use of W1 additive is expected to enhance S3 PG 76-28 binder's ability to wet and coat the surface of the Limestone 1 aggregate. Other studies also reported an increase in the spreading coefficient with the addition of WMA additive (Wasiuddin et al., 2008; Buddhala et al., 2011; Ghabchi et al., 2013).

As noted earlier, a higher work of adhesion ($W_{A/S}$) value indicates a stronger bond between asphalt binder and aggregate under dry condition. The SFE components of the binders were combined with the SFE components of Limestone 1 aggregate to determine the adhesion between combinations of different binders with Limestone 1 aggregate. From Figure 4.16(a), it was found that the S1 PG 64-22 binder exhibited a slight reduction in the $W_{A/S}$ value from 110.5 mJ/m^2 to 108.1 mJ/m^2 with the addition of chemical WMA additive. On the other hand, the $W_{A/S}$ for S3 PG 76-28 binder increased with the addition of 0.5% W1 additive. Therefore, it can be concluded that the S3 PG 76-28 containing W1 additive, when used in an asphalt mix with Limestone 1 aggregate, may exhibit increased durability and better bonding than the one without any additive.

Generally, the work of debonding (W_{ASW}^{wet}) for a specific binder-aggregate system in the presence of water is negative, which indicates that the process is thermodynamically favorable for debonding of asphalt binder and aggregate. A lower magnitude of $|W_{ASW}^{wet}|$ is desirable as it reduces the tendency of the binder-aggregate system to debond. On the contrary, a higher magnitude indicates a greater tendency of debonding between asphalt binder and aggregate. From Figure 4.16(a), the magnitude of the $|W_{ASW}^{wet}|$ value of S1 PG 64-22 binder was found to increase from 129.6 mJ/m^{2}to 132.2 mJ/m^2 indicating an increase in moisture-induced damage potential for binder-aggregate system upon addition of WMA additive. The $|W_{ASW}^{wet}|$ for S3 PG 76-28 binder with Limestone 1 aggregate was found to be 138.2 mJ/m^2, whereas the same values for binder containing 0.5% W1 additive was 132.5 mJ/m^2. Based on the results of the W_{ASW}^{wet}, it can be concluded that the addition of W1 additive may increase the moisture-induced damage resistance of an asphalt mix containing S3 PG 76-28 binder but may reduce it for S1 PG 64-22 binder.

The ER_1 and ER_2 parameters proposed by Bhasin et al. (2007b) were used to evaluate the moisture-induced damage potential of different combinations of S1 PG 64-22 and S3 PG 76-28 binders with the Limestone 1 aggregate and are presented in Figures 4.17 (a) and 4.17 (b). It was found that the ER_1 reduced from 0.85 to 0.82 with the addition of WMA additive to S1 PG 64-22 binder. However, for S3 PG 76-28 binder, the ER_1 value increased from 0.68 to 0.75 upon addition of 0.5% WMA additive. The ER_2 parameter was found to follow a similar trend as ER_1. Therefore, it can be concluded that the WMA additive is expected to help reduce the moisture-induced damage potential of the S3 PG 76-28 binder whereas will increase the moisture-induced damage potential for asphalt mixes with S1 PG 64-22 binder.

4.3.2. Effect of Antistripping agent

The effect of the addition of antistripping agent to RTFO-aged S1 PG 64-22 and RTFO-aged S3 PG 76-28 binders on their moisture-induced damage potential can be observed from Figure 4.16 (a) and 4.16 (b). The coating ability of the S1 PG 64-22 binder was found to reduce with the addition of antistripping agent. The magnitude of the $S_{A/S}$ was observed to reduce from 87.4 mJ/m^2 to 83.8 mJ/m^2 for S1 PG 64-22+0.5% A1 binder. Similar to the S1 PG 64-22+0.5% W1 binder, a slight reduction in the magnitude of work of adhesion and work of debonding was observed with the addition of antistripping agent. Therefore, Limestone 1 aggregate and the S1 PG 64-22+0.5% A1 binder are expected to produce a mix which will exhibit a higher moisture-induced damage potential than the neat binder. From Figure 4.17(a), the reduction of the ER_1

value from 0.85 to 0.82, with the addition of A1 additive, also indicated a reduction in resistance to moisture-induced damage. Similar reduction in moisture-induced damage resistance with using an antistripping agent was reported by Wasiuddin et al. (2007b) for basic aggregates.

The spreading coefficient ($S_{A/S}$) of the S3 PG 76-28 binder exhibited significant increase with the addition of A1 antistripping additive. Also, the work of adhesion ($W_{A/S}$) increased and the magnitude of work of debonding $|W_{ASW}^{wet}|$ reduced with Limestone 1 aggregate as A1 antistripping agent was added to the binder blend. The energy ratios were also found to increase significantly for S3 PG 76-28+0.5% A1 binder. As a result, the S3 PG 76-28+0.5% A1 binder and Limestone 1 aggregate system is expected to have a higher resistance to moisture-induced damage than Limestone 1 with S3 PG 76-28 binder without antistripping agent.

4.3.3. Effect of Reclaimed Asphalt Pavement (RAP)

The addition of simulated RAP binder was found to increase the spreading coefficient ($S_{A/S}$) and work of adhesion ($W_{A/S}$) for both S1 PG 64-22 and S3 PG 76-28 binders with Limestone 1 aggregate. Therefore, the aggregate is expected to be better coated with binder and the adhesion of binder-aggregate system are expected to be higher for both unmodified and polymer-modified binders containing R1 RAP. The magnitude of the work of debonding was also found to decrease after RAP addition. The reduction was higher for polymer-modified PG 76-28 binder. Also, the energy ratios of the binder-aggregate system were found to increase upon the addition of 20% simulated RAP. Ghabchi et al. (2014) reported a similar increase in energy ratios with simulated RAP. Overall, the addition of RAP is expected to reduce moisture-induced damage for all binder and Limestone 1 aggregate combinations.

4.3.4. Effect of Polyphosphoric Acid

From Figure 4.16(b), the $S_{A/S}$ was found to decrease with an increase in the PPA content in the blend. The PG 76-28 binder containing 1.5% PPA was found to exhibit a $S_{A/S}$ of 68.8 mJ/m^2 which is approximately 10% lower than the $S_{A/S}$ of the neat binder. This observation indicated that the use of PPA is expected to reduce binder's ability to wet and coat the surface of Limestone 1 aggregate.

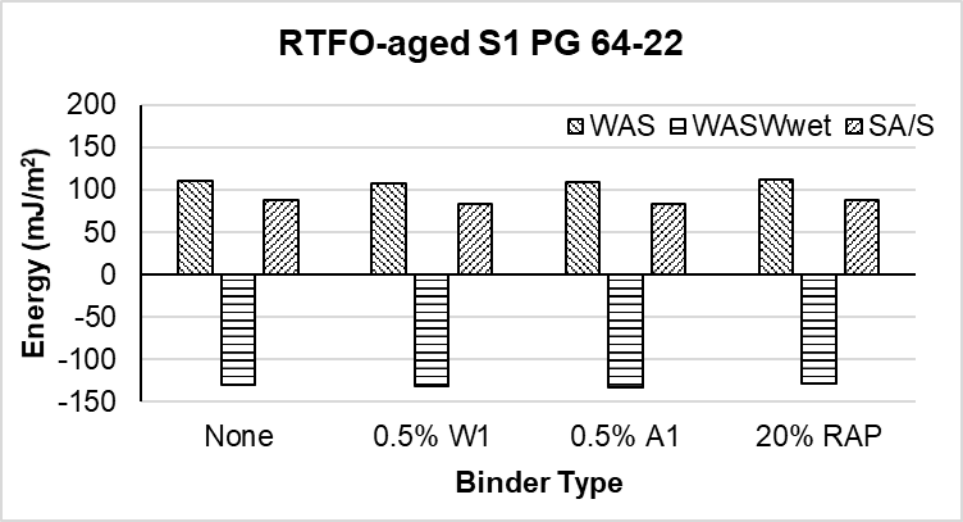

(a)

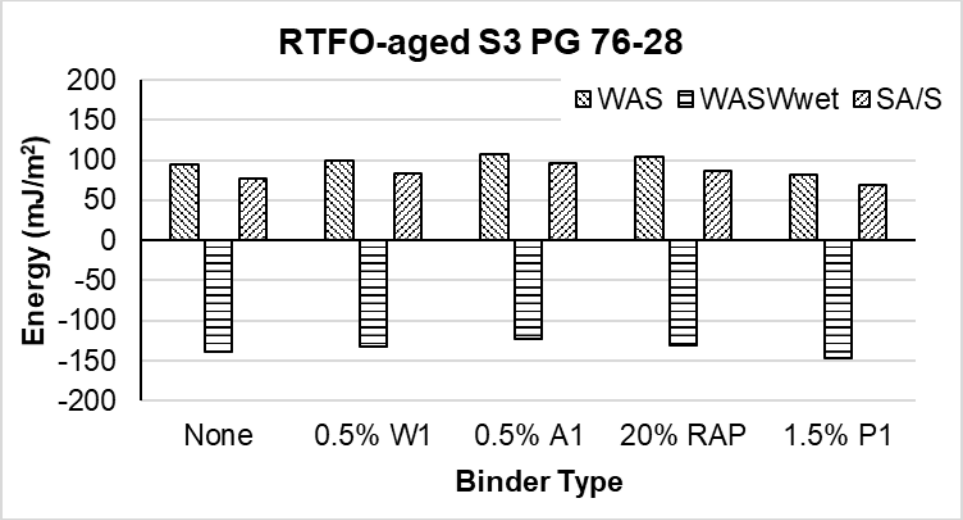

(b)

Figure 4.16 Work of adhesion, work of debonding and spreading coefficient of (a) RTFO-aged S1 PG 64-22 and (b) RTFO-aged S3 PG 76-28 binder with Limestone 1 aggregate

It was observed that the $W_{A/S}$ for PG 76-28 binder decreased due to the addition of 1.5% PPA. The work of adhesion for PG 76-28 binder containing 1.5% PPA was found to be 81.8 mJ/m^2, whereas the PG 76-28 binder exhibited a $W_{A/S}$ of 94.3 mJ/m^2. Also, the magnitude of the $|W_{ASW}^{wet}|$ was found to increase upon the addition of PPA. The $|W_{ASW}^{wet}|$for the PG 76-28 binder with limestone aggregate was found to be 138.2 mJ/m^2, whereas the same for the PPA-modified binder was 146.9 mJ/m^2. Based on the results of the $W_{A/S}$ and W_{ASW}^{wet}, it can be concluded that the addition of PPA may reduce the resistance of an asphalt mix containing Limestone 1 aggregate to moisture-induced damage. The ER_1 also reduced with the addition of PPA. The

reduction in the moisture damage resistance of a PPA-modified binders with limestone aggregate was also reported in other studies (Reinke and Glidden, 2010; Al-Qadi et al., 2014). Use of an anti-stripping agent with PPA-modified binder was recommended for a better moisture resistance performance (Fee et al., 2010).

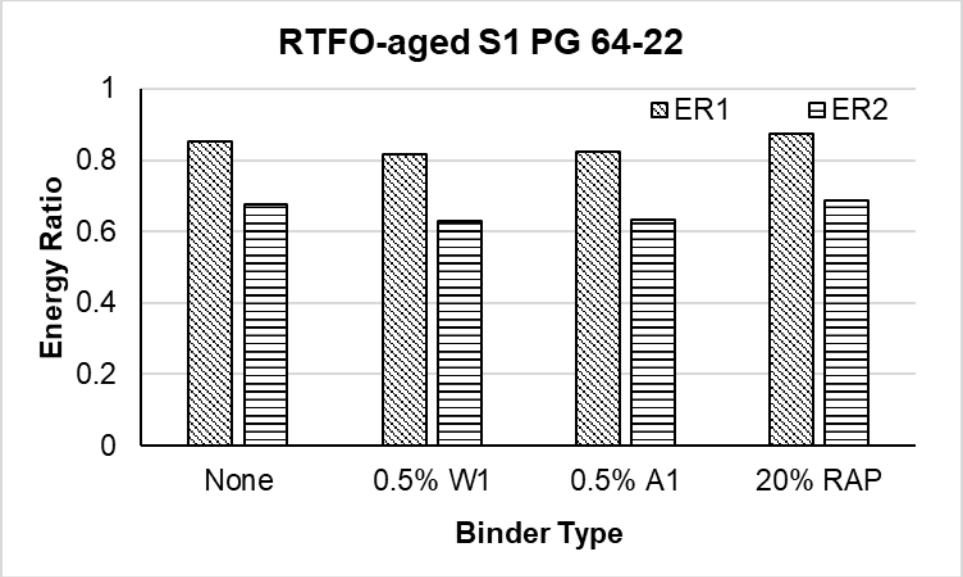

(a)

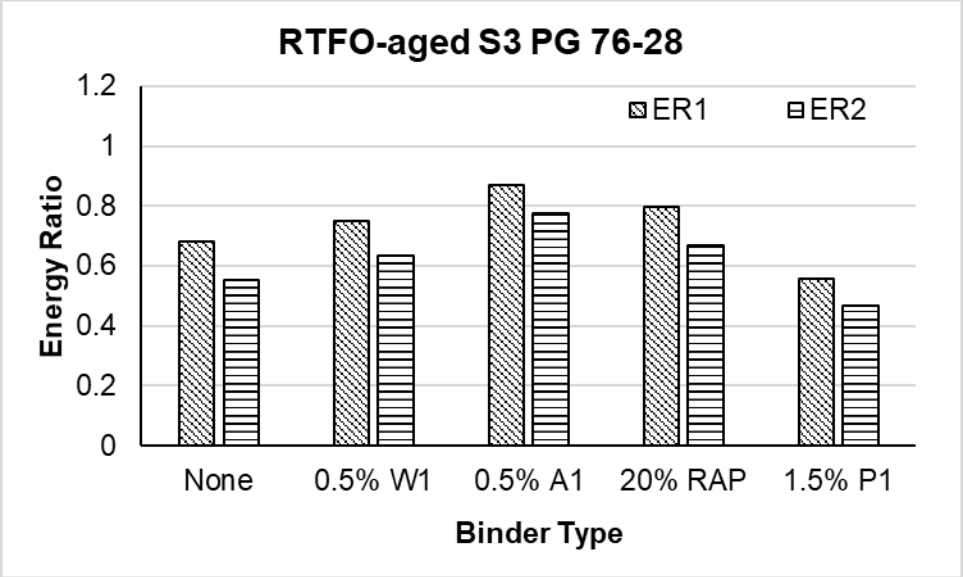

(b)

Figure 4.17 Energy ratios (ER_1 and ER_2) of (a) RTFO-aged S1 PG 64-22 and (b) RTFO-aged S3 PG 76-28 binder with Limestone 1 aggregate

4.3.5. Effect of Aging

Figure 4.18 (a) and 4.18 (b) present the spreading coefficient ($S_{A/S}$), work of adhesion ($W_{A/S}$), and work of debonding (W_{ASW}^{wet}) of the PAV-aged S1 PG 64-22 and PAV-aged S3 PG 76-28 binders with Limestone 1 aggregate, respectively. Comparing Figure 4.16(a) and 4.18 (a), the $S_{A/S}$ value of the S1 PG 64-22 binder was found to reduce with long-term aging. Also, the work of adhesion ($W_{A/S}$) reduced and work of debonding increased for PAV-aged S1 PG 64-22 binder. The ER_1 was also found to decrease from 0.85 to 0.80 indicating higher moisture-induced damage susceptibility for PAV-aged binder. A similar trend was observed for S1 PG 64-22+20% R1 binder. However, with long-term aging, no significant variation in moisture-induced damage potential was observed with the addition of WMA additive. Also, the S1 PG 64-22+0.5% A1 binder exhibited an increase in resistance to moisture-induced damage with aging as the ER_1 value increased from 0.82 for RTFO-aged to 0.86 for PAV-aged binder.

For S3 PG 76-28 binder, the moisture-induced damage potential of asphalt mixes was found to reduce with long-term aging for neat, WMA additive-modified and RAP-modified binders. For example, the ER_1 value for neat S3 PG 76-28 binder was found to increase from 0.68 to 1.07 with PAV-aging. Asphalt binder with polymer modification was observed to be less susceptible to oxidative aging than the non-polymer modified binder. As a result, the moisture-induced damage potential was found to be less affected by long-term aging. However, the antistripping agent was found to exhibit opposite trend, i.e. increase in moisture-induced damage potential with long-term aging. Wasiuddin et al. (2007b) also observed a similar phenomenon. According to Wasiuddin et al. (2007b), a reduction of basic nature of the antistripping agent-modified binder with aging is responsible for this increase in moisture-induced damage potential of the binder-aggregate system. The effect of PAV-aging on PPA-modified binder was also pursued but not successful. The S3 PG 76-28 binder became very stiff after PAV-aging which made it difficult to prepare good sample for dynamic Wilhelmy plate (DWP) test.

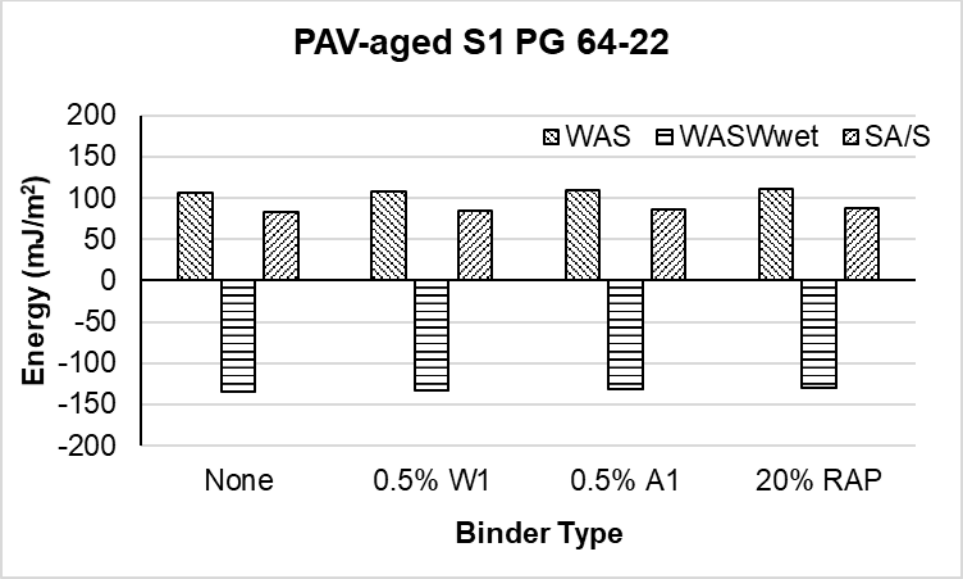

(a)

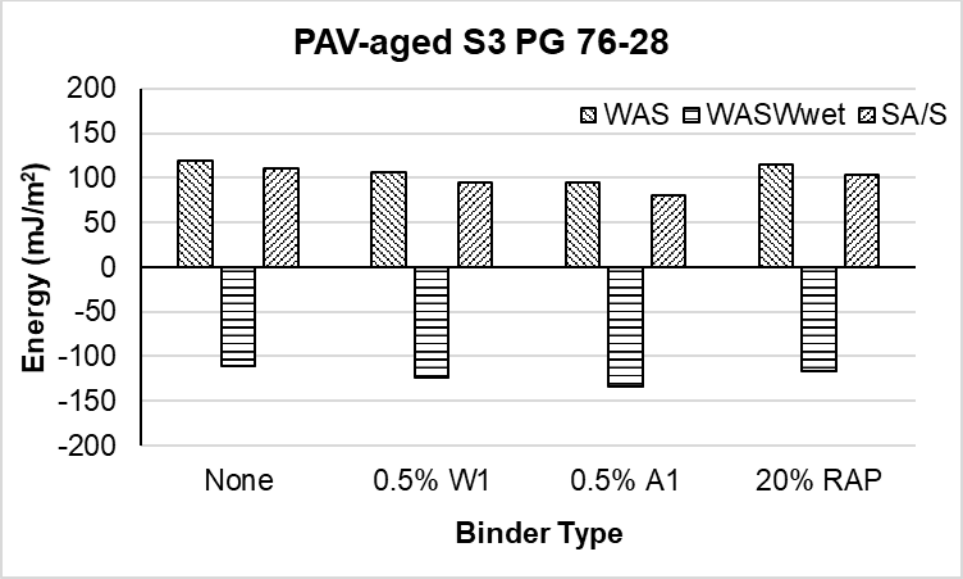

(b)

Figure 4.18 Work of adhesion, work of debonding and spreading coefficient of (a) PAV-aged S1 PG 64-22 and (b) PAV-aged S3 PG 76-28 binder with Limestone 1 aggregate

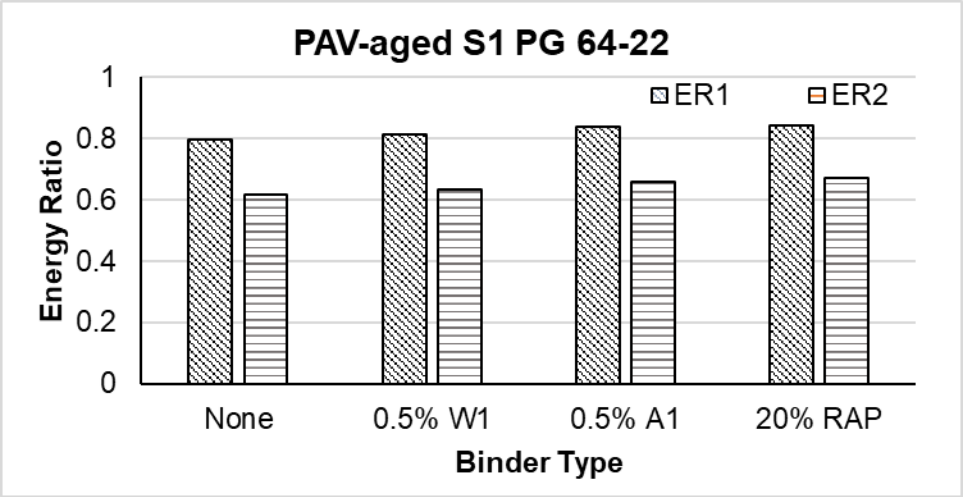

(a)

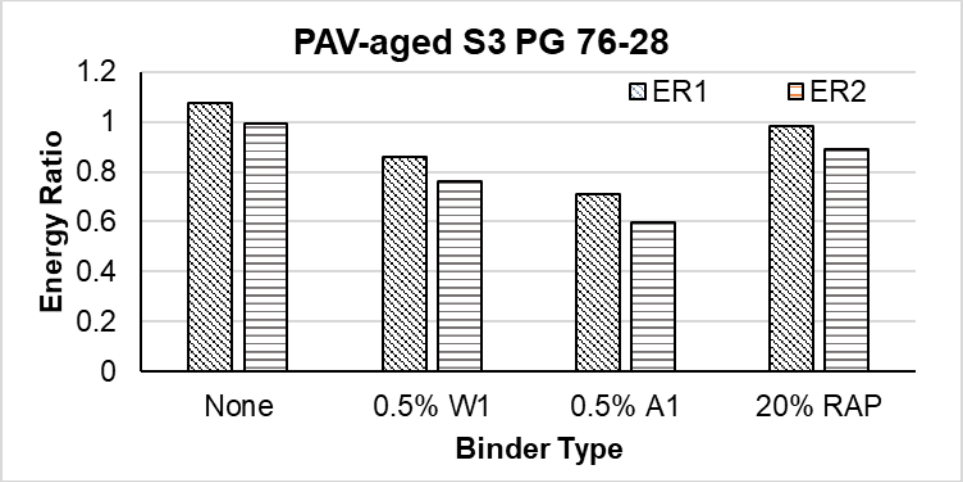

(b)

Figure 4.19 Energy ratios (ER_1 and ER_2) of (a) PAV-aged S1 PG 64-22 and (b) PAV-aged S3 PG 76-28 binder with Limestone 1 aggregate

4.3.6. Effect of Aggregate Type

The type, source and properties of aggregates are known to affect the moisture-induced damage potential of asphalt mixes. According to Tarrer and Wagh (1991) the properties of aggregates are single most important factor contributing to binder-aggregate bonding. Figure 4.20 presents the energy ratios of different aggregates tested in this study with the RTFO-aged S3 PG 76-28 binder. The ER_1 and ER_2 values were found to be different for different aggregates. Limestone 1 exhibited the highest ER_1 and ER_2 values indicating better resistance to moisture-induced damage than other aggregates. The granite and rhyolite aggregates were

found to have the highest moisture-induced damage potential when used with the S3 PG 76-28 binder in a mix. From Appendix I, similar trends of variations in moisture-induced damage potential were observed for limestone, granite and rhyolite aggregates with other binders. Tarrer and Wagh (1991) also reported that the limestone aggregate performed better than the granite aggregate in terms of moisture-induced damage.

Tarrer and Wagh (1991) reported that, the adhesion between asphalt and aggregate in the presence of water became weaker when the pH value increased to 9.0 and above. Tarrer and Wagh (1991) also reported that, typically, when an aggregate is coated with binder, selective adsorption of some components of binder, such as the more polar species of the binder took place on the aggregate surface and hydrogen bonds or salt links were formed. The water solubility of the hydrogen bonds and the salt links between the adsorbed binder components and the aggregate surface increased as the pH of the water presented at the aggregate surface increased. The granite aggregate was found to increase the pH of the water gradually and made the mix susceptible to moisture-induced damage. Also, the presence of limestone aggregate was reported to raise the pH of the water to a relatively high level. However, alkaline earth salts formed due ton the reaction of alkaline earth metals in limestone and the acids present in binder are very strong. The alkaline earth salts generally do not dissociate in water even at a high pH and resulted in a higher resistance to moisture-induced damage.

From Figure 4.20, it was also observed that the limestone from three different sources exhibited significant differences in their energy ratios with the same binder. For example, The ER_1 values for Limestone 1, Limestone 2 and Limestone 3 with the S3 PG 76-28 binder were 0.68, 0.53 and 0.49, respectively. Therefore, care should be taken in selecting similar types of aggregates (SFE-wise) from different sources to ensure compatibility.

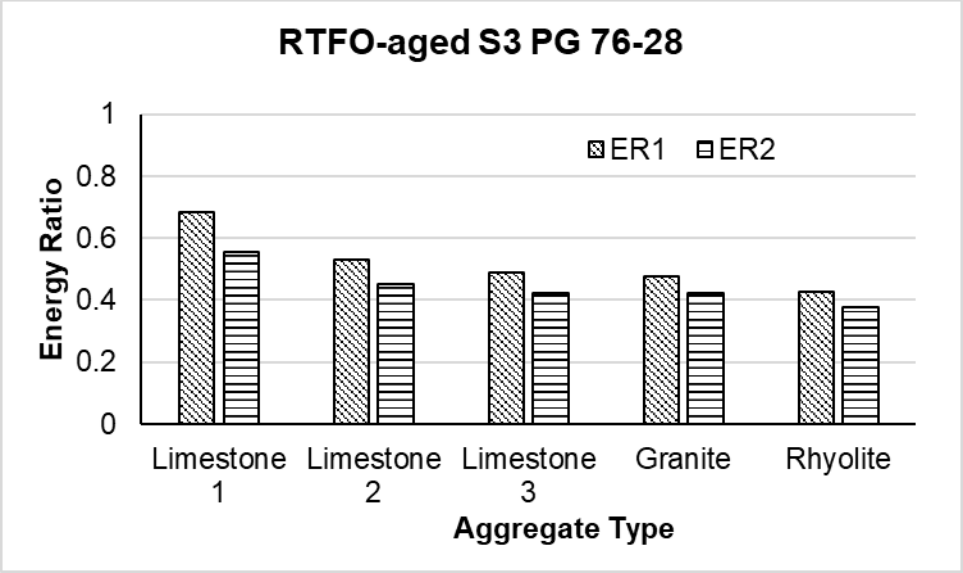

Figure 4.20 Energy ratios (ER_1 and ER_2) of RTFO-aged S3 PG 76-28 binder with different aggregates

4.4. Asphalt Mixes Test Results

4.4.1. Energy Ratio from SFE Technique

In previous sections, the compatibility of binders with only one type of aggregates were evaluated using energy ratio (ER_1 and ER_2) parameters. However, a mix design generally contains a number of different aggregates. Therefore, a different parameter is required to combine the effect of all the aggregates present in a mix design. It was also observed that the ER_1 and ER_2 followed a similar trend for all the binder-aggregate combinations and ER_1 required less effort in calculation than ER_2. Therefore, a modified ER_1 parameter, named composite energy ratio 1 (CER_1) was developed in this study to account for the effect of all the aggregates in the overall moisture-induced damage potential of an asphalt mix. First, the ER_1 for all the aggregates and binder combination present in a mix is calculated using Equation (18). The CER_1 is then calculated by taking weighted average of all the ER_1 based on the percent of aggregate present in a mix using Equation (18).

$$CER_1 = \frac{\sum_{i=1}^{n} p_i ER_{1(Agg-i)}}{\sum_{i}^{n} p_i} \quad (18)$$

where,

n = the number of aggregate stockpiles used in mix design;

p_i = the percentage of aggregate from stockpile i used in the mix;

$ER_{1\,(agg\text{-}i)}$ = Energy ratio between asphalt binder and aggregate from stockpile i.

The CER_1 parameters for the tested asphalt mixes were calculated using Equation (18) and presented in Figure 4.21. A majority of the aggregates were found to be rhyolite aggregate. It was observed that the addition of 0.5% W1 (Mix-2), 0.5% A1 (Mix-3) and 20% R1 (Mix-5) to mixes increased the CER_1 value indicating improvements in moisture-induced damage resistance for that binder-aggregates system. The addition of antistripping agent (Mix-3) was found to exhibit the highest increase in CER_1 value followed by Mix-5 and Mix-2. The CER_1 value of Mix-4 was not calculated as the SFE components of the PG 64-22 binder with PPA was not determined in this study. The following sections provide details about the moisture-induced damage potential of asphalt mixes from the performance tests conducted.

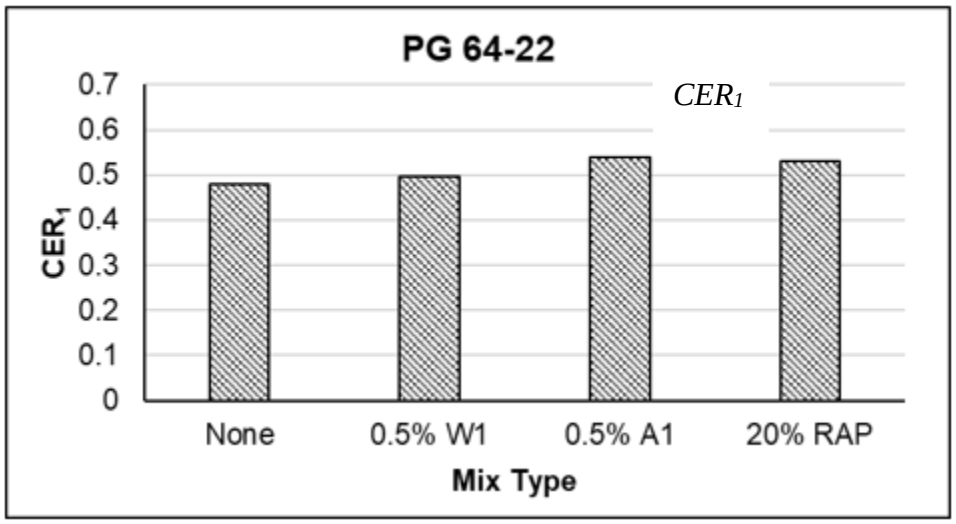

Figure 4.21 Composite energy ratio (CER_1) of tested asphalt mixes

4.4.2. Hamburg Wheel Tracking (HWT) Test

4.4.2.1. Conventional Method

Figure 4.22 presents the rut depths vs. number of wheel passes obtained from the HWT tests on all five mixes. The conventional rutting parameters for all mixes were determined from the HWT curves and are presented in Table 4.3. From Figure 4.22, the rut depths at 10,000 and 20,000 passes for Mix-1 (control mix) were found to be 2.8 and 14.9 mm, respectively. A stripping inflection point (SIP) was observed at 11,500 wheel passes for Mix-1, indicating a potential for moisture-induced damage. The creep and stripping slope for the Mix-1 were found

to be 4,120 and 880 passes/mm, respectively.

The effect of the addition of WMA additive to the binder was observed by comparing the rutting parameters of Mix-1 and Mix-2. From Figure 4.22, it was observed that the HWT test for Mix-2 stopped around 13,000 passes as the rut depths reached the maximum limit. At 10,000 passes, Mix-2 was found to exhibit a rut depth of 11.5 mm which was higher than that of Mix-1 (2.81 mm) at the same number of wheel passes. Also, the number of wheel passes required for 1 mm deformation at creep and the stripping phase were found to be lower for Mix-2 than Mix-1. Therefore, it can be concluded that the mix containing WMA is expected to exhibit higher rutting and moisture-induced damage than the control mix. These findings were found to be consistent with the results reported by (Prowell et al., 2007; Ghabchi et al., 2013).

The rut depths for the mix containing ASA (Mix-3) were found to be lower than those measured for the control mix (Mix-1) indicating an improvement in rutting resistance as a result of using ASA. For example, the rut depth after 10,000 and 20,000 wheel passes for Mix-3 were found to be 2.4 mm and 9.8 mm, respectively. Also, the creep slope (passes/mm) was found to increase from 4,120 to 5,426 with the addition of ASA. Furthermore, the stripping inflection point for Mix-3 was observed at 13,700 load cycle, the highest among the mixes. Therefore, addition of ASA is expected to reduce the moisture-induced damage potential of the mixes which is consistent with the findings of other studies (Wasiuddin et al., 2007b; Arabani and Hamedi, 2014; Abuawad et al., 2015).

The effect of the addition of PPA to the moisture-induced damage and rutting potential of asphalt mix (Mix-4) can be observed from Figure 4.22 and Table 4.3. The addition of PPA was found to make the mix susceptible to moisture-induced damage and rutting. The stripping inflection point for Mix-4 was observed at 5,500 load cycles with a stripping slope of 850 passes/mm. However, the post- compaction deformation for Mix-4 was found to be lower than the control mix indicating a higher rutting resistance at the initial stage. With an increase in wheel passes the Mix-4 specimens were damaged due to moisture and exhibited higher rut depths than those of the control mix specimens. A similar increase in rutting and moisture-induced damage potential with using a PPA-modified binder was observed in other studies (Orange et al., 2004; Fee et al., 2010; Al-Qadi et al., 2014; Rani, 2019). The mix containing 20% RAP (Mix-5) exhibited a higher moisture-induced damage potential than the control mix (Mix-1). The Mix-5 specimens were observed to exhibit a stripping inflection point at a lower number of wheel passes (around 9,000 passes) than the control mix (Mix-1). However, the stripping slope was found to be similar to that of the control mix.

4.4.2.2. Use of Texas A&M University Method for Analyzing the HWT Results

Yin et al. (2014) proposed two parameters, namely stripping number (LC_{SN}) and stripping life (LC_{ST}) for evaluating moisture-induced damage potential of asphalt mixes. A software called "HWTT Analysis- TAMU v3" was used to determine these parameters. Mixes with higher LC_{SN} and LC_{ST} values are expected to be less susceptible to moisture-induced damage than those having lower LC_{SN} values. Table 4.4 presents the LC_{SN} values for the mixes tested in a HWT. From Table 4.4, it was observed that Mix-4 exhibited the lowest LC_{SN} value (131 passes) among all mixes indicating a higher susceptibility to moisture-induced damage. On the other hand, the mix containing ASA (Mix-3) exhibited the highest LC_{SN} value (3,312 passes) than the control mix (1,228 passes).

According to Yin et al. (2014), LC_{ST} value represents the moisture-induced damage potential of a mix after it passes stripping number (LC_{SN}). From Table 4.4, it was observed that the LC_{ST} values for Mix-1, Mix-2, Mix-3, Mix-4 and Mix-5 were 18,019, 10,482, 18,402, 17,203 and 16,160, respectively. Considering LC_{ST} values, the control (Mix-1) and the mix containing ASA (Mix-3) were found to exhibit a higher a resistance to moisture-induced damage than the one containing WMA additive (Mix-2). Also, the mix containing PPA-modified binder (Mix-4) and the one containing RAP (Mix-5) exhibited lower LC_{ST} values compared to that of the control mix (Mix-1).

A higher value of viscoelastic strain increment ($\Delta\varepsilon_{10,000}^{vp}$) for a mix represents a better rutting resistance than that with a lower $\Delta\varepsilon_{10,000}^{vp}$value. Table 4.4 shows that the mix containing ASA (Mix-3) exhibited a higher $\Delta\varepsilon_{10,000}^{vp}$value than other mixes and thus has the highest rutting resistance among the mixes. The lowest rutting performance was observed for the mix containing PPA-modified binder (Mix-4). The mix with WMA additive also exhibited a lower resistance to rutting than the control mix (Mix-1).

Table 4.3 Different Parameters Obtained from HWT Test (Conventional Method)

Mix ID	Post-compaction (mm)	Creep Slope (mm/Pass)	Creep Slope (Passes/mm)	Stripping Inflection Point (SIP)	Stripping Slope (mm/Pass)	Stripping Slope (Passes/mm)
Mix-1	1.11	0.00024	4,120	11,500	0.00114	880
Mix-2	1.56	0.00058	1,714	5,800	0.00200	500
Mix-3	0.97	0.00018	5,426	13,700	0.00108	930
Mix-4	0.95	0.00031	3,204	5,500	0.00118	850
Mix-5	1.03	0.00041	2,421	9,000	0.00112	895

Table 4.4 Different Parameters Obtained from HWT Test (TAMU Method)

Mix ID	$\Delta\varepsilon_{10,000}^{vp}$	LC_{SN}	LC_{ST}
Mix-1	3.91E-06	1,228	18,019
Mix-2	9.32E-06	867	10,482
Mix-3	1.93E-06	3,312	18,402
Mix-4	3.17E-05	131	17,203
Mix-5	3.52E-06	1,776	16,160

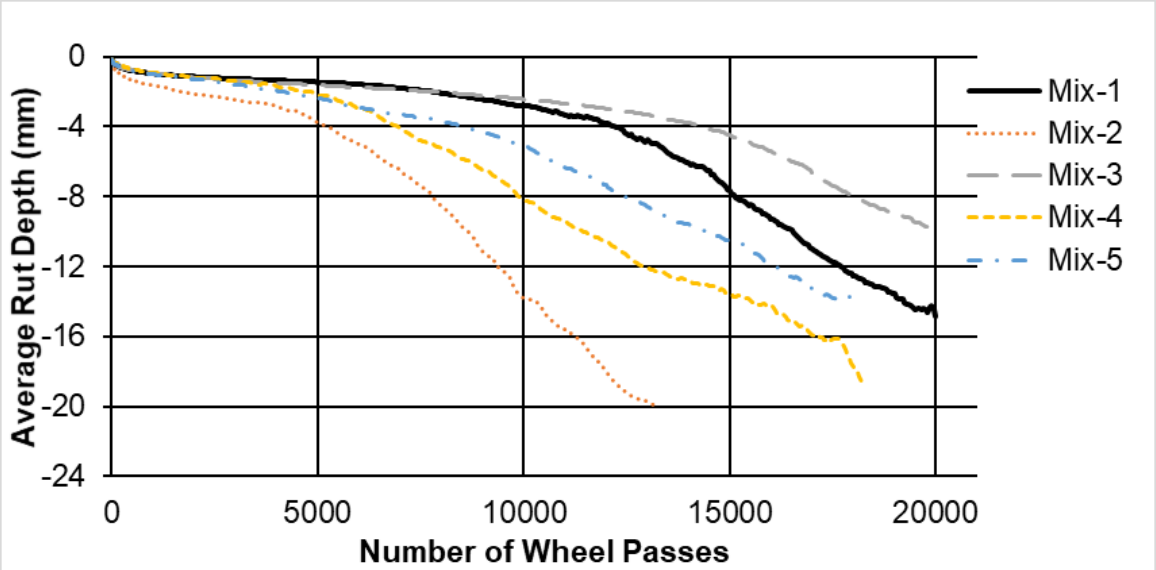

Figure 4.22 Rut depths vs. wheel passes from HWT test

4.4.3. Indirect Tensile Strength Test

4.4.3.1. Tensile strength ratio (TSR)

Figure 4.23 (a) presents the indirect tensile strength (ITS) values of the dry- and moisture-conditioned specimens and TSR values for all five mixes. From Figure 4.23 (a) it is evident that the ITS values for dry and moisture-conditioned Mix-4 and Mix-5 specimens are significantly higher than those of the other three mixes. For example, ITS values of the Mix-4 specimens at dry- (ITS_{dry}) and moisture-conditioned (ITS_{wet}) states were found to be 878 kPa and 639 kPa, respectively, whereas the same for the control mix were 638 kPa and 463 kPa, respectively. Therefore, addition of PPA and RAP to a mix is expected to increase the tensile strengths of the mixes which is consistent with the findings of other studies (Abuawad et al., 2015; Ghabchi et al., 2016). The addition of WMA additive and ASA did not result in a significant increase in ITS_{dry} value compared to the that of control mix. However, ITS_{wet} value was observed to increase with the addition of WMA additive and ASA to the mix. From Figure 4.23(a), the control mix (Mix-1) exhibited a TSR value of 0.73, which is lower than the specification requirement (TSR ≥ 0.80) used by Oklahoma DOT. It was observed that the addition of WMA additive and ASA increased the TSR values to 0.93 and 0.99, respectively, indicating a reduction in moisture-induced damage potential of the mixes. An increase in TSR value with the addition of ASA was also reported by LaCroix et al. (2016) and Abuawad et al. (2015). Although the incorporation of PPA in the mix increased both ITS_{dry} and ITS_{wet}, the TSR value (0.73) was found not to satisfy the specification requirement indicating its higher potential for moisture-induced damage than Mix-2 and Mix-3. A similar trend in TSR value with the addition of PPA was also reported by other researchers (Orange et al., 2004; Fee et al., 2010; Abuawad et al., 2015). From Figure 4.23(a), it was also observed that the addition of RAP resulted in TSR values less than 0.80 indicating a higher susceptibility to moisture-induced damage.

4.4.3.2. Toughness Index (TI) Ratio

Figure 4.23(b) presents the TI values of asphalt mixes under dry- (TI_{dry}) and moisture-conditioned (TI_{wet}) states. It was found that the moisture-conditioned specimens exhibited an increase in their plastic behavior compared to dry specimens for all mixes. For example, the TI_{dry} value for control mix (Mix-1) was found to be 0.78 which increased to 0.98 after moisture conditioning the sample according to AASHTO T 283 method (AASHTO, 2014). In dry condition, addition of WMA additive to mix (Mix-2) was found to result in an increase in plastic behavior.

However, addition of ASA, PPA and RAP causes a reduction in the TI value, indicating a reduction in plastic behavior of the mix. A reduction in TI value with an increase in RAP content was also reported by other researchers (Shu et al., 2008; Huang et al., 2010) .The mix with PPA (Mix-4) exhibited the highest reduction (approximately 20%) in TI value compared with the control mix (Mix-1). No significant effect on the TI_{wet} value was observed after the addition of WMA (Mix-2) and ASA (Mix-3) additives. However, Mix-4 and Mix-5 exhibited approximately 7% and 11% reduction in the TI_{wet} values, compared to control mix (Mix-1), respectively. Based on the TI ratio (TI_{wet}/TI_{dry}) from Figure 4.23(b), it was evident that the changes in the TI values for Mix-3 and Mix-4 were higher than that in Mix-1, Mix-2 and Mix-5. As an increase in the TI value indicates an increase in plastic behavior, mixes with high TI ratios are expected to perform worse relative to moisture-induced damage after the crack initiation. Therefore, Mix-4 is expected to exhibit the lowest resistance to moisture-induced damage than other three mixes.

4.4.4. LA-SCB test

The LA-SCB method was applied to characterize the fracture properties of asphalt mixes by using their critical strain energy release rate (J_c) values. Figure 4.24 presents the J-integral values of the dry- ($J_{c\text{-}dry}$) and MIST-conditioned ($J_{c\text{-}MIST}$) specimens for all mixes. From Figure 4.24, the addition of ASA was found to reduce the fracture resistance in dry-conditioned specimens, whereas, the addition of WMA additive and PPA did not exhibit a significant change in fracture resistance under dry condition. Mix-5 exhibited the highest J_c value among all the mixes both for dry- and MIST-conditioned specimens. A higher binder content (5.5%) present in Mix-5 could be the reason behind this observation. However, a significant change in J_c values was observed among the mixes after conditioning using a MIST equipment. For examples, Mix-1 was found to exhibit a J_c ratio of 0.60, whereas, Mix-2, Mix-3, Mix-4 and Mix-5 exhibited J_c ratios of 0.92, 1.07, 0.61 and 0.74, respectively. Therefore, the addition of WMA and ASA is expected to produce mixes which are less susceptible to moisture-induced damage, whereas, addition of PPA and RAP is expected to increase the moisture-induced damage potentials of the mixes.

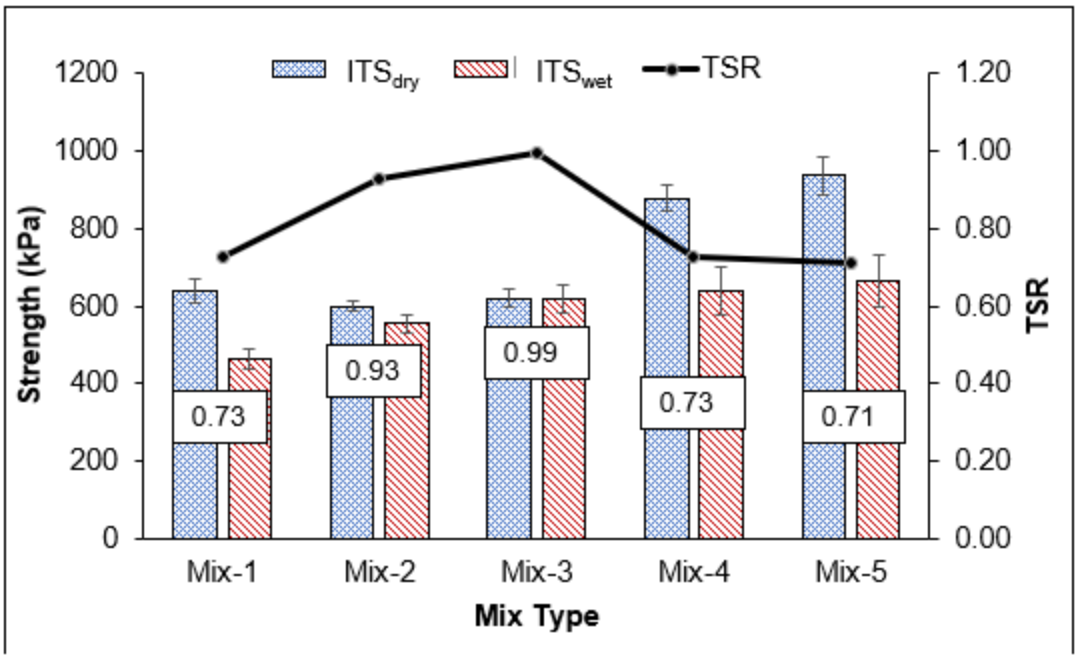

(a)

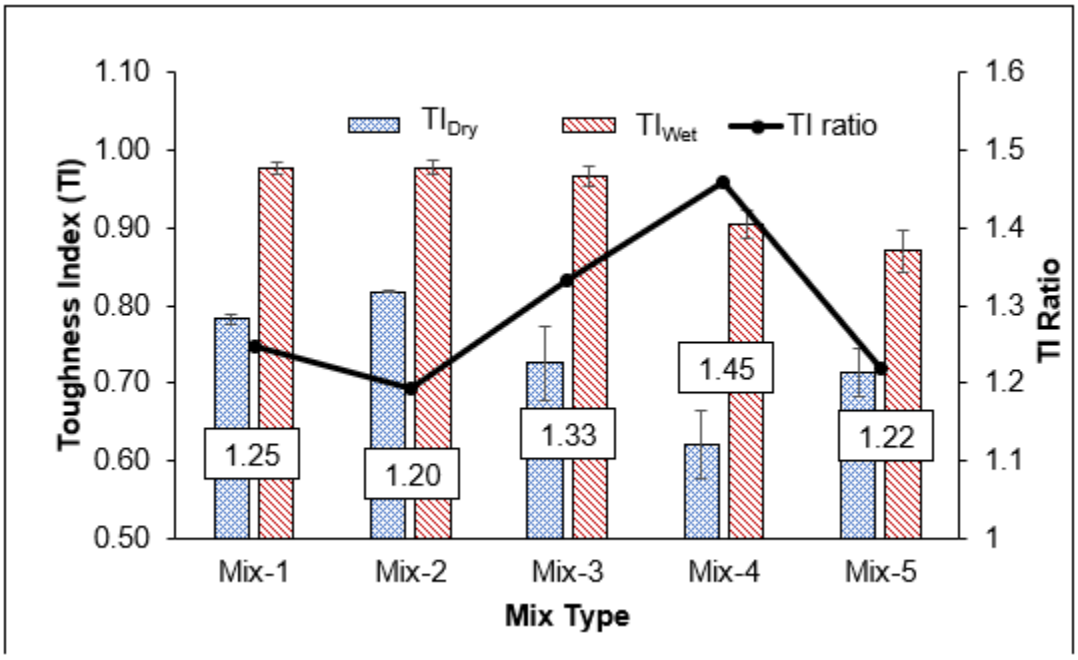

(b)

Figure 4.23 (a) Indirect tensile strength (ITS_{dry} and ITS_{wet}) and TSR values; (b) toughness index (TI_{dry} and TI_{wet}) and TI ratios of asphalt mixes from IDT test

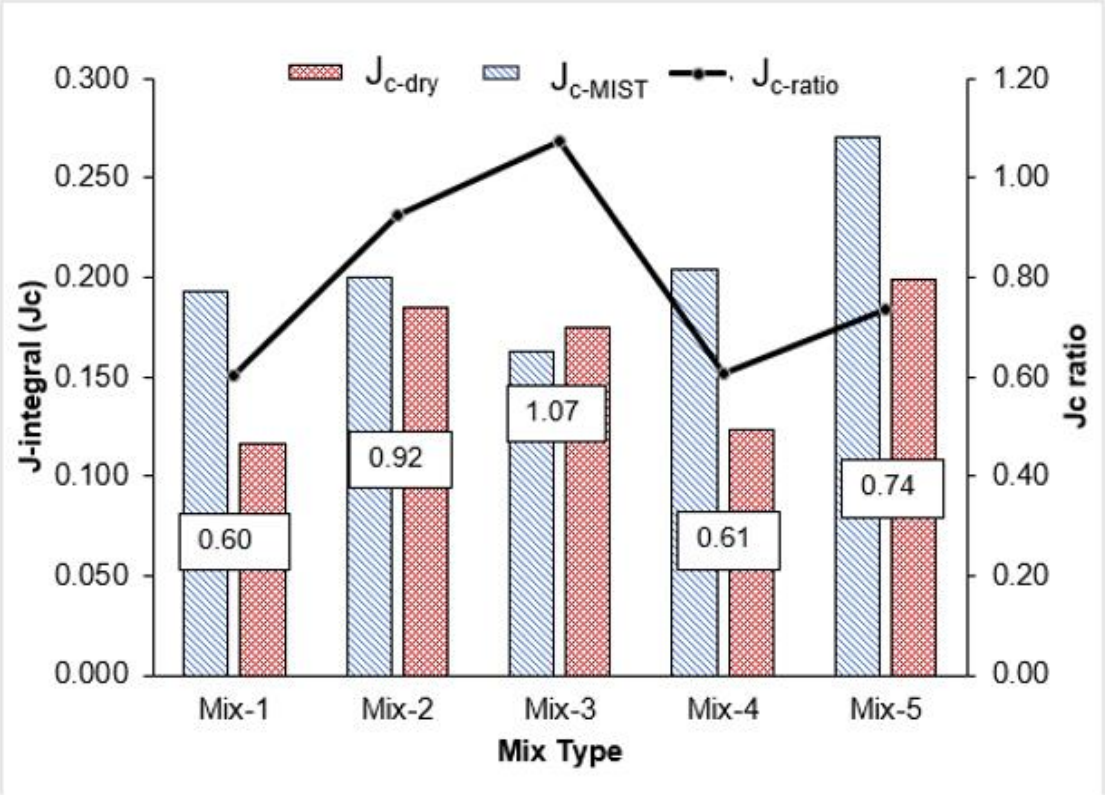

Figure 4.24 $J_{c\text{-}dry}$ and $J_{c\text{-}MIST}$ values and J_c Ratio of asphalt mixes from LA-SCB test

4.4.5. Comparison of Different Parameters

The effect of the addition of different additives on the moisture-induced damage potential of asphalt mixes is presented in Table 4.5. From Table 4.5, it can be observed that the effect of the addition of an additive vary with the test method and parameter used for evaluation of moisture-induced damage. for example, the SIP and LC_{SN} from HWT test exhibited an increase in the moisture-induced damage potential with the addition of WMA additive. However, TSR and TI ratio from IDT and J_c ratio from LA-SCB were found to indicate a reduction in the moisture-induced damage potential with the addition of WMA additive. This variation is expected to be resulted from the differences in the test mechanisms.

Table 4.6 presents the ranking of asphalt mixes with respect to their resistance to moisture-induced damage using different parameters. From Table 4.6, both the conventional (SIP) and TAMU (LC_{SN}) methods were found to provide very similar ranking of the asphalt mixes with respect to their moisture-induced damage potential. The SIP for Mix-4 was found to be the lowest followed by Mix-2, Mix-5, Mix-1 and Mix-3. In case of LC_{SN}, Mix-5 was found to perform

better than Mix-1. However, the TAMU method (a more mechanistic method) was found to exhibit less variability in results (Yin et al., 2014).

From Table 4.6, variation in ranking of the mixes was observed for the TSR and the TI ratio values obtained from the IDT test. According to TSR ratio, Mix-3 exhibited the highest resistance to moisture-induced damage followed by Mix-2, Mix-1, Mix-4 and Mix-5. However, TI ratio ranked the mixes in the following order: Mix-2, Mix-5, Mix-1, Mix-3 and Mix-4, from the lowest to the highest moisture susceptibility. Different post-peak behavior from dry- and moisture-conditioned specimens of a mix can be expected although it exhibits similar strength in both states. In case of J_c ratio and TSR values, Mix-2, Mix-3 and Mix-4 were found to exhibit similar ranks with regard to moisture-induced damage potentials. However, Mix-1 and Mix-5 were ranked as 3 and 5 with respect to TSR, whereas, ranked as 5 and 3 according to J_c ratio. Although both the J_c and TI values are indicators of fracture performance of a mix, the ranking of the mixes from J_c ratio were fond not consistent with TI ratio. The J_c or critical energy release rate was developed using linear elastic fracture mechanics principle to characterize fracture properties of asphalt mixes. According to Kim et al. (Kim et al., 2012), the J_c value represents the pre-peak fracture energy whereas TI is related to post-peak fracture energy. Therefore, rankings of mixes with respect to J_c ratio and TI ratio are expected to be different. Also, the HWT and TSR were found to rank the mixes differently. The HWT test is a torture test and simulates the rutting and stripping on submerged asphalt mix specimens under wheel load. On the other hand, TSR is the ratio of peak strength of asphalt mix specimen at wet and dry condition. In all the cases, mixes with ASA and PPA were found to exhibit the highest and the lowest moisture-induced damage resistance among the mixes, respectively. The Mix-2 (containing WMA additive) was found to have a high moisture-induced damage potential from HWT parameters. However, from the TSR results, an improved resistance to moisture-induced damage was observed with addition of WMA additive to the mix. The addition of RAP to mix was found to increase the susceptibility to moisture-induced damage based on the TSR value. However, the effect of the addition of different additives were found to be dependent on the evaluation mechanism.

Table 4.5 Effect of additives on moisture-induced damage potential of asphalt mixes

Mix ID	Additive used	SIP	LC_{SN}	TSR	TI ratio	J_c ratio
Mix-1	None	-	-	-	-	-
Mix-2	WMA	Increase	Increase	Reduction	Reduction	Reduction
Mix-3	ASA	Reduction	Reduction	Reduction	Increase	Reduction
Mix-4	PPA	Increase	Increase	Increase	Increase	Reduction
Mix-5	RAP	Increase	Reduction	Increase	Reduction	Reduction

Table 4.6 Ranking of mixes based on laboratory performance tests on asphalt mixes

Mix ID	SIP	LC_{SN}	TSR	TI ratio	J_c ratio
Mix-1	2	3	3	3	5
Mix-2	4	4	2	1	2
Mix-3	1	1	1	4	1
Mix-4	5	5	4	5	4
Mix-5	3	2	5	2	3

Table 4.7 presents a comparison of rankings of the different mixes with respect to SFE and other performance-based tests. Here, only three HMA mixes (i.e. Mix-1, Mix-3 and Mix-5) were considered for comparison because of the CER_1 values were not available for the other two mixes. It was observed that the CER_1, J_c ratio and LC_{SN} exhibited similar rankings of the mixes. Based on CER_1, J_c ratio and LC_{SN} parameter, the Mix-3 with antistripping agent exhibited the highest resistance to moisture-induced damage followed by Mix-5 and Mix-1. The other parameters, such as SIP, LC_{ST}, and TSR were found to rank the mixes differently. Therefore, based on the limited results available from this study, it can be concluded that the J_c ratio from SCB test and the LC_{SN} from HWT are expected to exhibit good correlations with the SFE technique and can be used as screening tools for evaluation of moisture-induced damage potential of asphalt mixes.

Table 4.7 Ranking of mixes from SFE, HWT, IDT and SCB tests

Mix ID	CER_1	SIP	LC_{SN}	LC_{ST}	TSR	J_c ratio
Mix-1	3	2	3	2	2	3
Mix-3	1	1	1	1	1	1
Mix-5	2	3	2	3	3	2

5. CONCLUSIONS

This study was undertaken to generate laboratory test data to help in selecting asphalt binder and aggregate to be used in Oklahoma asphalt mix based on their performance to resist moisture-induced damage. This study was limited to mechanistic evaluation of moisture-induced damage of asphalt binder-aggregate system using SFE technique and laboratory performance evaluation of five asphalt mixes. Also, relative performance of different additives was evaluated through laboratory performance tests on asphalt mixes and SFE technique. For the purpose of this study, unmodified and polymer-modified asphalt binders from different sources were collected. Different additives, such as warm mix asphalt (WMA) additive, anti-stripping agent (ASA), polyphosphoric acid (PPA) and reclaimed asphalt pavement (RAP) were mixed with the binder. The SFE components of the binder blends were determined using dynamic Wilhelmy plate (DWP) and sessile drop (SD) test methods at RTFO-aged and PAV-aged conditions. Also, aggregates from five different sources of Oklahoma were collected and the SFE components were determined using universal sorption device and sessile drop test. Furthermore, chemical analyses of the blended binders and aggregates were conducted to understand the effects of chemical compositions on the SFE components. To this end, asphalt mixes consisting of WMA additive, ASA, PPA and RAP were produced in the laboratory for moisture-induced damage evaluation using Hamburg wheel tracking (HWT), indirect tensile strength (IDT) and semi-circular bend (SCB) tests. Correlations between the moisture-induced damage performance parameters from laboratory performance tests and the SFE technique were also investigated. Based on the test results obtained from different laboratory tests conducted on asphalt mixes, aggregates and binders and their analyses, the following conclusions were made:

i. SFE technique was found to be a useful tool to screen asphalt mixes for moisture-induced damage.
ii. The effect of the addition of different additives on binders' contact angle with different probe liquids and binders' SFE components were observed to be dependent on binder types and sources.
iii. The addition of RAP is expected to reduce moisture-induced damage for all binder and aggregate combinations. However, the use of PPA is expected to reduce binder's ability to wet and coat the surface of the aggregate resulting in a reduction in moisture-induced damage resistance.

iv. From SFE technique, the granite and rhyolite aggregates were found to exhibit high and limestone aggregates exhibited low moisture-induced damage potential when used in an asphalt mix.

v. The LA-SCB test with MIST conditioning was found to be effective in evaluating the moisture-induced damage potential of asphalt mixes. The J_c ratio exhibited the potential to be used as an alternative method to conventional moisture-induced damage parameter.

vi. The SFE components were found not to exhibit good correlations with the elements detected from XRF of the binder blends. Also, it was observed that the presence of PPA can be detected from XRF test. The appearance of the acid functional group from FTIR test was found to be consistent with acid SFE components of the binder blends.

vii. From TAN test, the addition of W1 and A1 additives was found to reduce the acidic properties as well as acid value of the unmodified PG 64-22 binder. However, no significant change in the acid values were observed for polymer-modified PG 76-28 binder with the addition of W1 and A1 additive. The reaction of the polymer presents in the binder and the chemical constituents of W1 and A1 additives may be responsible for such changes in the acid values.

viii. The basic components of all the aggregates were found to be higher than their acidic and Lifshitz-van der Waals (Γ^{LW}) components from USD and SD tests. The highest and the lowest basic components were observed for granite and Limestone 1 aggregates, respectively.

ix. It was observed that all the limestone aggregates mostly composed of carbonaceous material. The granite and rhyolite were found to contain high amount of silica (SiO_2) which is expected to be responsible for higher hydrophilicity than the limestone aggregates.

x. The lime treatment was found to increase the basic SFE components of all the aggregates. The rhyolite aggregate exhibited the highest change in basic SFE component compared to that of other aggregate.

xi. The moisture-induced damage potential of asphalt mixes was found to reduce with long-term aging. Asphalt binder with polymer modification was observed to be less susceptible to oxidative aging than the non-polymer modified binder. As a result, the moisture-induced damage potential of polymer-modified binder was found to be less affected by long-term aging.

xii. From HWT test, the mixes with W1 additive were found to exhibit higher susceptibility to rutting and moisture-induced damage following PPA-modified binder than the control mix. However, the addition of A1 additive was found to improve the rutting and moisture-

induced damage resistance of the mix from both the conventional method and TAMU method.

xiii. An improved resistance to rutting and moisture-induced damage of asphalt mixes with the addition of A1 additive were also observed from TSR. However, the mix containing PPA was found to exhibit the lowest TSR value indicating the highest susceptibility to moisture-induced damage, while the tensile strength was found to be higher than the other mixes for both dry- and moisture-conditioned samples.

xiv. From TI results, moisture conditioning process was found to increase plastic behavior in all mixes. The knowledge of the post-peak behavior from the TI ratio can be used to evaluate post-peak changes in different mixes due to moisture conditioning.

xv. After comparing moisture-induced damage parameters from different tests, it was observed that the CER_1, J_c ratio and LC_{SN} exhibited similar ranking for the mixes.

Based on the limitation of this study following recommendations on future study are proposed:

i. Study is needed to determine the correlation between CER_1 and field moisture-induced damage performance of asphalt mixes.

ii. The minimum threshold value of CER_1 for asphalt mixes needs to be determined for Oklahoma mixes.

iii. The SFE database should be enriched with additional SFE data of asphalt binders and aggregates used in Oklahoma (fill voids in current database).

iv. Study needs to be conducted to verify the applicability of J_c ratio for evaluating moisture-induced damage with field performance data.

v. Another study can be conducted to evaluate the suitability of Illinois IFIT Test for moisture-induced damage.

6. SURFACE FREE ENERGY DATABASE

As a part of this project, a SFE database of asphalt binders and aggregates was developed and included in a spreadsheet called “SFE DATABASE FOR OKLAHOMA”. The spreadsheet can calculate the energy ratio CER_1 of asphalt binder with up to ten different aggregates combinations. The spreadsheet can be used to screen asphalt binder and aggregate in the mix design phase. It is suggested to use a number of asphalt binder-aggregate combinations and compare the CER_1 values to obtain optimum performance from a mix design. A lower CER_1 value is expected to result in a mix with higher moisture-induced damage resistance. To use the spreadsheet efficiently, please follow the steps mentioned below:

i. Open the “SFE DATABASE FOR OKLAHOMA” spreadsheet and go to the tab called “CER1”. The CER1 tab contains the program to calculate CER_1 value of binder-aggregate combination. The “Orig” and “PS” contains the SFE data for binder and aggregate.

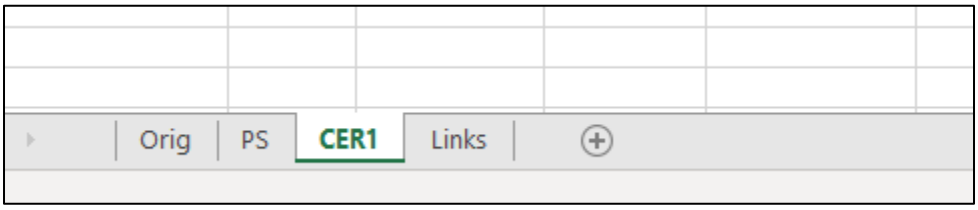

Figure 6.1 Step 1: select CER1 tab for analysis

ii. In Column called “ID(Design)”, write the Mix ID. It can be ID of the asphalt mix design.

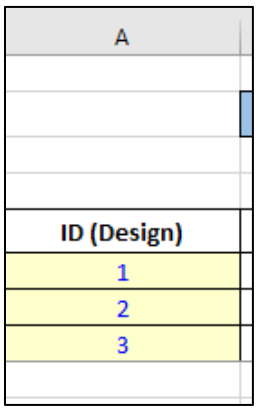

Figure 6.2 Step 2: write asphalt mix design ID in Column called “ID(Design)”

iii. Click on the column called “Binder Source” and select a source from the picklist. For example, binder source “S5”. The details of each source can be found in the spreadsheet.

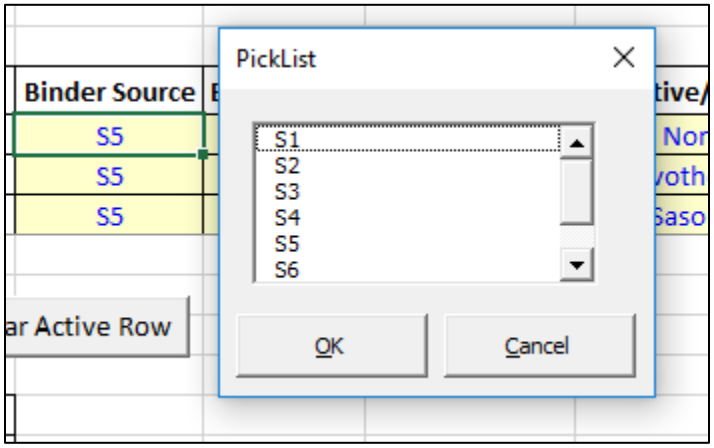

Figure 6.3 Step 3: select proper binder Source from “Binder Source” column

iv. Click on the column called “Binder Type” and a picklist will appear with the available binder types for that binder source. For example, if PG 64-22 binder from source S5 is going to be used in the mix, then, select “PG 64-22”.

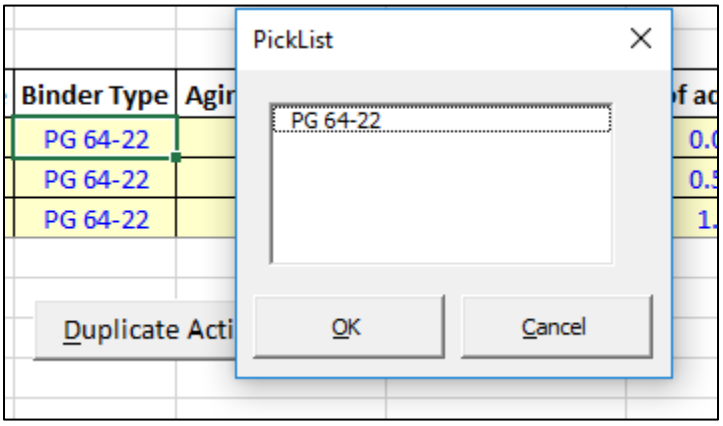

Figure 6.4 Step 4: select proper binder type from “Binder Type” column

v. The aging condition of the binder can be selected from the column called “Aging Condition”. Generally, the SFE data for three different aging conditions, such as unaged, RTFO-aged and PAV-aged are available in the database.

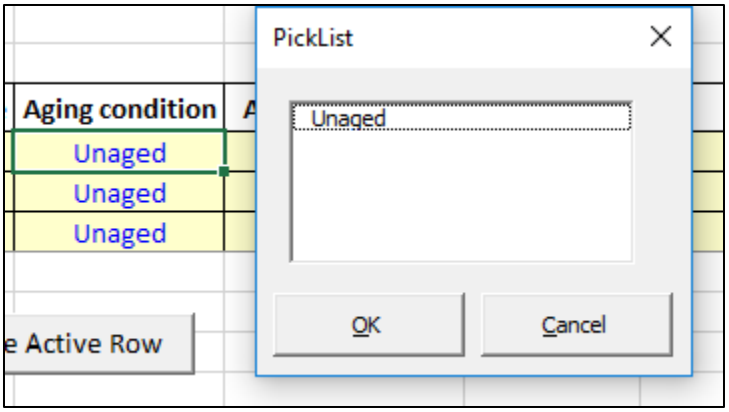

Figure 6.5 Step 5: select aging condition from “Aging Condition” column

vi. If any additive is being used for the asphalt mix, click on the column called “Additives/Others” and select the additive from the picklist. The amount of additive can be selected from the next column (% of Additives) through a picklist. If no additive is going to be used, select “None” from “Additive/Others” and “0” from the “% of Additives”.

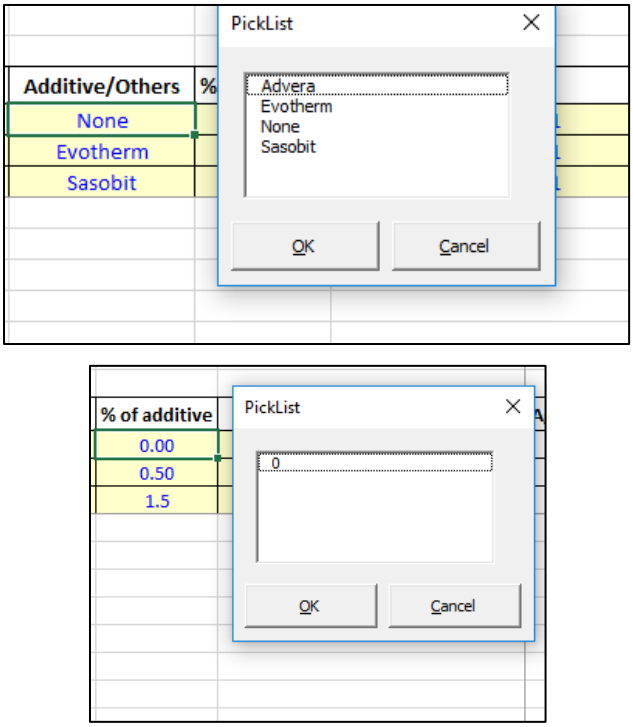

Figure 6.6 Step 6: select additive type and amount from “Additives/Others” and “% of Additives” columns

vii. Select the type of the aggregate from column called “Agg1” and write the amount in %Agg1. If multiple aggregates are present in the mix design, put those in the subsequent aggregate sections. For example, if 30% Limestone 1 aggrgate is being used in the design, select “Limestone 1” from “Agg1” and put “30” in “%Agg1”.

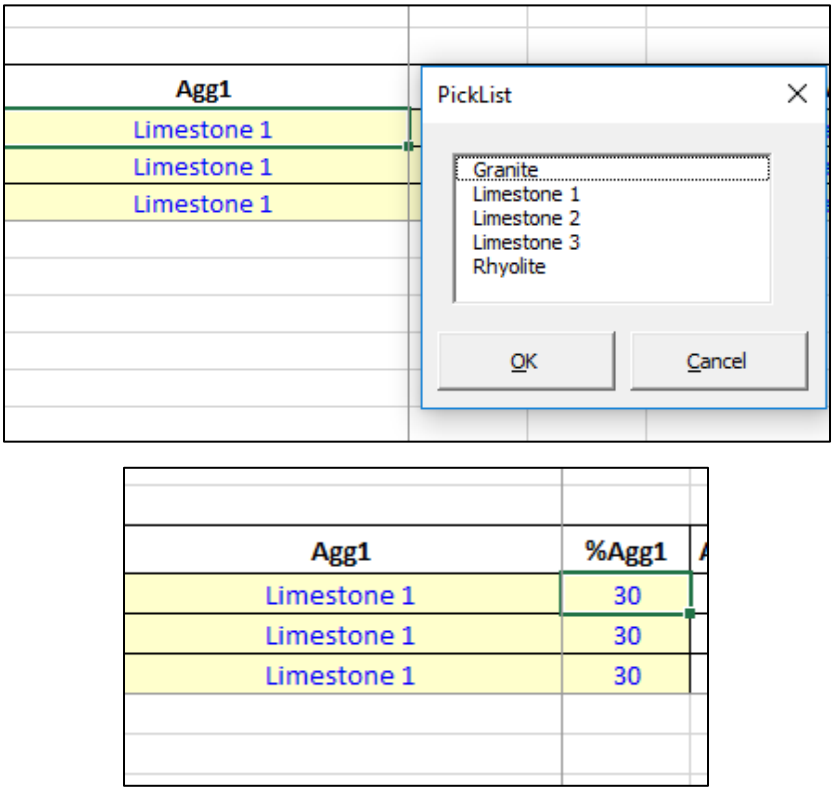

Figure 6.7 Step 7: select aggregate type and amount from “Agg1” and “%Agg1” columns

viii. The results of the binder-aggregate combination will be calculated by the program and exhibited in column called “CER1”.

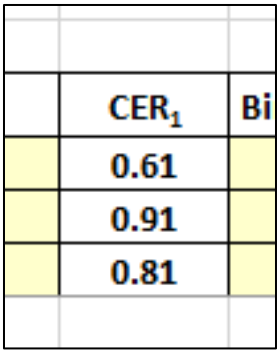

Figure 6.8 Step 8: note the CER_1 value from “CER_1” column for that binder-aggregate system

ix. To repeat another binder-aggregate combination, click on the button called “Duplicate Active Row”. Another row will appear and another binder-aggregate combination can be tried on that row.

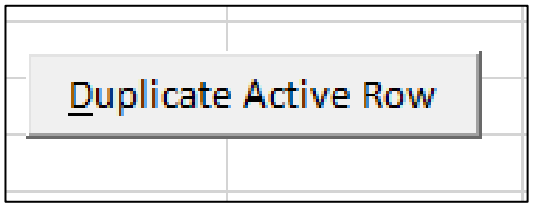

Figure 6.9 Step 9: To repeat another binder-aggregate combination, select “Duplicate Active Row”

x. To clear an active binder-aggregate combination, click on the button called “Clear Active Row”. All the calculations in the active row will be erased.

Figure 6.10 Step 10: To clear an active binder-aggregate combination, select “Clear Active Row”

Please note that, the SFE database prepared for this project is limited to the material tested during this project. The database needs to be updated periodically to accommodate new material test results. New data can be added to “Origin” and “PS” tab. Also, note that the SFE database does not contain SFE results for fine aggregate. Total percent of aggregate used in the calculation needs to be checked from the column called “Total Aggregate (%)”. The amount of total aggregate should always be equal to or less than 100.

Total Aggregate (%)	
ID (Design)	Agg(%)
1	90.00
2	90.00
3	90.00

Figure 6.11 Check for total amount of aggregate

7. IMPLEMENTATION/TECHNOLOGY TRANSFER

7.1. Implementation and Technology Transfer Workshop

Technology transfer has occurred continuously during this project. The research team worked very closely with asphalt binder and aggregate manufacturers in Oklahoma to collect materials of different compositions. Also, a local paving company namely Silver Star Construction Co. in Moore, Oklahoma helped in preparing the asphalt mix design and in collecting materials for asphalt mixes. Furthermore, a presentation titled “Workshop on Surface Free Energy Technique to Evaluate Moisture-induced Damage,” was made to a group of about 15 individuals consisting of ODOT Personnel and individuals from asphalt industries on January 08, 2019. The aim of the workshop was to discuss the SFE database developed during this project and demonstrated how moisture-induced damage potential of asphalt mixes can be evaluated mechanistically using this database. Also, a comparison of the SFE technique with other conventional and unconventional test methods used for evaluation of the moisture-induced damage potential was discussed in this workshop. One professional development hours (PDH) were offered to the interested participants.

7.2. Journal and Proceedings Papers

The scale and breadth of this project have drawn national and international attention. The research team has published/submitted 1 journal articles and 2 proceedings papers and made 3 platform and 4 poster presentations. Furthermore, test data from this project are integral part of a Ph.D. dissertation. The publication records of the research team related to the project are listed below:

7.2.1. Referred Journal Papers

- Ali, S.A., Ghabchi, R., Zaman, M., Rani, S. and Rahman, M.A. (2018). “Laboratory Characterization of Moisture-Induced Damage Potential of Asphalt Mixes Using Conventional and Unconventional Performance-Based Tests.” Submitted to International Journal of Road Materials and Pavement Design (Under review).

7.2.2. Referred Conference Papers

- Ali, S.A., Ghabchi, R., Rani, S., Rahman, M.A., and Zaman, M. (2018). “Feasibility of Using XRF for Assessment of Surface Free Energy Components of Asphalt binder.”

In proceeding of 5th GeoChina International Conference, HangZhou, China, held on July 23-25, 2018.

- Ali, S.A., Ghabchi, R., Zaman, M. Steger, R., Rani, S., and Rahman, M. A. (2018). "Mechanistic Evaluation of Effect of PPA on Moisture-induced Damage using SFE and XRF." In proceeding of ASCE International Conference on Transportation & Development (ICTD 2018), Philadelphia, Pennsylvania, held on July 15-18, 2018.

7.2.3. Presentations

- Ali, S.A., and Zaman, M. (2018). "Mechanistic Evaluation of Moisture-induced Damage of Asphalt Mixes using SFE and XRF." Presented at Graduate Student Research & Creativity Day, 2018, held at the University of Oklahoma, Norman, OK. Date: March 2th, 2018.
- Ali, S.A., Ghabchi, R., Zaman, M., Steger, R., Rani, S. and Rahman, M.A. (2018). "Development of a Surface Free Energy (SFE) Database for Screening of Mixes for Moisture-induced Damage in Oklahoma." Presented at the 2018 SPTC Summer Symposium, organized by Southern Plain Transportation Center, held at the Metro Tech Conference Center, Oklahoma City. Date: August 14th, 2018.
- Ali, S.A., Ghabchi, R., Zaman, M., Rani, S. and Rahman, M.A. (2018). "Laboratory Characterization of Moisture-Induced Damage Potential of Asphalt Mixes Using Conventional and Unconventional Performance-Based Tests." Presented at Transportation Research Record 98th Annual Meeting, Washington, D.C. Date: January 13-17, 2019.

7.2.4. Posters

- Ali, S.A., Ghabchi, R., Rani, S., Rahman M. A., and Zaman, M. (2017). "Development of a Surface Free Energy (SFE) Database for Screening of Mixes for Moisture-induced Damage in Oklahoma." Poster presented at 2017 Oklahoma Transportation Research Day, held at the Metro Technology Center, OKC, OK. Date: October 17th, 2017.
- Ali, S.A., Ghabchi, R., Rani, S., Rahman, M.A., and Zaman, M. (2018). "Feasibility of Using XRF for Assessment of Surface Free Energy Components of Asphalt binder." Poster presented at 5th GeoChina International Conference, HangZhou, China, held on July 23-25, 2018.

- Ali, S.A., Ghabchi, R., Zaman, M. Steger, R., Rani, S., and Rahman, M. A. (2018). “Mechanistic Evaluation of Effect of PPA on Moisture-induced Damage using SFE and XRF.” Poster presented at ASCE International Conference on Transportation & Development (ICTD 2018), Philadelphia, Pennsylvania, held on July 15-18, 2018.
- Ali, S.A., Ghabchi, R., Rani, S., Rahman M. A., and Zaman, M. (2018). “Evaluation of Surface Free Energy (SFE) Technique for Screening of Mixes for Moisture-induced Damage in Oklahoma.” Poster presented at 2018 Oklahoma Transportation Research Day, held at the Metro Tech Conference Center, Oklahoma City, OK. Date: October 23rd, 2018.

REFERENCES

Abuawad, I. M., Al-Qadi, I. L. and Trepanier, J. S. 2015. Mitigation of moisture damage in asphalt concrete: Testing techniques and additives/modifiers effectiveness. *Construction and Building Materials,* 84, 437-443.

Aksoy, A., Şamlioglu, K., Tayfur, S. and Özen, H. 2005. Effects of various additives on the moisture damage sensitivity of asphalt mixtures. *Construction and Building Materials,* 19(1), 11-18.

Al-Qadi, I. L., Abauwad, I. M., Dhasmana, H. and Coenen, A. R., 2014. *Effects of various asphalt binder additives/modifiers on moisture-susceptible asphaltic mixtures.* Illinois Center for Transportation, 0197-9191.

Alvarez, A. E., Ovalles, E. and Caro, S. 2012a. Assessment of the effect of mineral filler on asphalt–aggregate interfaces based on thermodynamic properties. *Construction and Building Materials,* 28(1), 599-606.

Alvarez, A. E., Ovalles, E. and Epps Martin, A. 2012b. Comparison of asphalt rubber-aggregate and polymer modified asphalt–aggregate systems in terms of surface free energy and energy indices. *Construction and Building Materials,* 35, 385-392.

Arabani, M. and Hamedi, G. H. 2010. Using the surface free energy method to evaluate the effects of polymeric aggregate treatment on moisture damage in hot-mix asphalt. *Journal of Materials in Civil Engineering,* 23(6), 802-811.

Arabani, M. and Hamedi, G. H. 2014. Using the surface free energy method to evaluate the effects of liquid antistrip additives on moisture sensitivity in hot mix asphalt. *International Journal of Pavement Engineering,* 15(1), 66-78.

Arnold, T. S., Needham, S. and Youtcheff Jr, J. 2009. Use of phosphoric acid as a modifier for hot-mix asphalt. *Transportation Research Circular E-C160, Polyphosphoric Acid Modification of Asphalt Binders*, 40-51.

Bagampadde, U., Isacsson, U. and Kiggundu, B. 2006. Impact of bitumen and aggregate composition on stripping in bituminous mixtures. *Materials and structures,* 39(3), 303-315.

Baumgardner, G. L. 2010. Why and how of polyphosphoric acid modification–an industry perspective. *Journal of the Association of Asphalt Paving Technologists,* 79.

Baumgardner, G. L., Masson, J., Hardee, J. R., Menapace, A. M. and Williams, A. G. 2005. Polyphosphoric acid modified asphalt: proposed mechanisms. *Journal of the Association of Asphalt Paving Technologists,* 74, 283-305.

Bhasin, A., 2007. *Development of methods to quantify bitumen-aggregate adhesion and loss of adhesion due to water.* Texas A&M University.

Bhasin, A., Howson, J., Masad, E., Little, D. and Lytton, R. 2007a. Effect of modification processes on bond energy of asphalt binders. *Transportation Research Record: Journal of the Transportation Research Board,* (1998), 29-37.

Bhasin, A., Little, D., Vasconcelos, K. and Masad, E. 2007b. Surface free energy to identify moisture sensitivity of materials for asphalt mixes. *Transportation Research Record: Journal of the Transportation Research Board,* (2001), 37-45.

Bhasin, A. and Little, D. N., 2006. *Characterizing surface properties of aggregates used in hot mix asphalt.*

Bhasin, A. and Little, D. N. 2007. Characterization of aggregate surface energy using the universal sorption device. *Journal of Materials in Civil Engineering,* 19(8), 634-641.

Bhasin, A., Masad, E., Little, D. and Lytton, R. 2006. Limits on adhesive bond energy for improved resistance of hot-mix asphalt to moisture damage. *Transportation Research Record: Journal of the Transportation Research Board,* (1970), 3-13.

Brunauer, S., Emmett, P. H. and Teller, E. 1938. Adsorption of gases in multimolecular layers. *Journal of the American chemical society,* 60(2), 309-319.

Buddhala, A., Hossain, Z., Wasiuddin, N. M., Zaman, M. and Edgar, A. 2011. Effects of an amine anti-stripping agent on moisture susceptibility of sasobit and aspha-min mixes by surface free energy analysis. *Journal of Testing and Evaluation,* 40(1), 91-99.

Caro, S., Masad, E., Bhasin, A. and Little, D. N. 2008a. Moisture susceptibility of asphalt mixtures, Part 1: mechanisms. *International Journal of Pavement Engineering,* 9(2), 81-98.

Caro, S., Masad, E., Bhasin, A. and Little, D. N. 2008b. Moisture susceptibility of asphalt mixtures, Part 2: characterisation and modelling. *International Journal of Pavement Engineering,* 9(2), 99-114.

Chong, K. and Kuruppu, M. 1984. New specimen for fracture toughness determination for rock and other materials. *International Journal of Fracture,* 26(2), R59-R62.

Cooper Jr, S. B., Cooper III, S. B., Mohammad, L. N. and Elseifi, M. A. 2016. Development of a Predictive Model Based on an Artificial Neural Network for the Semicircular Bend Test. *Transportation Research Record: Journal of the Transportation Research Board,* (2576), 83-90.

Curtis, C., Lytton, R. and Brannan, C. 1992. Influence of aggregate chemistry on the adsorption and desorption of asphalt. *Transportation Research Record,* (1362).

D'Angelo, J. A., Harm, E. E., Bartoszek, J. C., Baumgardner, G. L., Corrigan, M. R., Cowsert, J. E., Harman, T. P., Jamshidi, M., Jones, H. W. and Newcomb, D. E., 2008. *Warm-mix asphalt: European practice.*

D'Angelo, J. A. 2010. Effect of poly phosphoric acid on asphalt binder properties. *Journal of the Association of Asphalt Paving Technologists,* 79.

Fee, D., Maldonado, R., Reinke, G. and Romagosa, H. 2010. Polyphosphoric acid modification of asphalt. *Transportation Research Record: Journal of the Transportation Research Board,* (2179), 49-57.

Ghabchi, R., Barman, M., Singh, D., Zaman, M. and Mubaraki, M. A. 2016. Comparison of laboratory performance of asphalt mixes containing different proportions of RAS and RAP. *Construction and Building Materials,* 124, 343-351.

Ghabchi, R., Singh, D. and Zaman, M. 2014. Evaluation of moisture susceptibility of asphalt mixes containing RAP and different types of aggregates and asphalt binders using the surface free energy method. *Construction and Building Materials,* 73, 479-489.

Ghabchi, R., Singh, D. and Zaman, M. 2015. Laboratory evaluation of stiffness, low-temperature cracking, rutting, moisture damage, and fatigue performance of WMA mixes. *Road Materials and Pavement Design,* 16(2), 334-357.

Ghabchi, R., Singh, D., Zaman, M. and Tian, Q. 2013. Mechanistic evaluation of the effect of WMA additives on wettability and moisture susceptibility properties of asphalt mixes. *Journal of Testing and Evaluation,* 41(6), 933-942.

Gorkem, C. and Sengoz, B. 2009. Predicting stripping and moisture induced damage of asphalt concrete prepared with polymer modified bitumen and hydrated lime. *Construction and Building Materials,* 23(6), 2227-2236.

Harvey, J. T. and Lu, Q. 2005. Investigation of Conditions for Moisture Damage in Asphalt Concrete and Appropriate Laboratory Test Methods.

Hefer, A. W., Bhasin, A. and Little, D. N. 2006. Bitumen surface energy characterization using a contact angle approach. *Journal of Materials in Civil Engineering,* 18(6), 759-767.

Hefer, A. W., Little, D. N. and Lytton, R. L. 2005. A synthesis of theories and mechanisms of bitumen-aggregate adhesion including recent advances in quantifying the effects of water. *Journal of the Association of Asphalt Paving Technologists,* 74, 139-196.

Hesp, S. A. and Shurvell, H. F. 2010. X-ray fluorescence detection of waste engine oil residue in asphalt and its effect on cracking in service. *International Journal of Pavement Engineering,* 11(6), 541-553.

Hesp, S. A. and Shurvell, H. F. 2013. Quality assurance testing of asphalt containing waste engine oil. *International Journal of Pavements*.

Hossain, Z., Lewis, S., Zaman, M., Buddhala, A. and O'Rear, E. 2012. Evaluation for warm-mix additive-modified asphalt binders using spectroscopy techniques. *Journal of Materials in Civil Engineering,* 25(2), 149-159.

Huang, B., Shu, X. and Vukosavljevic, D. 2010. Laboratory investigation of cracking resistance of hot-mix asphalt field mixtures containing screened reclaimed asphalt pavement. *Journal of Materials in Civil Engineering,* 23(11), 1535-1543.

Jingyan, L., Xiaoli, C. and Songbai, T. 2012. Research on determination of total acid number of petroleum using mid-infrared attenuated total reflection spectroscopy. *Energy & Fuels,* 26(9), 5633-5637.

Khodaii, A., Tehrani, H. K. and Haghshenas, H. 2012. Hydrated lime effect on moisture susceptibility of warm mix asphalt. *Construction and Building Materials,* 36, 165-170.

Kim, M., Mohammad, L. and Elseifi, M. 2012. Characterization of fracture properties of asphalt mixtures as measured by semicircular bend test and indirect tension test. *Transportation Research Record: Journal of the Transportation Research Board,* (2296), 115-124.

Koc, M., 2013. *Development of testing protocols for direct measurements of contact angles on aggregate and asphalt binder surfaces using a sessile drop device.* Oklahoma State University.

Koc, M. and Bulut, R. 2013. Assessment of a sessile drop device and a new testing approach measuring contact angles on aggregates and asphalt binders. *Journal of Materials in Civil Engineering,* 26(3), 391-398.

LaCroix, A., Regimand, A. and James, L. 2016. Proposed Approach for Evaluation of Cohesive and Adhesive Properties of Asphalt Mixtures for Determination of Moisture Sensitivity. *Transportation Research Record: Journal of the Transportation Research Board,* (2575), 61-69.

Lamontagne, J., Dumas, P., Mouillet, V. and Kister, J. 2001. Comparison by Fourier transform infrared (FTIR) spectroscopy of different ageing techniques: application to road bitumens. *Fuel,* 80(4), 483-488.

Langmuir, I. 1918. The adsorption of gases on plane surfaces of glass, mica and platinum. *Journal of the American chemical society,* 40(9), 1361-1403.

Le Guern, M., Chailleux, E., Farcas, F., Dreessen, S. and Mabille, I. 2010. Physico-chemical analysis of five hard bitumens: Identification of chemical species and molecular organization before and after artificial aging. *Fuel,* 89(11), 3330-3339.

Li, X.-J. and Marasteanu, M. 2010. Using semi circular bending test to evaluate low temperature fracture resistance for asphalt concrete. *Experimental Mechanics,* 50(7), 867-876.

Li, X., Braham, A. F., Marasteanu, M. O., Buttlar, W. G. and Williams, R. C. 2008. Effect of factors affecting fracture energy of asphalt concrete at low temperature. *Road Materials and Pavement Design,* 9(sup1), 397-416.

Liu, Y., Apeagyei, A., Ahmad, N., Grenfell, J. and Airey, G. 2014. Examination of moisture sensitivity of aggregate–bitumen bonding strength using loose asphalt mixture and physico-chemical surface energy property tests. *International Journal of Pavement Engineering,* 15(7), 657-670.

Masad, E., Arambula, E., Ketcham, R., Abbas, A. and Martin, A. E. 2007. Nondestructive measurements of moisture transport in asphalt mixtures. *Asphalt Paving Technology-Proceedings,* 76, 919.

Masad, E. A., Zollinger, C., Bulut, R., Little, D. N. and Lytton, R. L. 2006. Characterization of HMA moisture damage using surface energy and fracture properties (with discussion). *Journal of the Association of Asphalt Paving Technologists,* 75.

Mirzababaei, P. 2016. Effect of zycotherm on moisture susceptibility of Warm Mix Asphalt mixtures prepared with different aggregate types and gradations. *Construction and Building Materials,* 116, 403-412.

Moghadas Nejad, F., Hamedi, G. H. and Azarhoosh, A. 2012. Use of surface free energy method to evaluate effect of hydrate lime on moisture damage in hot-mix asphalt. *Journal of Materials in Civil Engineering,* 25(8), 1119-1126.

Mohammad, L. N., Kim, M. and Challa, H., 2016. *Development of performance-based specifications for Louisiana asphalt mixtures.*

Mouillet, V., Lamontagne, J., Durrieu, F., Planche, J.-P. and Lapalu, L. 2008. Infrared microscopy investigation of oxidation and phase evolution in bitumen modified with polymers. *Fuel,* 87(7), 1270-1280.

Mull, M., Stuart, K. and Yehia, A. 2002. Fracture resistance characterization of chemically modified crumb rubber asphalt pavement. *Journal of Materials Science,* 37(3), 557-566.

Orange, G., Martin, J.-V., Menapace, A., Hemsley, M. and Baumgardner, G. 2004. Rutting and moisture resistance of asphalt mixtures containing polymer and polyphosphoric acid modified bitumen. *Road Materials and Pavement Design,* 5(3), 323-354.

Ozer, H., Al-Qadi, I. L., Singhvi, P., Khan, T., Rivera-Perez, J. and El-Khatib, A. 2016. Fracture characterization of asphalt mixtures with high recycled content using Illinois semicircular bending test method and flexibility index. *Transportation Research Record: Journal of the Transportation Research Board,* (2575), 130-137.

Prowell, B., Hurley, G. and Crews, E. 2007. Field performance of warm-mix asphalt at national center for asphalt technology test track. *Transportation Research Record: Journal of the Transportation Research Board,* (1998), 96-102.

Rani, S., 2019. *Characterization of Rutting in Asphalt Pavements using Laboratory Testing.* Dissertation (Ph.D.). University of Oklahoma.

Reinke, G. and Glidden, S. 2010. Analytical procedures for determining phosphorus content in asphalt binders and impact of aggregate on quantitative recovery of phosphorus from

asphalt binders. *Asphalt Paving Technology-Proceedings Association of Asphalt Technologists,* 79, 695.

Saeidi, H. and Aghayan, I. 2016. Investigating the effects of aging and loading rate on low-temperature cracking resistance of core-based asphalt samples using semi-circular bending test. *Construction and Building Materials,* 126, 682-690.

Saha, G. and Biligiri, K. P. 2016. Fracture properties of asphalt mixtures using semi-circular bending test: a state-of-the-art review and future research. *Construction and Building Materials,* 105, 103-112.

Shu, X., Huang, B. and Vukosavljevic, D. 2008. Laboratory evaluation of fatigue characteristics of recycled asphalt mixture. *Construction and Building Materials,* 22(7), 1323-1330.

Soleimani, A., Walsh, S. and Hesp, S. 2009. Asphalt cement loss tangent as surrogate performance indicator for control of thermal cracking. *Transportation Research Record: Journal of the Transportation Research Board,* (2126), 39-46.

Tan, Y. and Guo, M. 2013. Using surface free energy method to study the cohesion and adhesion of asphalt mastic. *Construction and Building Materials,* 47, 254-260.

Tarefder, R. A. and Ahmad, M. 2014. Evaluating the relationship between permeability and moisture damage of asphalt concrete pavements. *Journal of Materials in Civil Engineering,* 27(5), 04014172.

Tarefder, R. A. and Zaman, A. M. 2009. Nanoscale evaluation of moisture damage in polymer modified asphalts. *Journal of Materials in Civil Engineering,* 22(7), 714-725.

Tarrer, A. and Wagh, V., 1991. *The effect of the physical and chemical characteristics of the aggregate on bonding.* Strategic Highway Research Program, National Research Council Washington, DC, USA.

Taylor, M. A. and Khosla, N. P., 1983. *Stripping of asphalt pavements: State of the art (discussion, closure).*

Thoroppady Kittu, A., 2013. *Surface energy characteristics of granite and limestone aggregates with respect to 2D and 3D surface roughness measurements.* Oklahoma State University.

Tóth, J. 1981. A uniform interpretation of gas/solid adsorption. *Journal of Colloid and Interface Science,* 79(1), 85-95.

Tunnicliff, D. G. and Root, R. E., Testing asphalt concrete for effectiveness of antistripping additives. ed. *Proceedings of the Association of Asphalt Paving Technologists*, 1983, 535-560.

Van Oss, C. J., Chaudhury, M. K. and Good, R. J. 1988. Interfacial Lifshitz-van der Waals and polar interactions in macroscopic systems. *Chemical Reviews,* 88(6), 927-941.

Vargas-Nordcbeck, A., Leiva-Villacorta, F., Aguiar-Moya, J. P. and Loria-Salazar, L. 2016. Evaluating moisture susceptibility of asphalt concrete mixtures through simple performance tests. *Transportation Research Record: Journal of the Transportation Research Board,* (2575), 70-78.

Wagoner, M. P., Buttlar, W. G. and Paulino, G. H. 2005. Development of a single-edge notched beam test for asphalt concrete mixtures. *Journal of Testing and Evaluation,* 33(6), 452-460.

Wasiuddin, N., Zaman, M. and O'Rear, E. 2008. Effect of sasobit and aspha-min on wettability and adhesion between asphalt binders and aggregates. *Transportation Research Record: Journal of the Transportation Research Board,* (2051), 80-89.

Wasiuddin, N. M., Fogle, C. M., Zaman, M. M. and Edgar, A. 2007a. Characterization of Thermal Degradation of qa Liquid Amine Anti-Strip Additives in Asphalt qa Binders Due to RTFO and PAV-Aging. *Journal of Testing and Evaluation,* 35(4), 387-394.

Wasiuddin, N. M., Fogle, C. M., Zaman, M. M. and O'Rear, E. A. 2007b. Effect of Antistrip Additives on Surface Free Energy Characteristics of Asphalt Binders for Moisture-Induced Damage Potential. *Journal of Testing and Evaluation,* 35(1).

Wasiuddin, N. M., Zaman, M. M. and Edgar, A. 2010. Polymeric aggregate treatment using styrene-butadiene rubber (SBR) for moisture-induced damage potential. *International Journal of Pavement Research and Technology,* 3(1), 1-9.

Wei, J., Dong, F., Li, Y. and Zhang, Y. 2014. Relationship analysis between surface free energy and chemical composition of asphalt binder. *Construction and Building Materials,* 71, 116-123.

West, R., Rodezno, C., Julian, G., Prowell, B., Frank, B., Osborn, L. and Kriech, T. 2014. NCHRP Report 779: Field Performance of Warm Mix Asphalt Technologies. *Transportation Research Board of the National Academies, Washington, DC*.

Wu, Z., Mohammad, L. N., Wang, L. and Mull, M. A. 2005. Fracture resistance characterization of superpave mixtures using the semi-circular bending test. *Journal of ASTM International,* 2(3), 1-15.

Xiao, F., Zhao, W., Gandhi, T. and Amirkhanian, S. N. 2010. Influence of antistripping additives on moisture susceptibility of warm mix asphalt mixtures. *Journal of Materials in Civil Engineering,* 22(10), 1047-1055.

Yildirim, Y. and Kennedy, T. W., 2002. *Hamburg wheel tracking device results on plant and field cores produced mixtures.* Citeseer.

Yin, F., Arambula, E., Lytton, R., Martin, A. and Cucalon, L. 2014. Novel method for moisture susceptibility and rutting evaluation using Hamburg wheel tracking test. *Transportation Research Record: Journal of the Transportation Research Board,* (2446), 1-7.

Yoon, H. H. and Tarrer, A. R. 1988. Effect of aggregate properties on stripping. *Transportation Research Board of the National Academies, Washington, DC,* (1171), 37-43.

Zhang, D. and Luo, R. 2017. Modeling of adsorption isotherms of probe vapors on aggregates for accurate determination of aggregate surface energy components. *Construction and Building Materials,* 134, 374-387.

APPENDIX A

Contact Angles and SFE Components of Binders from DWP Test

Table A1 Contact angles of binders with different probe liquids from DWP Test

Binder Source	Binder Type	Aging Condition	Additive	Water Average (°)	Water SD (°)	Glycerin Average (°)	Glycerin SD (°)	Formamide Average (°)	Formamide SD (°)
S1	PG 64-22	RTFO	None	107.91	0.10	94.27	0.11	90.46	0.13
S1	PG 64-22	RTFO	0.5% W1	107.75	0.16	94.12	0.36	89.83	0.38
S1	PG 64-22	RTFO	0.5% A1	106.98	0.09	93.95	0.14	89.74	0.32
S1	PG 64-22	RTFO	20% R1	107.08	0.26	93.13	0.18	89.18	0.21
S1	PG 64-22	PAV	None	107.13	0.59	95.17	0.19	91.17	0.21
S1	PG 64-22	PAV	0.5% W1	107.48	0.74	94.95	0.20	91.00	0.27
S1	PG 64-22	PAV	0.5% A1	107.30	0.62	94.69	0.26	91.19	0.34
S1	PG 64-22	PAV	20% R1	107.02	0.55	95.14	0.12	91.72	0.80
S2	PG 64-22	RTFO	None	112.06	0.62	100.19	0.25	96.98	0.97
S2	PG 64-22	RTFO	0.5% W1	112.38	0.65	101.37	0.53	99.50	0.81
S2	PG 64-22	RTFO	0.5% A1	113.38	0.30	100.57	0.29	97.95	0.86
S2	PG 64-22	RTFO	20% R1	104.20	1.14	98.30	0.46	95.17	0.29
S2	PG 64-22	PAV	None	111.82	0.21	99.73	0.63	95.85	0.29
S2	PG 64-22	PAV	0.5% W1	110.40	0.51	98.76	0.70	95.07	0.85
S2	PG 64-22	PAV	0.5% A1	110.15	0.12	99.01	0.50	95.79	0.44
S2	PG 64-22	PAV	20% R1	110.22	0.64	100.24	0.79	95.72	0.55
S3	PG 76-28	RTFO	None	114.37	0.26	101.17	0.20	97.45	0.39
S3	PG 76-28	RTFO	0.5% W1	115.14	0.40	101.11	0.73	98.18	0.56
S3	PG 76-28	RTFO	0.5% A1	115.81	0.61	100.36	0.78	98.51	0.32
S3	PG 76-28	RTFO	20% R1	113.43	0.27	99.00	0.28	95.96	0.44
S3	PG 76-28	RTFO	1.5% P1	117.70	0.65	108.83	0.41	106.10	0.80
S3	PG 76-28	PAV	None	115.52	0.29	100.37	0.08	100.66	0.23
S3	PG 76-28	PAV	0.5% W1	115.39	0.45	100.05	0.52	98.01	0.59
S3	PG 76-28	PAV	0.5% A1	117.46	0.34	101.16	0.76	97.54	0.38
S3	PG 76-28	PAV	20% R1	114.42	0.63	98.70	0.43	97.53	0.83
S4	PG 76-28	RTFO	None	118.83	0.64	111.81	0.49	107.30	1.00
S4	PG 76-28	RTFO	0.5% W1	118.12	0.89	107.19	0.81	103.32	0.92
S4	PG 76-28	RTFO	0.5% A1	118.73	0.72	110.15	0.52	105.44	0.40
S4	PG 76-28	RTFO	20% R1	115.84	0.62	105.78	1.07	102.46	0.83
S4	PG 76-28	PAV	None	117.03	1.60	109.69	0.18	104.18	1.93
S4	PG 76-28	PAV	0.5% W1	118.93	0.56	107.82	0.85	106.56	0.53
S4	PG 76-28	PAV	0.5% A1	118.93	0.55	106.49	0.46	103.07	1.03
S4	PG 76-28	PAV	20% R1	115.10	0.35	103.99	0.79	101.26	0.56

Table A2 Surface free energy components of binders from DWP Test

Binder Source	Binder Type	Aging Condition	Additive	Γ^+ (mJ/m^2)	Γ^- (mJ/m^2)	Γ^{LW} (mJ/m^2)	Γ^{AB} (mJ/m^2)	Γ^{Total} (mJ/m^2)	Γ^+/Γ^-
S1	PG 64-22	RTFO	None	1.81	0.68	9.31	2.22	11.53	2.65
S1	PG 64-22	RTFO	0.5% W1	1.51	0.64	10.40	1.97	12.37	2.36
S1	PG 64-22	RTFO	0.5% A1	1.49	0.83	10.32	2.23	12.55	1.80
S1	PG 64-22	RTFO	20% R1	1.85	0.69	9.84	2.26	12.10	2.70
S1	PG 64-22	PAV	None	1.39	1.06	9.68	2.43	12.10	1.32
S1	PG 64-22	PAV	0.5% W1	1.51	0.91	9.57	2.35	11.91	1.66
S1	PG 64-22	PAV	0.5% A1	1.84	0.98	8.66	2.68	11.34	1.88
S1	PG 64-22	PAV	20% R1	1.75	1.18	8.47	2.87	11.34	1.48
S2	PG 64-22	RTFO	None	1.50	0.69	7.00	2.04	9.03	2.16
S2	PG 64-22	RTFO	0.5% W1	2.19	1.01	4.60	2.97	7.56	2.18
S2	PG 64-22	RTFO	0.5% A1	1.98	0.51	5.82	2.00	7.82	3.91
S2	PG 64-22	RTFO	20% R1	0.96	3.57	7.75	3.69	11.44	0.27
S2	PG 64-22	PAV	None	1.16	0.60	8.39	1.67	10.06	1.95
S2	PG 64-22	PAV	0.5% W1	1.28	0.82	8.25	2.05	10.31	1.56
S2	PG 64-22	PAV	0.5% A1	1.47	1.01	7.34	2.44	9.78	1.46
S2	PG 64-22	PAV	20% R1	0.63	1.05	9.82	1.63	11.45	0.60
S3	PG 76-28	RTFO	None	1.28	0.29	7.67	1.23	8.90	4.38
S3	PG 76-28	RTFO	0.5% W1	1.89	0.23	6.16	1.31	7.47	8.34
S3	PG 76-28	RTFO	0.5% A1	3.02	0.14	4.47	1.31	5.78	21.27
S3	PG 76-28	RTFO	20% R1	2.05	0.26	6.74	1.46	8.21	7.83
S3	PG 76-28	RTFO	1.5% P1	0.88	0.79	4.81	1.67	6.49	1.12
S3	PG 76-28	PAV	None	5.11	0.33	1.87	2.61	4.48	15.29
S3	PG 76-28	PAV	0.5% W1	2.88	0.16	4.80	1.34	6.14	18.54
S3	PG 76-28	PAV	0.5% A1	1.72	0.01	7.24	0.22	7.46	250.17
S3	PG 76-28	PAV	20% R1	3.92	0.22	3.72	1.85	5.56	18.01
S4	PG 76-28	RTFO	None	0.12	0.79	7.32	0.61	7.92	0.15
S4	PG 76-28	RTFO	0.5% W1	0.65	0.34	6.86	0.94	7.80	1.92
S4	PG 76-28	RTFO	0.5% A1	0.17	0.53	7.96	0.59	8.55	0.32
S4	PG 76-28	RTFO	20% R1	0.88	0.67	6.24	1.53	7.78	1.31
S4	PG 76-28	PAV	None	0.03	0.77	9.81	0.28	10.10	0.03
S4	PG 76-28	PAV	0.5% W1	2.06	0.51	2.89	2.04	4.94	4.06
S4	PG 76-28	PAV	0.5% A1	1.03	0.18	6.09	0.86	6.96	5.69
S4	PG 76-28	PAV	20% R1	1.42	0.62	5.51	1.88	7.39	2.26

APPENDIX B

XRF Test Results of Binders

Table B1 XRF test results of the binders

Binder Source	Binder Type	Aging Condition	Additive	Al (ppm)	Si (ppm)	P (ppm)	S (ppm)	Cl (ppm)	Ca (ppm)	V (ppm)	Fe (ppm)	Ni (ppm)	Cu (ppm)	Zn (ppm)	Sr (ppm)	Sn (ppm)	Pb (ppm)	Others (ppm)
S1	PG 64-22	RTFO	None	331.0	78.2	120.0	46507.0	60.1	13.0	183.0	39.0	78.2	3.0	3.4	0.0	13.8	0.0	95.3
S1	PG 64-22	RTFO	0.5% W1	375.0	89.7	122.0	47192.0	65.7	12.7	185.0	38.9	78.3	3.5	3.4	0.0	12.2	0.0	95.2
S1	PG 64-22	RTFO	0.5% A1	350.0	80.8	122.0	46722.0	64.7	9.8	182.0	42.4	78.0	3.2	3.7	0.0	14.2	0.0	95.2
S1	PG 64-22	RTFO	20% R1	345.0	73.3	120.0	44699.0	56.3	8.3	179.0	38.8	76.0	3.4	3.0	0.0	14.2	0.0	95.4
S2	PG 64-22	RTFO	None	294.0	82.3	99.0	37887.0	38.3	5.6	354.0	68.1	66.5	3.3	2.5	0.0	12.6	0.0	96.1
S2	PG 64-22	RTFO	0.5% W1	296.0	72.4	101.6	37168.0	36.9	6.8	349.0	66.0	66.3	3.5	2.6	0.0	13.8	0.0	96.2
S2	PG 64-22	RTFO	0.5% A1	297.0	76.6	99.4	37182.0	43.1	8.5	353.0	69.9	66.1	3.2	2.8	0.0	13.8	0.0	96.2
S2	PG 64-22	RTFO	20% R1	294.0	79.7	103.0	38653.0	40.9	6.6	315.0	63.7	69.9	2.7	2.9	0.0	15.1	0.0	96.0
S3	PG 76-28	RTFO	None	241.0	116.0	80.1	28666.0	46.3	26.1	45.2	183.0	25.2	3.3	8.4	1.2	14.5	2.5	97.1
S3	PG 76-28	RTFO	0.5% W1	273.0	117.0	83.2	28936.0	51.3	33.8	47.2	181.0	26.0	3.2	9.0	1.3	12.9	2.6	97.0
S3	PG 76-28	RTFO	0.5% A1	248.0	123.0	78.9	29109.0	50.2	28.3	43.5	181.0	25.4	3.5	8.1	1.3	14.5	2.3	97.0
S3	PG 76-28	RTFO	20% R1	259.0	105.0	83.5	30.7	47.7	20.9	71.1	151.0	35.4	3.9	7.4	1.0	15.9	1.7	96.9
S3	PG 76-28	RTFO	1.5% P1	264.0	142.0	3385.0	26979.0	34.1	26.4	42.4	170.0	24.1	3.1	8.4	1.2	22.0	2.7	96.9
S4	PG 76-28	RTFO	None	192.0	89.2	603.0	21028.0	30.7	12.5	119.0	95.8	49.1	3.4	3.1	0.0	12.5	0.0	97.8
S4	PG 76-28	RTFO	0.5% W1	186.0	98.7	612.0	21127.0	0.0	10.1	118.0	96.8	48.5	3.2	3.3	0.0	13.4	0.0	97.8
S4	PG 76-28	RTFO	0.5% A1	188.0	87.7	606.0	20700.0	0.0	9.3	118.0	95.2	49.8	3.1	2.9	0.0	14.8	0.0	97.8
S4	PG 76-28	RTFO	20% R1	222.0	86.4	495.0	25076.0	0.0	8.9	128.0	85.6	56.3	3.3	2.7	0.0	13.9	0.0	97.4

APPENDIX C

TAN Test Results of Binders

Table C1 TAN Test Results of Binders

Binder Source	Binder Type	Aging Condition	Additive	Acid Values (mg KOH/g)
S1	PG 64-22	RTFO	None	0.61
S1	PG 64-22	RTFO	0.5% W1	0.40
S1	PG 64-22	RTFO	0.5% A1	0.41
S3	PG 76-28	RTFO	None	0.40
S3	PG 76-28	RTFO	0.5% W1	0.39
S3	PG 76-28	RTFO	0.5% A1	0.46
S3	PG 76-28	RTFO	1.5% P1	14.32

APPENDIX D

FTIR Test Results of Binders

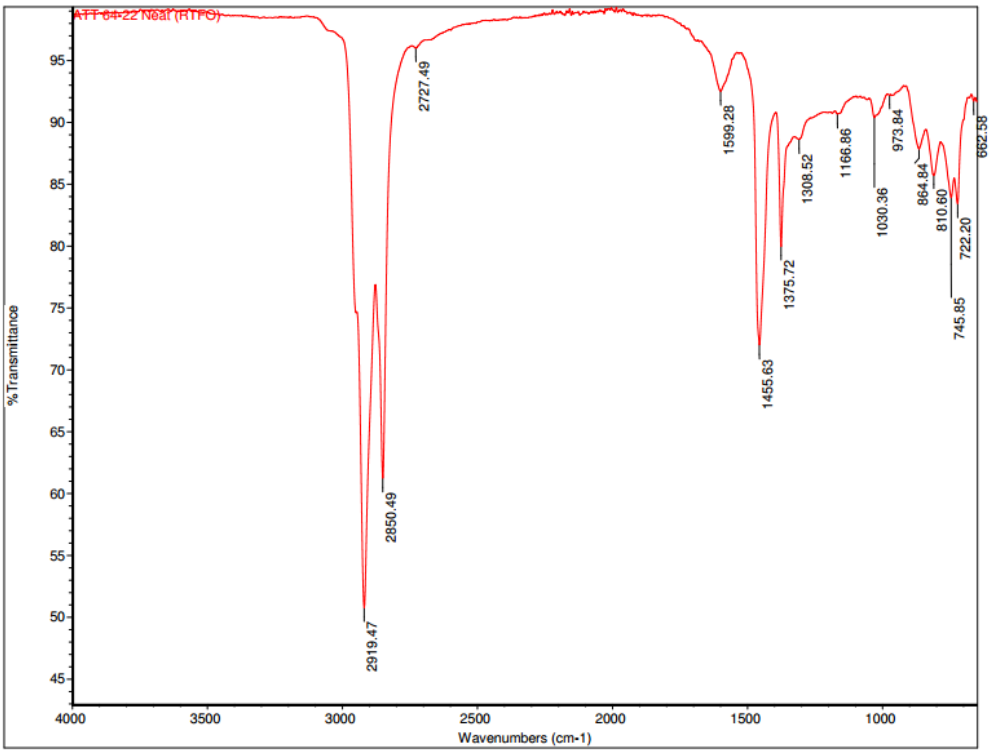

Figure D1 FTIR result for S1 PG 64-22

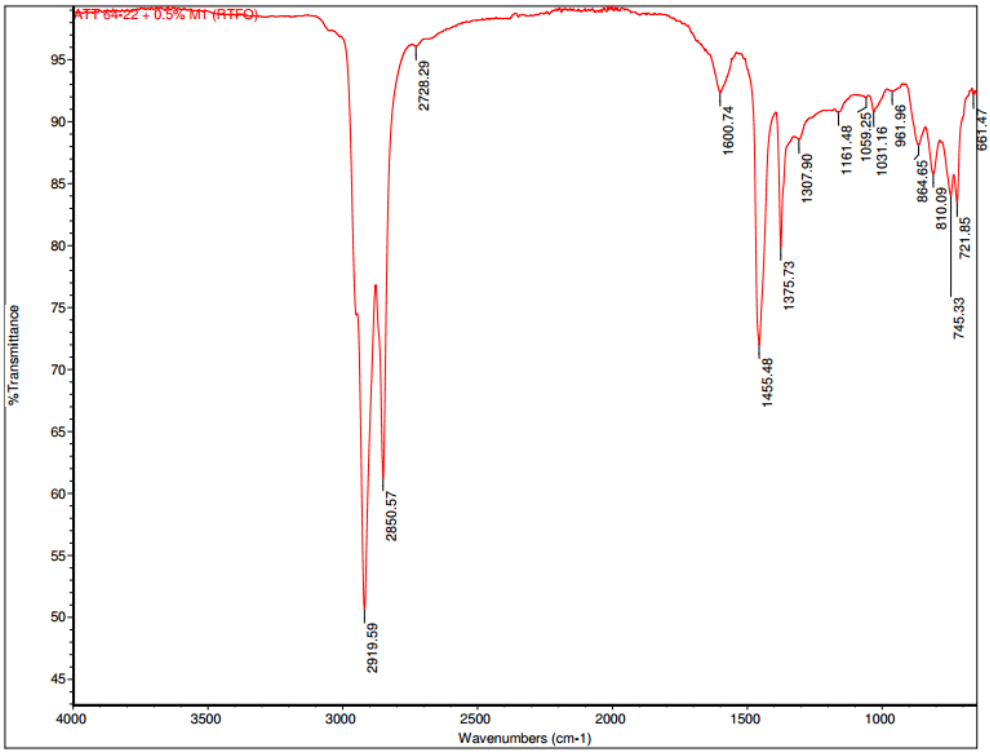

Figure D2 FTIR result for S1 PG 64-22 + 0.5% W1

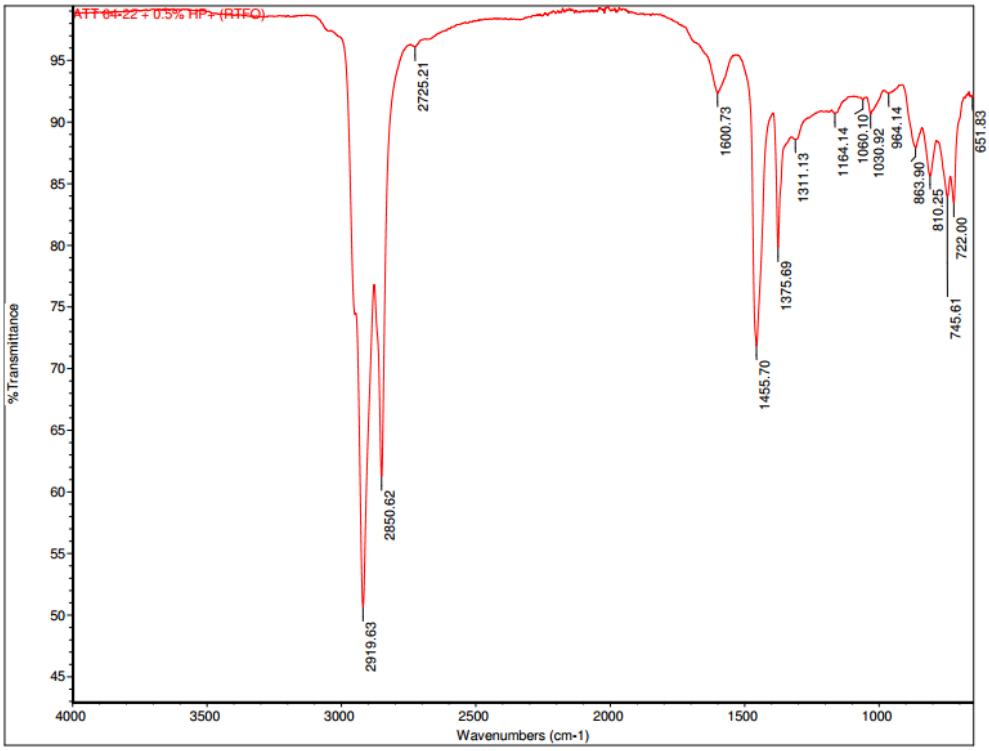

Figure D3 FTIR result for S1 PG 64-22 + 0.5% A1

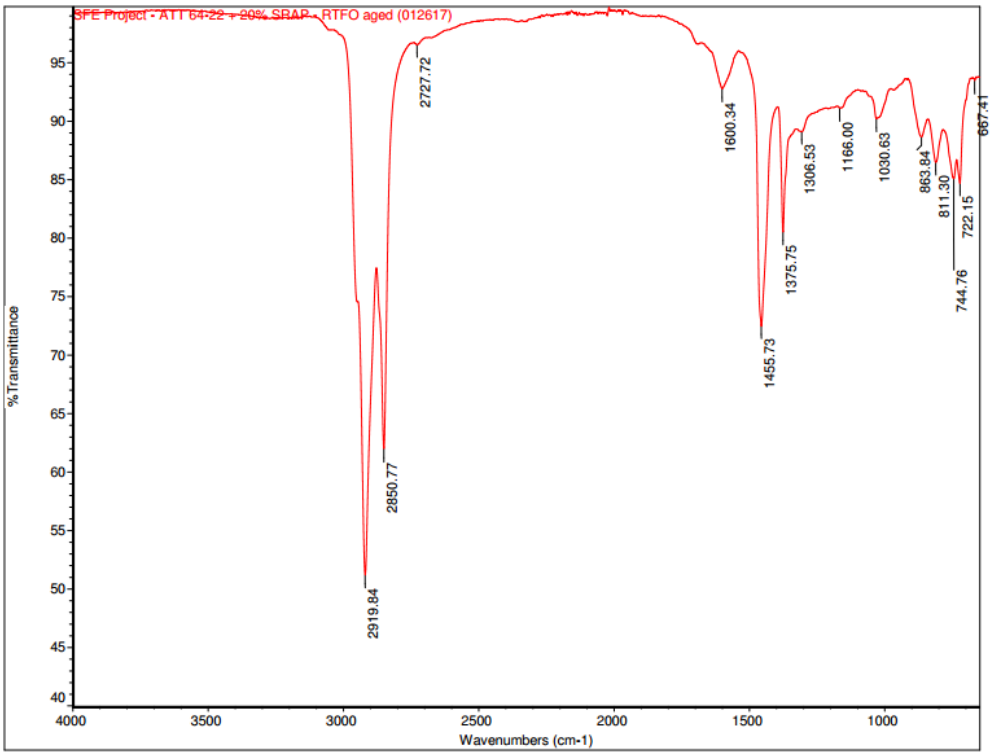

Figure D4 FTIR result for S1 PG 64-22 + 20% R1

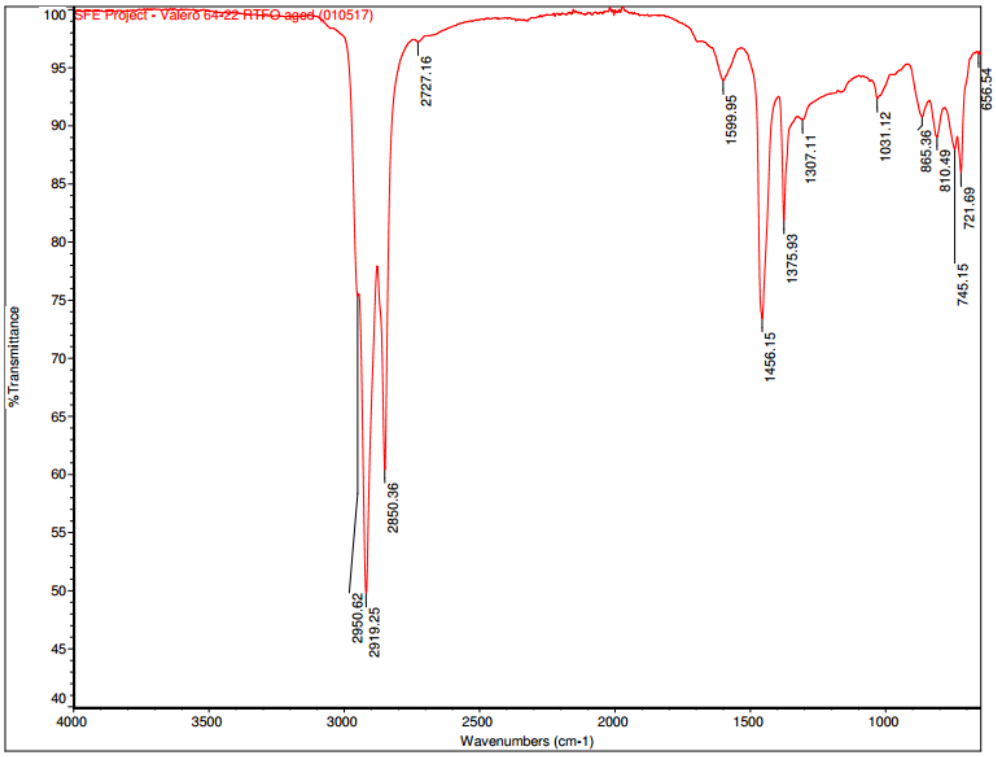

Figure D5 FTIR result for S2 PG 64-22

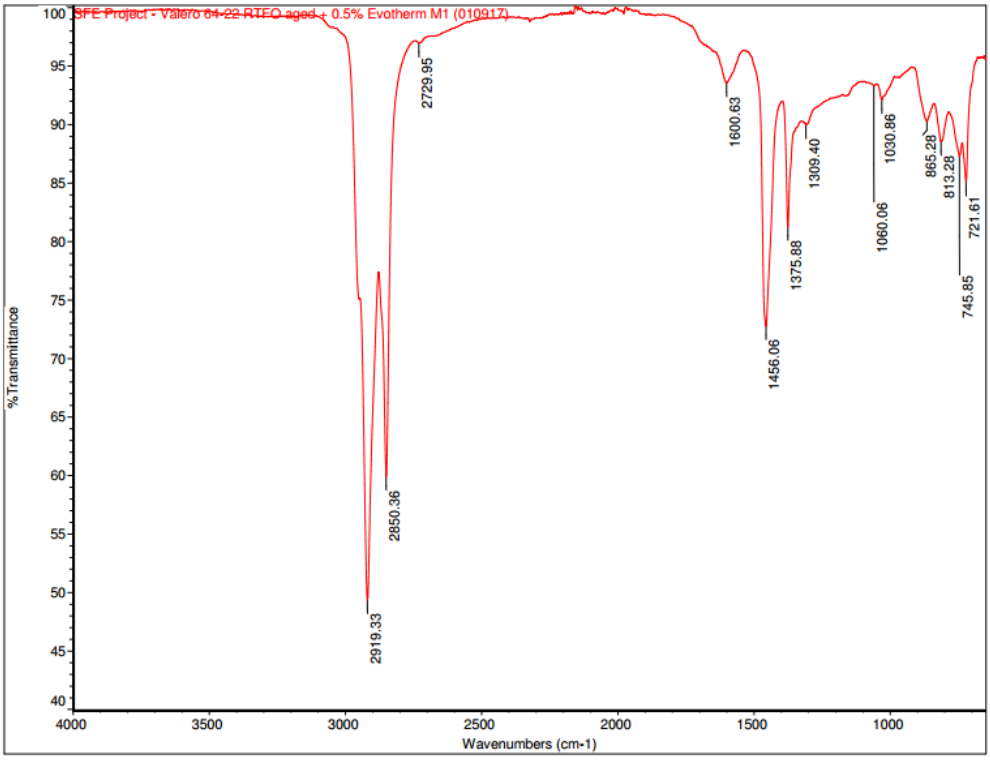

Figure D6 FTIR result for S2 PG 64-22 + 0.5% W1

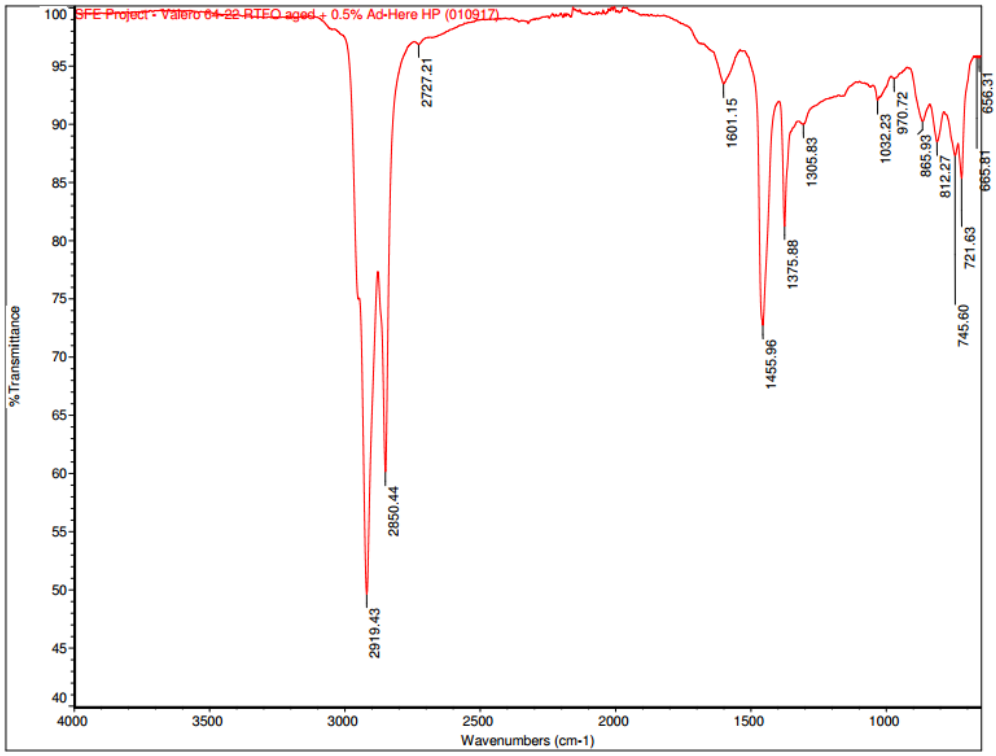

Figure D7 FTIR result for S2 PG 64-22 + 0.5% A1

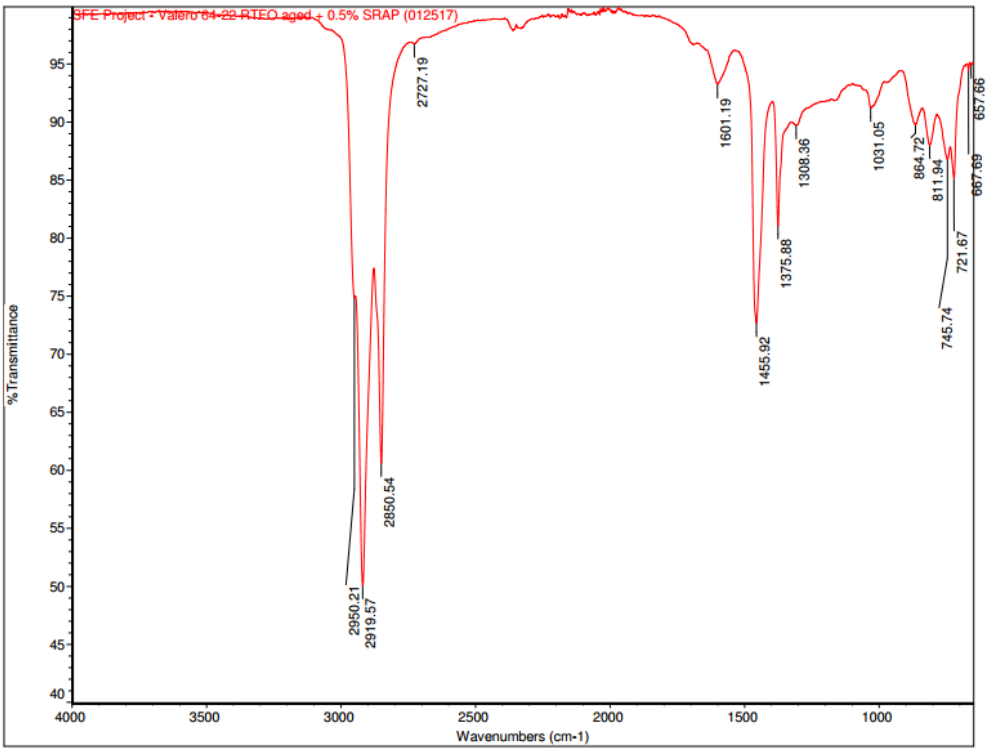

Figure D8 FTIR result for S2 PG 64-22 + 20% R1

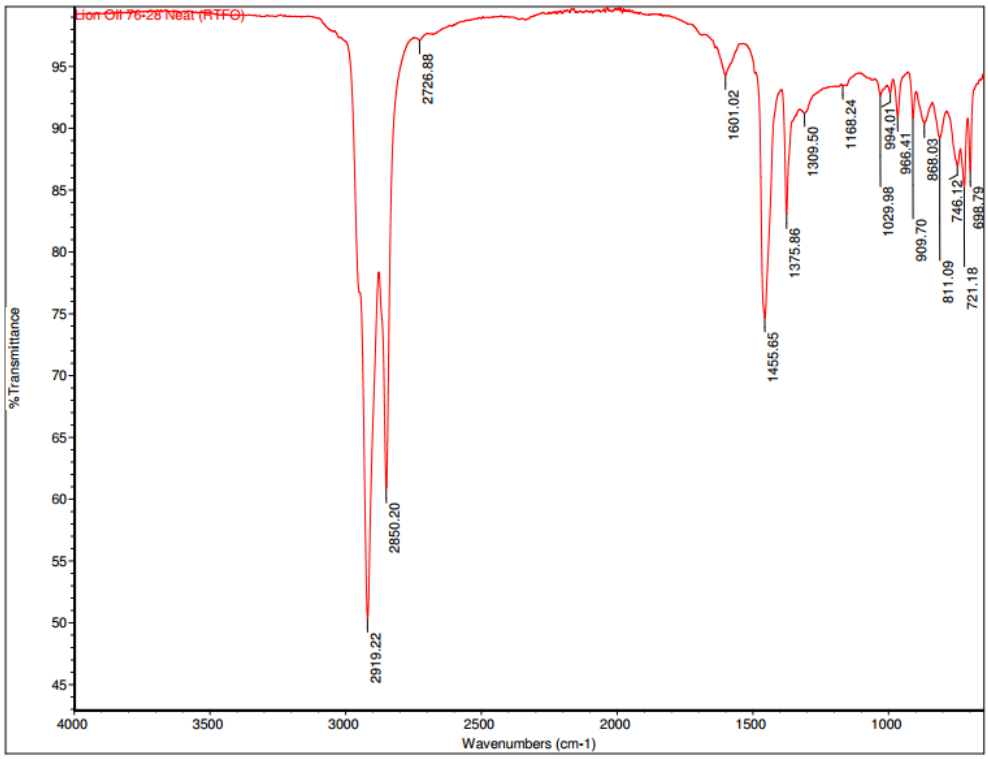

Figure D9 FTIR result for S3 PG 76-28

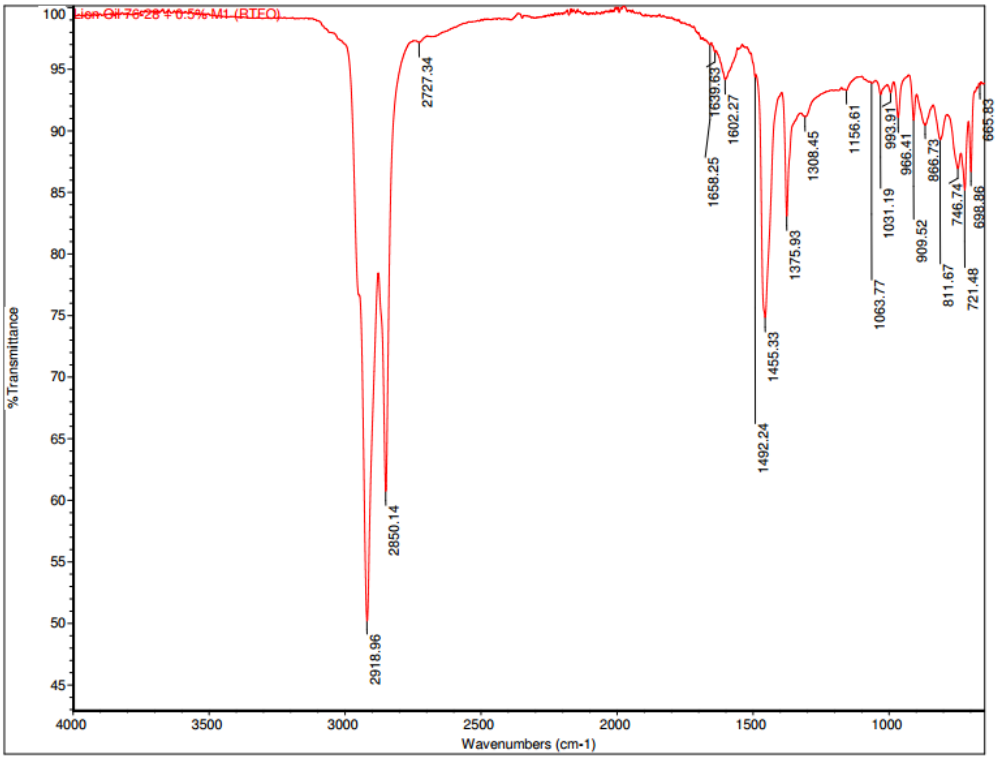

Figure D10 FTIR result for S3 PG 76-28 + 0.5% W1

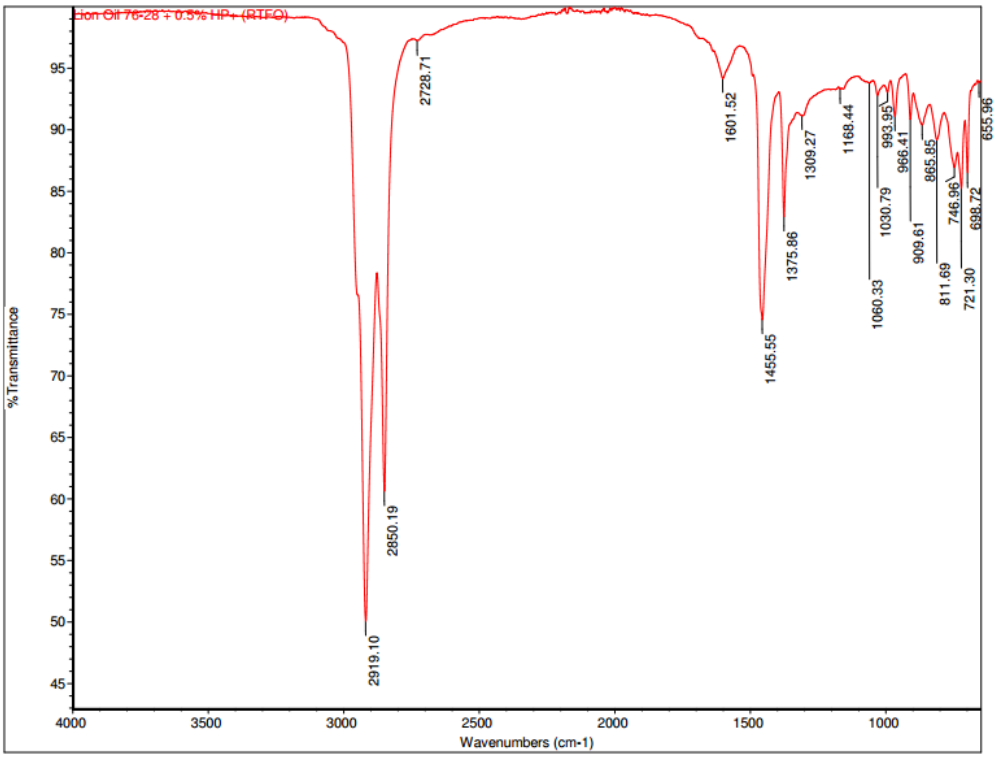

Figure D11 FTIR result for S3 PG 76-28 + 0.5% A1

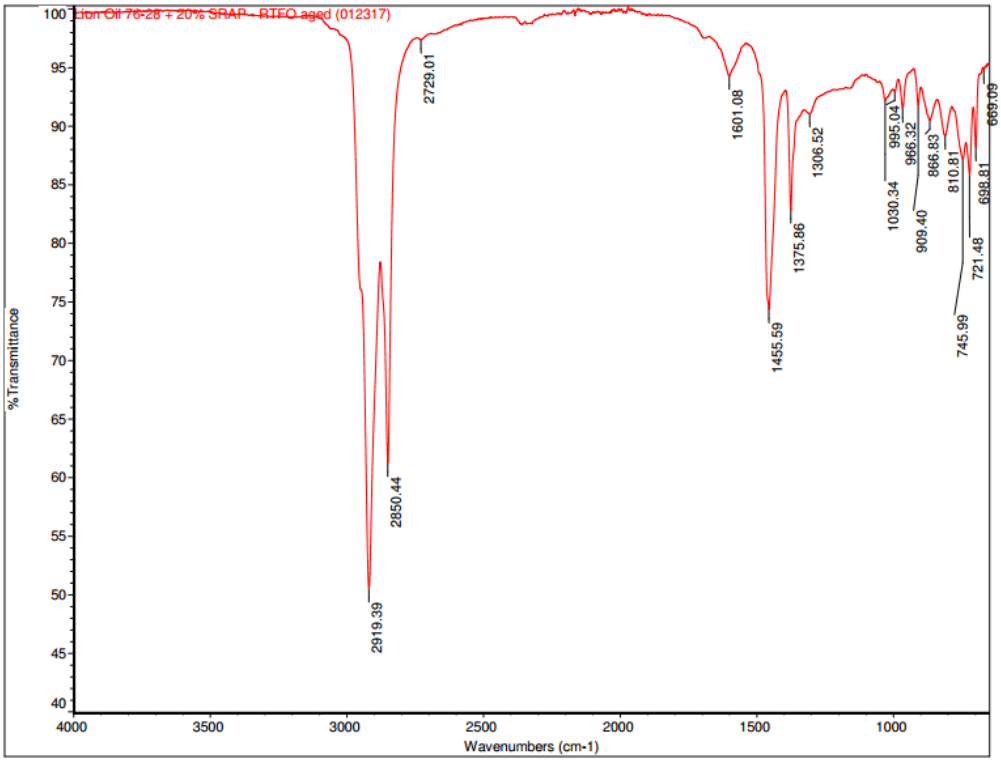

Figure D12 FTIR result for S3 PG 76-28 + 20% R1

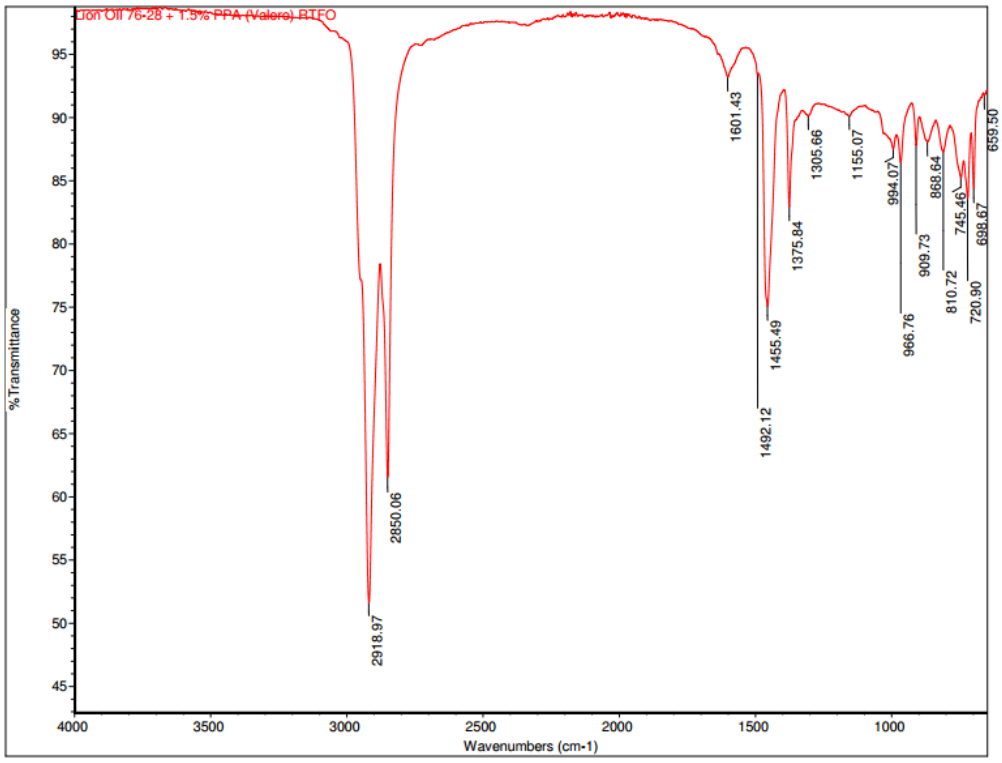

Figure D13 FTIR result for S3 PG 76-28 + 1.5% P1

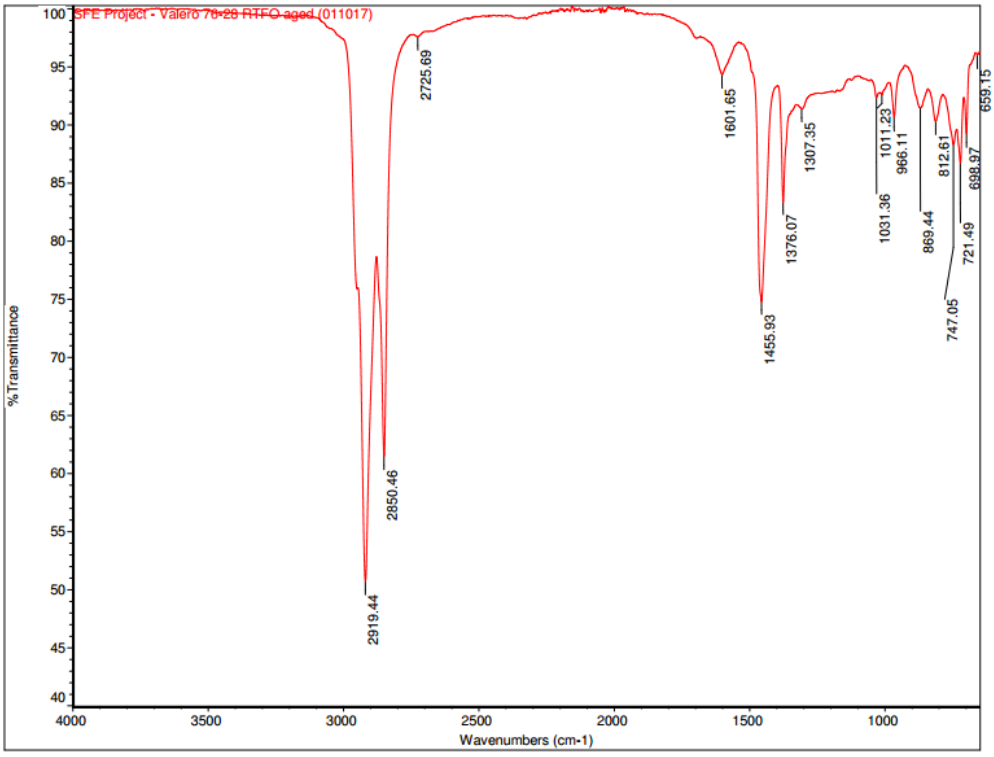

Figure D14 FTIR result for S4 PG 76-28

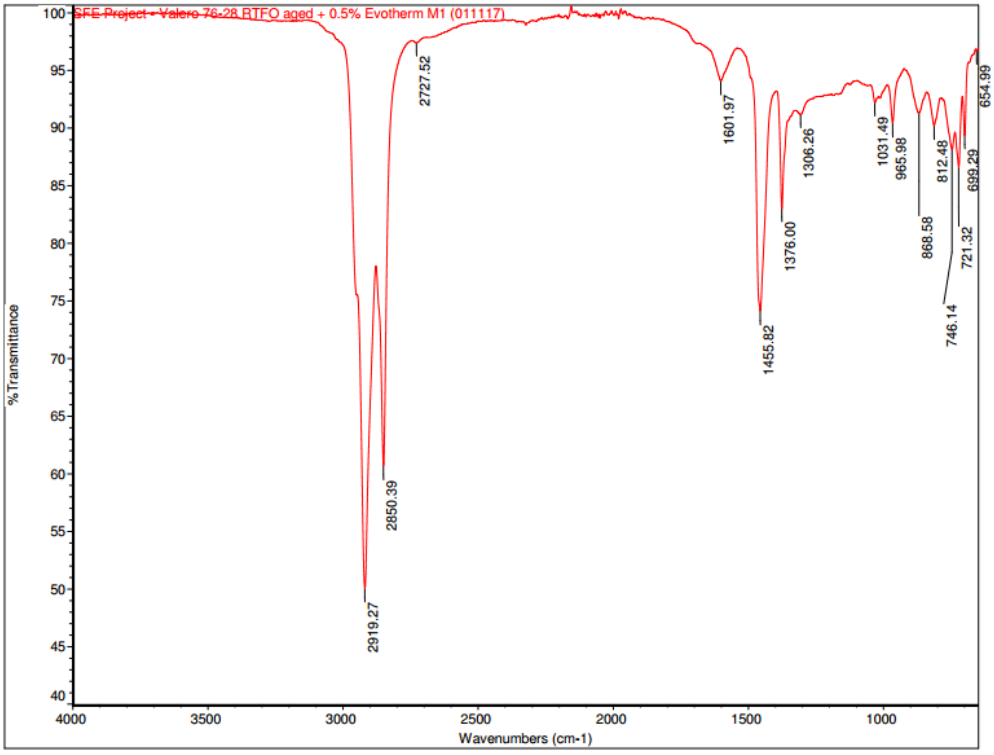

Figure D15 FTIR result for S4 PG 76-28 + 0.5% W1

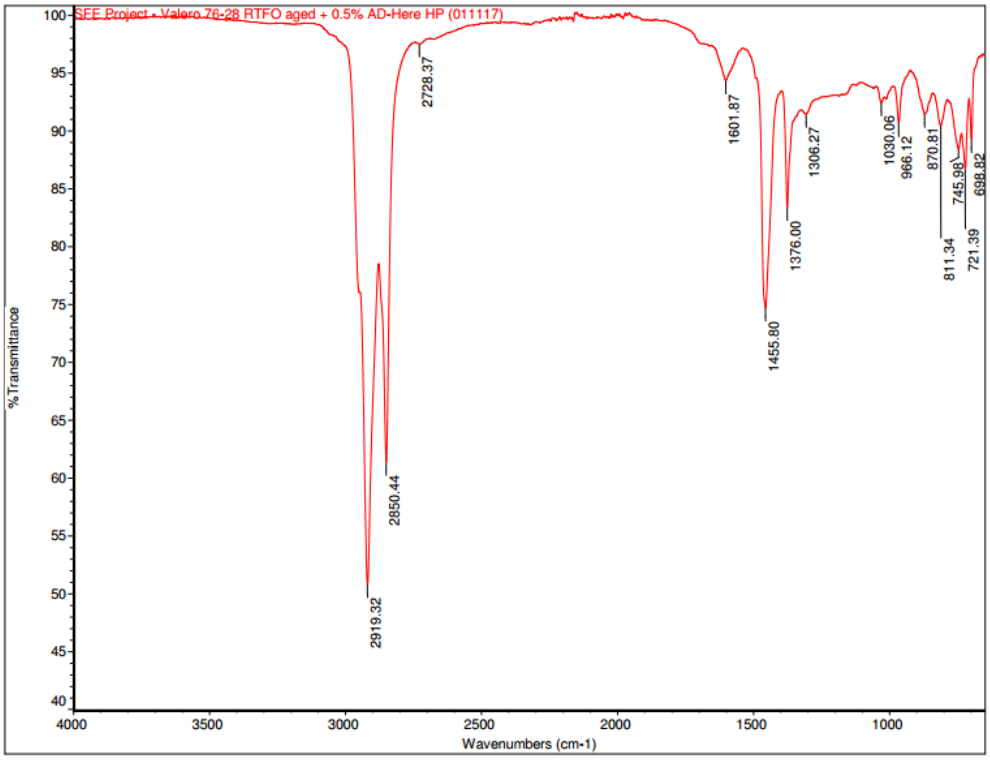

Figure D16 FTIR result for S4 PG 76-28 + 0.5% A1

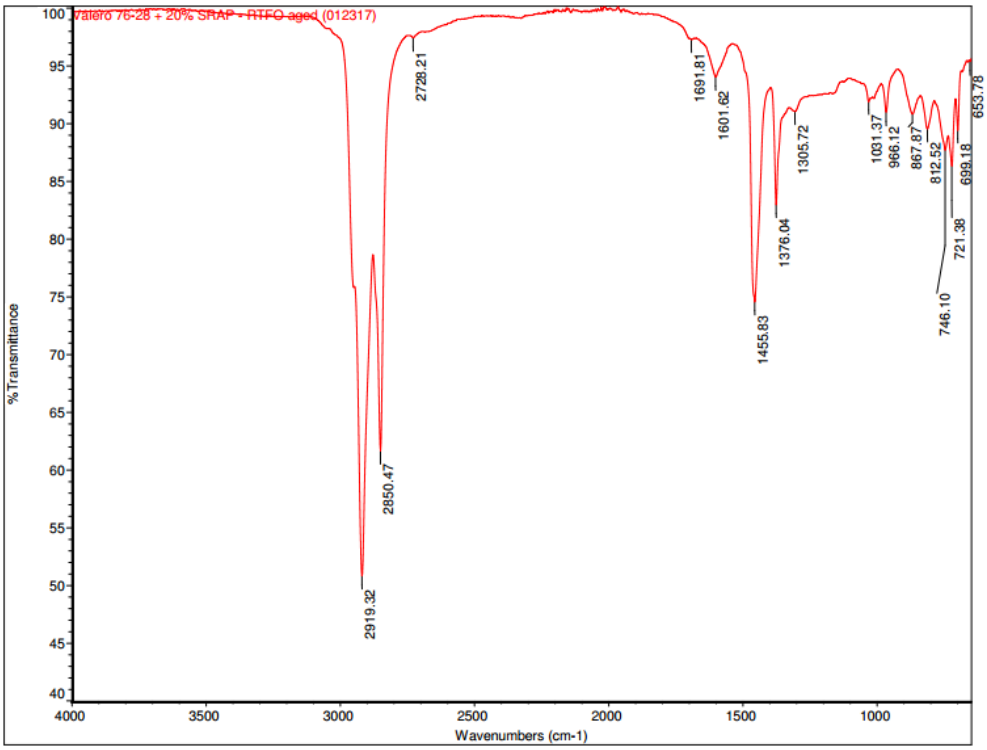

Figure D17 FTIR result for S4 PG 76-28 + 20% R1

APPENDIX E

Contact Angles and SFE Components of Binders from SD Test

Table E1 Contact angles of binders with different probe liquids from SD Test

Binder Source	Binder Type	Aging Condition	Additive	Water Average (°)	Water SD (°)	Ethylene Glycol Average (°)	Ethylene Glycol SD (°)	Diiodomethane Average (°)	Diiodomethane SD (°)
S1	PG 64-22	RTFO	None	95.35	2.05	74.87	2.90	45.28	3.25
S1	PG 64-22	RTFO	0.5% W1	92.63	2.11	73.78	3.03	44.63	2.35
S1	PG 64-22	RTFO	0.5% A1	91.60	1.76	75.90	1.56	42.85	2.80
S1	PG 64-22	RTFO	20% R1	97.78	1.43	77.17	1.74	46.05	1.86
S2	PG 64-22	RTFO	None	98.48	1.36	81.25	1.37	61.30	1.85
S2	PG 64-22	RTFO	0.5% W1	96.38	2.05	80.58	1.58	60.87	2.02
S2	PG 64-22	RTFO	0.5% A1	96.95	1.76	79.35	2.27	54.48	1.83
S2	PG 64-22	RTFO	20% R1	99.20	1.31	83.62	1.65	60.12	1.35
S3	PG 76-28	RTFO	None	99.37	1.64	82.92	2.25	60.30	1.98
S3	PG 76-28	RTFO	0.5% W1	97.05	1.04	81.48	1.30	58.50	1.55
S3	PG 76-28	RTFO	0.5% A1	95.90	2.22	82.40	1.36	58.38	1.78
S3	PG 76-28	RTFO	20% R1	100.70	1.41	83.67	2.49	63.13	1.49
S3	PG 76-28	RTFO	1.5% P1	93.15	1.35	80.25	2.24	63.34	1.91
S4	PG 76-28	RTFO	None	101.68	1.39	83.32	2.22	63.02	1.53
S4	PG 76-28	RTFO	0.5% W1	98.25	2.02	81.68	2.41	62.73	1.80
S4	PG 76-28	RTFO	0.5% A1	99.58	1.19	83.02	2.07	60.82	1.99
S4	PG 76-28	RTFO	20% R1	102.20	1.32	85.23	2.00	62.67	1.32

Table E2 Surface free energy components of binders from SD Test

Binder Source	Binder Type	Aging Condition	Additive	Γ^+ (mJ/m^2)	Γ^- (mJ/m^2)	Γ^{LW} (mJ/m^2)	Γ^{AB} (mJ/m^2)	Γ^{Total} (mJ/m^2)	Γ^+/Γ^-
S1	PG 64-22	RTFO	None	2.56	0.46	36.86	2.17	39.03	5.58
S1	PG 64-22	RTFO	0.5% W1	3.77	0.50	37.21	2.74	39.95	7.58
S1	PG 64-22	RTFO	0.5% A1	5.06	0.91	38.15	4.28	42.43	5.57
S1	PG 64-22	RTFO	20% R1	1.95	0.56	36.45	2.08	38.53	3.50
S2	PG 64-22	RTFO	None	2.98	0.21	27.83	1.59	29.41	14.13
S2	PG 64-22	RTFO	0.5% W1	4.00	0.24	28.08	1.97	30.05	16.47
S2	PG 64-22	RTFO	0.5% A1	3.10	0.40	31.74	2.23	33.97	7.72
S2	PG 64-22	RTFO	20% R1	3.18	0.44	28.51	2.37	30.88	7.20
S3	PG 76-28	RTFO	None	2.91	0.36	28.40	2.04	30.44	8.12
S3	PG 76-28	RTFO	0.5% W1	3.77	0.40	29.44	2.47	31.90	9.35
S3	PG 76-28	RTFO	0.5% A1	4.80	0.56	29.51	3.27	32.77	8.63
S3	PG 76-28	RTFO	20% R1	2.51	0.25	26.77	1.58	28.35	10.13
S3	PG 76-28	RTFO	1.5% P1	6.29	0.22	26.65	2.35	29.00	28.64
S4	PG 76-28	RTFO	None	1.97	0.20	26.84	1.25	28.09	9.95
S4	PG 76-28	RTFO	0.5% W1	3.28	0.19	27.00	1.59	28.60	16.88
S4	PG 76-28	RTFO	0.5% A1	2.84	0.33	28.10	1.95	30.05	8.48
S4	PG 76-28	RTFO	20% R1	2.15	0.35	27.04	1.73	28.77	6.19

APPENDIX F

SFE Components of Aggregates from USD Test

Table F1 Surface free energy components of un-treated aggregates from USD Test

Aggregate Type	SSA (m^2/g)	Γ^{LW} (mJ/m^2)	Γ^{+} (mJ/m^2)	Γ^{-} (mJ/m^2)	Γ^{Total} (mJ/m^2)
Limestone 1	0.30	56.73	33.78	416.94	294.10
Limestone 2	0.87	59.66	45.88	884.19	462.49
Limestone 3	1.50	56.97	31.69	1435.14	483.51
Granite	0.74	58.40	1.46	2477.59	178.69
Rhyolite	1.83	52.93	50.61	2423.40	753.40

Table F2 Surface free energy components of lime-treated aggregates from USD Test

Aggregate Type	SSA (m^2/g)	Γ^{LW} (mJ/m^2)	Γ^{+} (mJ/m^2)	Γ^{-} (mJ/m^2)	Γ^{Total} (mJ/m^2)
Limestone 1	0.58	58.04	20.17	520.21	262.88
Limestone 2	1.09	57.38	28.20	899.88	375.99
Limestone 3	1.70	58.04	34.91	1141.82	457.33
Granite	0.49	60.55	36.50	5360.24	945.15
Rhyolite	1.30	46.78	138.14	6026.01	1871.56

APPENDIX G

XRF Test Results of Aggregates

Table G1 Mineral composition of aggregates from XRF tests

Aggregate Type `	Na_2O (%)	MgO (%)	Al_2O_3 (%)	SiO_2 (%)	P_2O_5 (%)	K_2O (%)	CaO (%)	TiO_2 (%)	MnO_2 (%)	Fe_2O_3 (%)	Others (%)
Limestone 1	0.0	2.9	1.2	6.6	0.0	0.5	85.4	0.1	0.0	2.0	1.3
Limestone 2	0.0	1.4	1.0	6.5	0.0	0.2	90.2	0.0	0.0	0.3	0.3
Limestone 3	0.0	2.0	1.5	9.7	0.0	0.2	85.8	0.0	0.0	0.4	0.3
Granite	3.9	0.1	11.4	74.8	0.0	5.9	0.8	0.2	0.1	2.4	0.4
Rhyolite	3.1	1.4	12.2	68.9	0.3	4.0	1.5	1.3	0.2	6.8	0.5

APPENDIX H

Contact Angles and SFE Components of Aggregates from SD Test

Table H1 Contact angles of aggregates with different probe liquids from SD test

Aggregate Type	Water Average (°)	Water SD (°)	Ethylene Glycol Average (°)	Ethylene Glycol SD (°)	Diiodomethane Average (°)	Diiodomethane SD (°)
Limestone 1	53.7	1.4	31.9	1.2	37.2	1.8
Limestone 2	59.4	1.6	23.3	1.2	40.0	3.0
Limestone 3	63.8	3.0	31.8	4.0	42.1	2.6
Granite	51.1	2.2	34.6	1.4	48.5	1.8

Table H2 SFE components of aggregates from SD test

Aggregate Type	Γ^{LW} (mJ/m^2)	Γ^{+} (mJ/m^2)	Γ^{-} (mJ/m^2)	Γ^{Total} (mJ/m^2)
Limestone 1	40.99	0.16	26.56	45.13
Limestone 2	39.61	0.88	16.96	47.35
Limestone 3	38.54	0.68	14.62	44.35
Granite	35.10	0.34	32.21	41.70

APPENDIX I

Energy parameters of binder-aggregate system from DWP and USD Tests

Table I1 Energy parameters of binders with Limestone 1 aggregate

Binder Source	Binder Type	Aging Condition	Additive	W_{AS} (mJ/m^2)	W_{ASW}^{wet} (mJ/m^2)	$S_{A/S}$ (mJ/m^2)	ER_1	ER_2
S1	PG 64-22	RTFO	None	110.49	-129.59	87.42	0.85	0.67
S1	PG 64-22	RTFO	0.5% W1	108.09	-132.18	83.36	0.82	0.63
S1	PG 64-22	RTFO	0.5% A1	108.90	-132.31	83.80	0.82	0.63
S1	PG 64-22	RTFO	20% R1	112.50	-128.57	88.30	0.87	0.69
S1	PG 64-22	PAV	None	107.02	-134.00	82.81	0.80	0.62
S1	PG 64-22	PAV	0.5% W1	107.89	-132.70	84.07	0.81	0.63
S1	PG 64-22	PAV	0.5% A1	111.16	-129.65	88.48	0.86	0.68
S1	PG 64-22	PAV	20% R1	110.43	-130.72	87.75	0.84	0.67
S2	PG 64-22	RTFO	None	99.49	-135.63	81.42	0.73	0.60
S2	PG 64-22	RTFO	0.5% W1	104.35	-130.39	89.22	0.80	0.68
S2	PG 64-22	RTFO	0.5% A1	102.02	-131.55	86.37	0.78	0.66
S2	PG 64-22	RTFO	20% R1	103.83	-140.77	80.94	0.74	0.57
S2	PG 64-22	PAV	None	96.67	-138.74	76.55	0.70	0.55
S2	PG 64-22	PAV	0.5% W1	100.07	-137.00	79.46	0.73	0.58
S2	PG 64-22	PAV	0.5% A1	102.09	-135.29	82.53	0.75	0.61
S2	PG 64-22	PAV	20% R1	91.51	-145.79	68.61	0.63	0.47
S3	PG 76-28	RTFO	None	94.25	-138.17	76.46	0.68	0.55
S3	PG 76-28	RTFO	0.5% W1	99.07	-132.46	84.12	0.75	0.64
S3	PG 76-28	RTFO	0.5% A1	107.23	-123.54	95.67	0.87	0.77
S3	PG 76-28	RTFO	20% R1	103.48	-130.04	87.06	0.80	0.67
S3	PG 76-28	RTFO	1.5% P1	81.75	-146.87	68.78	0.56	0.47
S3	PG 76-28	PAV	None	119.61	-111.48	110.65	1.07	0.99
S3	PG 76-28	PAV	0.5% W1	106.87	-124.36	94.59	0.86	0.76
S3	PG 76-28	PAV	0.5% A1	95.13	-133.76	80.21	0.71	0.60
S3	PG 76-28	PAV	20% R1	115.27	-117.08	104.15	0.98	0.89
S4	PG 76-28	RTFO	None	64.99	-162.36	49.15	0.40	0.30
S4	PG 76-28	RTFO	0.5% W1	79.18	-148.97	63.57	0.53	0.43
S4	PG 76-28	RTFO	0.5% A1	67.61	-159.85	50.51	0.42	0.32
S4	PG 76-28	RTFO	20% R1	85.46	-145.27	69.90	0.59	0.48
S4	PG 76-28	PAV	None	63.92	-165.45	43.73	0.39	0.26
S4	PG 76-28	PAV	0.5% W1	92.54	-134.70	82.66	0.69	0.61
S4	PG 76-28	PAV	0.5% A1	83.55	-143.70	69.64	0.58	0.48
S4	PG 76-28	PAV	20% R1	93.13	-138.44	78.35	0.67	0.57

Table I2 Energy parameters of binders with Limestone 2 aggregate

Binder Source	Binder Type	Aging Condition	Additive	W_{AS} (mJ/m^2)	W_{ASW}^{wet} (mJ/m^2)	$S_{A/S}$ (mJ/m^2)	ER_1	ER_2
S1	PG 64-22	RTFO	None	138.31	-207.36	115.24	0.67	0.56
S1	PG 64-22	RTFO	0.5% W1	133.78	-212.08	109.05	0.63	0.51
S1	PG 64-22	RTFO	0.5% A1	134.65	-212.14	109.55	0.63	0.52
S1	PG 64-22	RTFO	20% R1	140.67	-206.00	116.47	0.68	0.57
S1	PG 64-22	PAV	None	132.18	-214.42	107.98	0.62	0.50
S1	PG 64-22	PAV	0.5% W1	133.82	-212.36	110.00	0.63	0.52
S1	PG 64-22	PAV	0.5% A1	139.44	-206.96	116.77	0.67	0.56
S1	PG 64-22	PAV	20% R1	138.26	-208.49	115.57	0.66	0.55
S2	PG 64-22	RTFO	None	124.90	-215.81	106.84	0.58	0.50
S2	PG 64-22	RTFO	0.5% W1	134.66	-205.68	119.53	0.65	0.58
S2	PG 64-22	RTFO	0.5% A1	130.50	-208.66	114.85	0.63	0.55
S2	PG 64-22	RTFO	20% R1	126.75	-223.44	103.87	0.57	0.46
S2	PG 64-22	PAV	None	119.37	-221.63	99.25	0.54	0.45
S2	PG 64-22	PAV	0.5% W1	124.03	-218.64	103.42	0.57	0.47
S2	PG 64-22	PAV	0.5% A1	127.69	-215.28	108.13	0.59	0.50
S2	PG 64-22	PAV	20% R1	109.45	-233.44	86.55	0.47	0.37
S3	PG 76-28	RTFO	None	117.45	-220.56	99.66	0.53	0.45
S3	PG 76-28	RTFO	0.5% W1	126.55	-210.57	111.61	0.60	0.53
S3	PG 76-28	RTFO	0.5% A1	141.16	-195.19	129.60	0.72	0.66
S3	PG 76-28	RTFO	20% R1	132.11	-207.00	115.70	0.64	0.56
S3	PG 76-28	RTFO	1.5% P1	101.80	-232.40	88.83	0.44	0.38
S3	PG 76-28	PAV	None	163.36	-173.33	154.39	0.94	0.89
S3	PG 76-28	PAV	0.5% W1	140.08	-196.75	127.80	0.71	0.65
S3	PG 76-28	PAV	0.5% A1	120.79	-213.69	105.87	0.57	0.50
S3	PG 76-28	PAV	20% R1	153.78	-184.17	142.65	0.83	0.77
S4	PG 76-28	RTFO	None	74.09	-258.86	58.24	0.29	0.23
S4	PG 76-28	RTFO	0.5% W1	96.34	-237.40	80.73	0.41	0.34
S4	PG 76-28	RTFO	0.5% A1	77.69	-255.36	60.60	0.30	0.24
S4	PG 76-28	RTFO	20% R1	105.47	-230.85	89.92	0.46	0.39
S4	PG 76-28	PAV	None	69.80	-265.16	49.61	0.26	0.19
S4	PG 76-28	PAV	0.5% W1	121.31	-211.52	111.43	0.57	0.53
S4	PG 76-28	PAV	0.5% A1	104.21	-228.63	90.30	0.46	0.39
S4	PG 76-28	PAV	20% R1	117.72	-219.45	102.94	0.54	0.47

Table I3 Energy parameters of binders with Limestone 3 aggregate

Binder Source	Binder Type	Aging Condition	Additive	W_{AS} (mJ/m^2)	W_{ASW}^{wet} (mJ/m^2)	$S_{A/S}$ (mJ/m^2)	ER_1	ER_2
S1	PG 64-22	RTFO	None	157.26	-257.50	134.19	0.61	0.52
S1	PG 64-22	RTFO	0.5% W1	150.85	-264.10	126.12	0.57	0.48
S1	PG 64-22	RTFO	0.5% A1	151.35	-264.53	126.25	0.57	0.48
S1	PG 64-22	RTFO	20% R1	159.86	-255.90	135.66	0.62	0.53
S1	PG 64-22	PAV	None	147.97	-267.73	123.76	0.55	0.46
S1	PG 64-22	PAV	0.5% W1	150.59	-264.69	126.76	0.57	0.48
S1	PG 64-22	PAV	0.5% A1	158.23	-257.27	135.55	0.62	0.53
S1	PG 64-22	PAV	20% R1	156.28	-259.56	133.59	0.60	0.51
S2	PG 64-22	RTFO	None	142.01	-267.79	123.95	0.53	0.46
S2	PG 64-22	RTFO	0.5% W1	155.71	-253.72	140.58	0.61	0.55
S2	PG 64-22	RTFO	0.5% A1	150.93	-257.32	135.28	0.59	0.53
S2	PG 64-22	RTFO	20% R1	137.39	-281.89	114.51	0.49	0.41
S2	PG 64-22	PAV	None	134.15	-275.93	114.04	0.49	0.41
S2	PG 64-22	PAV	0.5% W1	139.41	-272.36	118.79	0.51	0.44
S2	PG 64-22	PAV	0.5% A1	144.22	-267.84	124.66	0.54	0.47
S2	PG 64-22	PAV	20% R1	118.91	-293.07	96.01	0.41	0.33
S3	PG 76-28	RTFO	None	133.69	-273.41	115.90	0.49	0.42
S3	PG 76-28	RTFO	0.5% W1	146.99	-259.23	132.04	0.57	0.51
S3	PG 76-28	RTFO	0.5% A1	167.88	-237.56	156.33	0.71	0.66
S3	PG 76-28	RTFO	20% R1	153.33	-254.86	136.92	0.60	0.54
S3	PG 76-28	RTFO	1.5% P1	114.30	-289.00	101.33	0.40	0.35
S3	PG 76-28	PAV	None	198.38	-207.40	189.41	0.96	0.91
S3	PG 76-28	PAV	0.5% W1	166.05	-239.87	153.76	0.69	0.64
S3	PG 76-28	PAV	0.5% A1	141.05	-262.53	126.12	0.54	0.48
S3	PG 76-28	PAV	20% R1	184.28	-222.76	173.15	0.83	0.78
S4	PG 76-28	RTFO	None	76.64	-325.39	60.79	0.24	0.19
S4	PG 76-28	RTFO	0.5% W1	107.23	-295.60	91.63	0.36	0.31
S4	PG 76-28	RTFO	0.5% A1	81.69	-320.45	64.59	0.25	0.20
S4	PG 76-28	RTFO	20% R1	118.01	-287.40	102.45	0.41	0.36
S4	PG 76-28	PAV	None	69.31	-334.74	49.12	0.21	0.15
S4	PG 76-28	PAV	0.5% W1	142.48	-259.44	132.60	0.55	0.51
S4	PG 76-28	PAV	0.5% A1	118.89	-283.03	104.98	0.42	0.37
S4	PG 76-28	PAV	20% R1	134.47	-271.79	119.69	0.49	0.44

Table I4 Energy parameters of binders with granite aggregate

Binder Source	Binder Type	Aging Condition	Additive	W_{AS} (mJ/m^2)	W_{ASW}^{wet} (mJ/m^2)	$S_{A/S}$ (mJ/m^2)	ER_1	ER_2
S1	PG 64-22	RTFO	None	182.52	-308.57	159.45	0.59	0.52
S1	PG 64-22	RTFO	0.5% W1	173.64	-317.65	148.91	0.55	0.47
S1	PG 64-22	RTFO	0.5% A1	172.97	-319.25	147.87	0.54	0.46
S1	PG 64-22	RTFO	20% R1	185.51	-306.57	161.32	0.61	0.53
S1	PG 64-22	PAV	None	167.53	-324.50	143.32	0.52	0.44
S1	PG 64-22	PAV	0.5% W1	171.98	-319.63	148.15	0.54	0.46
S1	PG 64-22	PAV	0.5% A1	182.27	-309.56	159.59	0.59	0.52
S1	PG 64-22	PAV	20% R1	178.65	-313.52	155.97	0.57	0.50
S2	PG 64-22	RTFO	None	164.26	-321.88	146.19	0.51	0.45
S2	PG 64-22	RTFO	0.5% W1	182.42	-303.34	167.29	0.60	0.55
S2	PG 64-22	RTFO	0.5% A1	178.53	-306.06	162.88	0.58	0.53
S2	PG 64-22	RTFO	20% R1	144.49	-351.13	121.61	0.41	0.35
S2	PG 64-22	PAV	None	153.53	-332.89	133.41	0.46	0.40
S2	PG 64-22	PAV	0.5% W1	158.88	-329.22	138.27	0.48	0.42
S2	PG 64-22	PAV	0.5% A1	164.72	-323.67	145.16	0.51	0.45
S2	PG 64-22	PAV	20% R1	129.26	-359.05	106.37	0.36	0.30
S3	PG 76-28	RTFO	None	156.36	-327.08	138.57	0.48	0.42
S3	PG 76-28	RTFO	0.5% W1	175.94	-306.61	161.00	0.57	0.53
S3	PG 76-28	RTFO	0.5% A1	206.30	-275.47	194.75	0.75	0.71
S3	PG 76-28	RTFO	20% R1	183.33	-301.20	166.92	0.61	0.55
S3	PG 76-28	RTFO	1.5% P1	129.19	-350.44	116.22	0.37	0.33
S3	PG 76-28	PAV	None	247.28	-234.83	238.31	1.05	1.01
S3	PG 76-28	PAV	0.5% W1	203.32	-278.93	191.04	0.73	0.68
S3	PG 76-28	PAV	0.5% A1	172.05	-307.85	157.13	0.56	0.51
S3	PG 76-28	PAV	20% R1	227.58	-255.79	216.45	0.89	0.85
S4	PG 76-28	RTFO	None	77.36	-401.01	61.52	0.19	0.15
S4	PG 76-28	RTFO	0.5% W1	121.77	-357.39	106.17	0.34	0.30
S4	PG 76-28	RTFO	0.5% A1	85.50	-392.98	68.40	0.22	0.17
S4	PG 76-28	RTFO	20% R1	133.56	-348.18	118.00	0.38	0.34
S4	PG 76-28	PAV	None	65.99	-414.40	45.80	0.16	0.11
S4	PG 76-28	PAV	0.5% W1	170.65	-307.60	160.77	0.55	0.52
S4	PG 76-28	PAV	0.5% A1	139.72	-338.54	125.81	0.41	0.37
S4	PG 76-28	PAV	20% R1	156.22	-326.37	141.44	0.48	0.43

Table I5 Energy parameters of binders with rhyolite aggregate

Binder Source	Binder Type	Aging Condition	Additive	W_{AS} (mJ/m^2)	W_{ASW}^{wet} (mJ/m^2)	$S_{A/S}$ (mJ/m^2)	ER_1	ER_2
S1	PG 64-22	RTFO	None	188.56	-353.23	165.49	0.53	0.47
S1	PG 64-22	RTFO	0.5% W1	179.37	-362.61	154.64	0.49	0.43
S1	PG 64-22	RTFO	0.5% A1	180.03	-362.88	154.93	0.50	0.43
S1	PG 64-22	RTFO	20% R1	191.50	-351.28	167.30	0.55	0.48
S1	PG 64-22	PAV	None	176.11	-366.62	151.90	0.48	0.41
S1	PG 64-22	PAV	0.5% W1	179.63	-362.67	155.80	0.50	0.43
S1	PG 64-22	PAV	0.5% A1	190.31	-352.21	167.63	0.54	0.48
S1	PG 64-22	PAV	20% R1	187.89	-354.97	165.21	0.53	0.47
S2	PG 64-22	RTFO	None	170.80	-366.02	152.74	0.47	0.42
S2	PG 64-22	RTFO	0.5% W1	191.07	-345.38	175.94	0.55	0.51
S2	PG 64-22	RTFO	0.5% A1	183.61	-351.67	167.97	0.52	0.48
S2	PG 64-22	RTFO	20% R1	163.68	-382.63	140.80	0.43	0.37
S2	PG 64-22	PAV	None	159.35	-377.77	139.24	0.42	0.37
S2	PG 64-22	PAV	0.5% W1	166.24	-372.55	145.63	0.45	0.39
S2	PG 64-22	PAV	0.5% A1	173.29	-365.80	153.73	0.47	0.42
S2	PG 64-22	PAV	20% R1	138.23	-400.78	115.33	0.34	0.29
S3	PG 76-28	RTFO	None	159.48	-374.65	141.69	0.43	0.38
S3	PG 76-28	RTFO	0.5% W1	178.24	-355.00	163.29	0.50	0.46
S3	PG 76-28	RTFO	0.5% A1	207.30	-325.17	195.75	0.64	0.60
S3	PG 76-28	RTFO	20% R1	185.89	-349.33	169.48	0.53	0.49
S3	PG 76-28	RTFO	1.5% P1	137.06	-393.27	124.09	0.35	0.32
S3	PG 76-28	PAV	None	250.62	-282.18	241.66	0.89	0.86
S3	PG 76-28	PAV	0.5% W1	204.51	-328.44	192.23	0.62	0.59
S3	PG 76-28	PAV	0.5% A1	169.62	-360.98	154.69	0.47	0.43
S3	PG 76-28	PAV	20% R1	229.50	-304.56	218.38	0.75	0.72
S4	PG 76-28	RTFO	None	85.53	-443.53	69.68	0.19	0.16
S4	PG 76-28	RTFO	0.5% W1	125.84	-404.02	110.23	0.31	0.27
S4	PG 76-28	RTFO	0.5% A1	91.57	-437.60	74.47	0.21	0.17
S4	PG 76-28	RTFO	20% R1	140.36	-392.08	124.80	0.36	0.32
S4	PG 76-28	PAV	None	73.84	-457.23	53.65	0.16	0.12
S4	PG 76-28	PAV	0.5% W1	176.24	-352.71	166.36	0.50	0.47
S4	PG 76-28	PAV	0.5% A1	141.82	-387.13	127.91	0.37	0.33
S4	PG 76-28	PAV	20% R1	162.53	-370.76	147.75	0.44	0.40

APPENDIX J

Energy parameters of binder-aggregate system from SD Tests

Table J1 Energy parameters of binders with Limestone 1 aggregate

Binder Source	Binder Type	Aging Condition	Additive	W_{AS} (mJ/m^2)	W_{ASW}^{wet} (mJ/m^2)	$S_{A/S}$ (mJ/m^2)	ER_1	ER_2
S1	PG 64-22	RTFO	None	94.78	44.78	16.72	2.12	0.37
S1	PG 64-22	RTFO	0.5% W1	98.70	44.69	18.80	2.21	0.42
S1	PG 64-22	RTFO	0.5% A1	103.03	42.73	18.17	2.41	0.43
S1	PG 64-22	RTFO	20% R1	92.29	43.99	15.24	2.10	0.35
S2	PG 64-22	RTFO	None	85.71	44.08	26.89	1.94	0.61
S2	PG 64-22	RTFO	0.5% W1	88.87	43.90	28.77	2.02	0.66
S2	PG 64-22	RTFO	0.5% A1	90.80	43.71	22.85	2.08	0.52
S2	PG 64-22	RTFO	20% R1	87.29	42.40	25.53	2.06	0.60
S3	PG 76-28	RTFO	None	86.31	42.97	25.42	2.01	0.59
S3	PG 76-28	RTFO	0.5% W1	90.00	43.01	26.19	2.09	0.61
S3	PG 76-28	RTFO	0.5% A1	92.74	42.06	27.19	2.21	0.65
S3	PG 76-28	RTFO	20% R1	82.97	43.34	26.28	1.91	0.61
S3	PG 76-28	RTFO	1.5% P1	92.33	43.77	34.32	2.11	0.78
S4	PG 76-28	RTFO	None	81.16	43.82	24.98	1.85	0.57
S4	PG 76-28	RTFO	0.5% W1	85.55	44.00	28.35	1.94	0.64
S4	PG 76-28	RTFO	0.5% A1	85.72	43.05	25.61	1.99	0.59
S4	PG 76-28	RTFO	20% R1	82.17	42.55	24.64	1.93	0.58

Table J2 Energy parameters of binders with Limestone 2 aggregate

Binder Source	Binder Type	Aging Condition	Additive	W_{AS} (mJ/m^2)	W_{ASW}^{wet} (mJ/m^2)	$S_{A/S}$ (mJ/m^2)	ER_1	ER_2
S1	PG 64-22	RTFO	None	90.88	46.92	12.82	1.94	0.27
S1	PG 64-22	RTFO	0.5% W1	94.11	46.14	14.21	2.04	0.31
S1	PG 64-22	RTFO	0.5% A1	98.06	43.79	13.19	2.24	0.30
S1	PG 64-22	RTFO	20% R1	88.89	46.63	11.84	1.91	0.25
S2	PG 64-22	RTFO	None	81.49	45.89	22.66	1.78	0.49
S2	PG 64-22	RTFO	0.5% W1	84.11	45.18	24.01	1.86	0.53
S2	PG 64-22	RTFO	0.5% A1	86.61	45.56	18.66	1.90	0.41
S2	PG 64-22	RTFO	20% R1	83.15	44.31	21.39	1.88	0.48
S3	PG 76-28	RTFO	None	82.26	44.96	21.37	1.83	0.48
S3	PG 76-28	RTFO	0.5% W1	85.48	44.53	21.67	1.92	0.49
S3	PG 76-28	RTFO	0.5% A1	87.82	43.18	22.27	2.03	0.52
S3	PG 76-28	RTFO	20% R1	79.11	45.52	22.41	1.74	0.49
S3	PG 76-28	RTFO	1.5% P1	86.52	44.00	28.51	1.97	0.65
S4	PG 76-28	RTFO	None	77.61	46.30	21.43	1.68	0.46
S4	PG 76-28	RTFO	0.5% W1	81.14	45.64	23.95	1.78	0.52
S4	PG 76-28	RTFO	0.5% A1	81.70	45.07	21.59	1.81	0.48
S4	PG 76-28	RTFO	20% R1	78.64	45.06	21.10	1.75	0.47

Table J3 Energy parameters of binders with Limestone 3 aggregate

Binder Source	Binder Type	Aging Condition	Additive	W_{AS} (mJ/m^2)	W_{ASW}^{wet} (mJ/m^2)	$S_{A/S}$ (mJ/m^2)	ER_1	ER_2
S1	PG 64-22	RTFO	None	88.74	49.70	10.68	1.79	0.21
S1	PG 64-22	RTFO	0.5% W1	91.76	48.71	11.86	1.88	0.24
S1	PG 64-22	RTFO	0.5% A1	95.46	46.11	10.60	2.07	0.23
S1	PG 64-22	RTFO	20% R1	86.87	49.52	9.81	1.75	0.20
S2	PG 64-22	RTFO	None	79.46	48.78	20.64	1.63	0.42
S2	PG 64-22	RTFO	0.5% W1	81.91	47.90	21.81	1.71	0.46
S2	PG 64-22	RTFO	0.5% A1	84.46	48.33	16.52	1.75	0.34
S2	PG 64-22	RTFO	20% R1	81.03	47.11	19.27	1.72	0.41
S3	PG 76-28	RTFO	None	80.21	47.82	19.32	1.68	0.40
S3	PG 76-28	RTFO	0.5% W1	83.27	47.23	19.46	1.76	0.41
S3	PG 76-28	RTFO	0.5% A1	85.43	45.71	19.88	1.87	0.44
S3	PG 76-28	RTFO	20% R1	77.17	48.50	20.48	1.59	0.42
S3	PG 76-28	RTFO	1.5% P1	84.05	46.45	26.04	1.81	0.56
S4	PG 76-28	RTFO	None	75.79	49.41	19.61	1.53	0.40
S4	PG 76-28	RTFO	0.5% W1	79.09	48.50	21.89	1.63	0.45
S4	PG 76-28	RTFO	0.5% A1	79.66	47.96	19.56	1.66	0.41
S4	PG 76-28	RTFO	20% R1	76.75	48.09	19.21	1.60	0.40

Table J4 Energy parameters of binders with granite aggregate

Binder Source	Binder Type	Aging Condition	Additive	W_{AS} (mJ/m^2)	W_{ASW}^{wet} (mJ/m^2)	$S_{A/S}$ (mJ/m^2)	ER_1	ER_2
S1	PG 64-22	RTFO	None	90.90	38.28	12.84	2.37	0.34
S1	PG 64-22	RTFO	0.5% W1	95.16	38.53	15.26	2.47	0.40
S1	PG 64-22	RTFO	0.5% A1	99.82	36.90	14.96	2.71	0.41
S1	PG 64-22	RTFO	20% R1	88.25	37.33	11.20	2.36	0.30
S2	PG 64-22	RTFO	None	82.64	38.39	23.82	2.15	0.62
S2	PG 64-22	RTFO	0.5% W1	86.08	38.49	25.98	2.24	0.67
S2	PG 64-22	RTFO	0.5% A1	87.48	37.78	19.54	2.32	0.52
S2	PG 64-22	RTFO	20% R1	84.29	36.79	22.53	2.29	0.61
S3	PG 76-28	RTFO	None	83.22	37.26	22.33	2.23	0.60
S3	PG 76-28	RTFO	0.5% W1	87.08	37.47	23.27	2.32	0.62
S3	PG 76-28	RTFO	0.5% A1	90.10	36.80	24.55	2.45	0.67
S3	PG 76-28	RTFO	20% R1	79.86	37.62	23.17	2.12	0.62
S3	PG 76-28	RTFO	1.5% P1	90.18	39.00	32.18	2.31	0.82
S4	PG 76-28	RTFO	None	77.84	37.88	21.66	2.05	0.57
S4	PG 76-28	RTFO	0.5% W1	82.63	38.47	25.44	2.15	0.66
S4	PG 76-28	RTFO	0.5% A1	82.62	37.34	22.51	2.21	0.60
S4	PG 76-28	RTFO	20% R1	78.95	36.71	21.41	2.15	0.58